(2)

ARL-TR-91-19

Copy No. 4

ACOUSTIC BLOCH WAVE PROPAGATION IN A PERIODIC WAVEGUIDE

Technical Report under Contract N00014-84-K-0574 and Grant N00014-89-J-1109

Charles E. Bradley

APPLIED RESEARCH LABORATORIES
THE UNIVERSITY OF TEXAS AT AUSTIN
POST OFFICE BOX 8029, AUSTIN, TEXAS 78713-8029

24 July 1991

Technical Report

Approved for public release;
distribution unlimited.

Prepared for:

OFFICE OF NAVAL RESEARCH
PHYSICS DIVISION, CODE 1112
ARLINGTON, VA 22217-5000

REPORT DOCUMENTATION PAGE

Form Approved
OMB No. 0704-0188

1. AGENCY USE ONLY (Leave blank)	2. REPORT DATE	3. REPORT TYPE AND DATES COVERED
	24 Jul 91	technical

4. TITLE AND SUBTITLE
Acoustic Bloch Wave Propagation in a Periodic Waveguide
Technical Report under Contract N00014-84-K-0574 and Grant N00014-89-J-1109

5. FUNDING NUMBERS
N00014-84-K-0574
and
N00014-89-J-1109

6. AUTHOR(S)
Bradley, Charles E.

7. PERFORMING ORGANIZATION NAMES(S) AND ADDRESS(ES)
Applied Research Laboratories
The University of Texas at Austin
P.O. Box 8029
Austin, TX 78713-8029

8. PERFORMING ORGANIZATION REPORT NUMBER
ARL-TR-91-19

9. SPONSORING/MONITORING AGENCY NAME(S) AND ADDRESS(ES)
Office of Naval Research
Physics Division
Code 1112
Arlington, VA 22217-5000

10. SPONSORING/MONITORING AGENCY REPORT NUMBER

11. SUPPLEMENTARY NOTES

12a. DISTRIBUTION/AVAILABILITY STATEMENT
Approved for public release; distribution unlimited.

12b. DISTRIBUTION CODE

13. ABSTRACT (Maximum 200 words)

The propagation of linear, dissipative acoustic Bloch waves in a periodic waveguide is investigated theoretically and experimentally. The waveguide under study is a rigid, fluid-filled, rectangular waveguide that is loaded with a periodic array of rigidly terminated rectangular side branches. Conditions for the existence of Bloch waves in the periodic waveguide are presented. Analytic expressions for the dispersion relation, the impedance function, and the Bloch wave function are derived. Measurements verify the predicted passband/stopband structure of the dispersion relation and show good agreement with the theory.

14. SUBJECT TERMS
(see reverse side)

15. NUMBER OF PAGES
99

16. PRICE CODE

17. SECURITY CLASSIFICATION OF REPORT	18. SECURITY CLASSIFICATION OF THIS PAGE	19. SECURITY CLASSIFICATION OF ABSTRACT	20. LIMITATION OF ABSTRACT
UNCLASSIFIED	UNCLASSIFIED	UNCLASSIFIED	SAR

14. (cont'd)

acoustic Bloch wave
acoustic filter
band structure
Bloch wave
Bloch wave dispersion
Bloch wave impedance
dispersion
dispersive wave
dissipative Bloch wave
guided wave
periodic structure
periodic waveguide
stopband

TABLE OF CONTENTS

Page

Page

LIST OF FIGURES

Page

PREFACE

This report is adapted from the master's thesis of the same title by Charles E. Bradley. Mr. Bradley began his graduate studies in the Department of Mechanical Engineering in September 1987, and his degree was granted in December 1990. The report incorporates a few changes and additions not included in the thesis version.

The research was carried out at Applied Research Laboratories, The University of Texas at Austin. Support for the project came from the Office of Naval Research (ONR) under Contract N00014-84-K-0574 and Grant N00014-89-J-1109. Scientific Officer for ONR was L. E. Hargrove.

1. INTRODUCTION

The study of wave propagation in periodic structures began over three centuries ago with Newton's attempt to derive the speed of propagation of sound. Since that time, work concerning waves in periodic structures has branched into such diverse fields as linear particle accelerator design, microwave antennae and filter design, and the quantum mechanical theories of condensed matter. While much of the recent work in this field of study has not addressed acoustic waves, the acoustical case is still a very active field of study. Nearly all of the work in acoustics, however, concerns the problem of waves in elastic solids - most of that work concerning phonons, the quantized elementary acoustic excitation. The present study concentrates on the behavior of *fluid-borne* sound in a periodically varying waveguide.

The motivating interest in this study is that the waves which occur in periodic media, known as Bloch waves (Kittel, 1986), have very unusual dispersion and attenuation characteristics. The author's interest in the dispersive nature of Bloch waves sprung from an interest in nonlinear acoustic propagation in strongly dispersive media. While the nonlinear case will be treated in a subsequent study, the goal of this work is to characterize the linear behavior of acoustic waves in a periodic waveguide.

The work presented here is a theoretical and experimental investigation of acoustic Bloch wave propagation in a periodic waveguide. The waveguide under study is rectangular and loaded periodically with rigidly terminated rectangular side branches. The theoretical analysis is for a rigid waveguide filled with an arbitrary homogeneous, viscous, heat conducting fluid. The experimental portion of the work is the study of Bloch waves in an air filled aluminum waveguide.

1.1 Characteristic Properties of Bloch Wave Propagation

While nonuniformity of a wave system (the wave medium or the wave medium and its boundary) certainly affects the propagation of waves in that system, *periodic* nonuniformity has a particularly profound effect. The wave system, even a nondissipative wave system, selectively attenuates waves on the basis of their frequency. The frequency selective property of periodic structures has a banded structure: the strongly attenuated waves occupy bands of the frequency spectrum known as stopbands. Between neighboring stopbands are regions of the frequency spectrum known as passbands, the waves associated with which propagate with little or no attenuation.

The dispersion relation for a periodic structure is a functional relationship between the temporal frequency ω and the Bloch spatial frequency or Bloch wave number q (Brillouin, 1946). The Bloch wave number can frequently be interpreted as being a sort of "effective" wave number or "net" wave number, though this interpretation should be used carefully. The same is true of the Bloch wavelength $\lambda_B = 2\pi/q$. As might be expected, the stopband waves are exponentially attenuated and are associated, even in the nondissipative case, with Bloch wave numbers that have an imaginary component. Figure 1.1 shows a typical Bloch wave dispersion curve (or

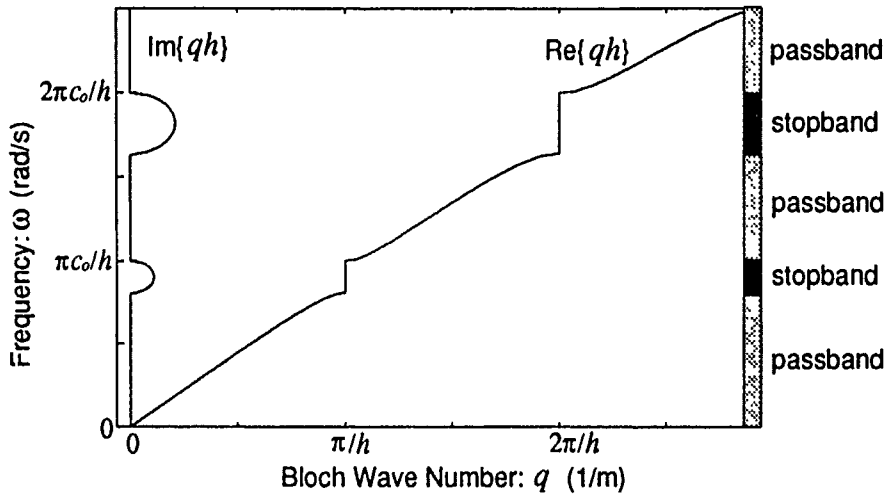

FIGURE 1.1
A typical dispersion curve for forward propagating Bloch waves in a periodic structure with periodicity h. The stopbands, which occur at intervals of π/h along the Bloch wave number axis, are frequency bands in which $\mathrm{Im}\{q\} \neq 0$ and $\mathrm{Re}\{q\} =$ constant.

AS-91-331

Brillouin diagram, as these curves are sometimes called (Elachi, 1976)) for nondissipative propagation. Several noteworthy characteristics of Bloch wave dispersion are as follows:

- At passband frequencies the Bloch wave number is real and a nonlinear function of frequency (i.e., passband Bloch waves are dispersive).
- At stopband frequencies, the Bloch wave number has a nonzero imaginary component, which is associated with the exponential attenuation of the wave.
- At stopband frequencies the real component of the Bloch wave number remains constant throughout the band. The stopbands are therefore *bands of frequencies associated with a single Bloch wavelength!* Like the passband Bloch waves, therefore, the stopband Bloch waves are dispersive.

- The passbands and stopbands occur at intervals of π/h along the Bloch wave number axis, where h is the periodicity of the periodic structure.

A few words need to be said about the graphical presentation of the Bloch wave dispersion relation. The variety of presentation schemes appearing in the literature often leads to confusion. It turns out that if one remains consistent with respect to several conventions, all of the information regarding the dispersion of the Bloch waves can be contained in a graph that is confined to the first so called Brillouin zone ($-\pi/h \leq q \leq +\pi/h$). Such a presentation, called the "reduced zone" scheme, is frequently used by solid state physicists (Kittel, 1986). Figure 1.1 is an example of the "extended zone" scheme, which is used in most of the present work. A third scheme, the "periodic zone" scheme, is shown in Sec. 3.4 in relation to the so called travelling wave spectral representation of Bloch wave functions.

1.2 Classes of Periodic Structures

The term "periodic structure" is used as a generic label for a wave system (the medium or the combination of the medium and its boundary) that has some sort of spatially repeating structure. Periodic structures can be regarded as belonging to one of three classes: (1) the periodic medium, (2) the periodically inhomogeneous medium, and (3) the periodically bounded medium.

The sound speed calculations made by Newton are based on a model of a continuum which defines the first class of periodic structures. Brillouin (1946) points out that Newton modeled the one-dimensional fluid continuum in the lumped element approximation: the medium is effectively a series of masses connected by springs. The mass of each element is related to the fluid density and the spring constant is related to the bulk modulus of elasticity of the fluid.[1] Though Newton did not know of the atomic lattice arrangement of crystalline solids, his lumped element model of a fluid is essentially that used currently to model such solids. A wave medium of this type, in which the *fabric of the medium itself* is intrinsically periodic, is referred to as a periodic medium. The majority of the works concerning waves in periodic media is in the area of lattice dynamics in the field of solid state physics. The dispersion in this case is referred to as phonon dispersion, which is important in the modeling of the thermal, optical, and ohmic electrical properties of solids (Kittel, 1986). An extensive source of information on the periodic medium and, to a lesser extent, the other two classes of periodic structures is the classic monograph by Brillouin (1946).

[1] It is of historical interest to note that Newton assumed the ratio of pressure to density to be constant (Boyle's law). Though it was not known at the time, implicit in Boyle's law is the assumption that the acoustic process takes place *isothermally*. Over 100 years later, about 1816, Laplace realized that the thermodynamic process is more accurately *adiabatic* and corrected Newton's calculations.

The second class of periodic structures, the periodically inhomogeneous medium, is somewhat self explanatory. Periodically inhomogeneous media are simply continua that exhibit some sort of periodically repeating inhomogeneity. An example from acoustics is a fluid having a periodic variation in ambient density or sound speed. Easily the largest body of work involving periodically inhomogeneous media is that concerning the quantum theory of electrical conductivity. In the quantum theory, the electron is represented by De Broglie/Schrödinger matter waves which propagate in an electrical conductor, which is a crystalline solid. The properties of the "medium" in which such waves propagate are determined by the potential of the crystal lattice, which varies periodically. In the quantum mechanical interpretation, the dispersion relation (a frequency-wave number relation) is an energy-momentum relation[2] and the band structure of the dispersion relation is the well known "band structure of solids" The stopband frequencies or forbidden frequencies are the forbidden energy bands or the "band gaps" that lie at the heart of the quantum theories of electrical conductivity, resistivity, and semi-conductivity (Kittel, 1986). An interesting application which exploits the properties of the periodically inhomogeneous medium is the distributed feedback laser, in which the lasing medium is imposed with a periodic spatial modulation in the refractive index (Elachi, 1976).

The subject of this study is an example of the third class of periodic structures, the periodically bounded medium. These structures are systems composed of a homogeneous medium with a periodically varying boundary. Work involving such media has been all but entirely confined to the realm of guided microwave propagation. Some examples of applications of this work are the slotted waveguide antenna (Hessel, 1969), the travelling wave filter (Collin, 1960), and the linear particle accelerator. The linear particle accelerator (which is a periodic waveguide) is a particularly interesting application in which the "space harmonic" property of Bloch waves is exploited to allow efficient exchange of energy between the microwave field and the accelerating particles (Slater, 1948; Slater, 1950). Another interesting application exploits the stopband properties of Rayleigh waves propagating along a corrugated elastic surface. Stopband frequency Rayleigh waves incident upon a corrugated section of a surface are very nearly 100% reflected. Such efficient reflections allow very high Q surface wave resonant tanks to be built for use as microwave frequency oscillators and filters (Bell and Li, 1976). Some of the unusual problems encountered in attempting to transmit information acoustically through a periodic waveguide (in this case the drill string of a deep petrochemical well) are discussed by Drumheller (1989).

A body of work that treats media which could arguably be placed in either the first or the third class of periodic structures also exists. The media in question are transverse or flexural wave media which are loaded in some periodic manner, such as the skin of aircraft with a rib-like support structure. Examples are the work of

[2] $E = \hbar\omega$ and $p = \hbar k$, where E is the energy, $\hbar$ is Planck's constant, k is the wave number, p is the momentum, and ω is the frequency.

Ungar (1966), Sen Gupta (1970), Mead (1970), and Mead (1973), which all treat the problem of a periodically supported beam or plate. A fascinating example of this class of work is that of J. D. Maynard, who models quantum mechanical events with waves in a classical acoustic wave system. For example, Maynard and He (1986) used a thin wire loaded periodically with small masses to model a crystalline solid. In such a system, transverse and longitudinal waves can be taken to be analogous to De Broglie/Schrödinger electron waves and phonons, respectively. Measurements of theoretically predicted quantum mechanical events, such as Anderson localization and phonon assisted hopping, were successfully made in the periodically loaded wire system.

1.3 Previous Work

Previous work in the area of acoustic wave propagation in a periodic, fluid filled waveguide is, to the author's knowledge, limited to purely theoretical investigations in which the periodic deviations from uniformity are small. An appropriate dimensionless variable representing the magnitude of the deviation from uniformity is in each case taken as the small parameter in a perturbation analysis.

Samuels (1959) and Salant (1972) treat the case of propagation in a two dimensional (parallel plate) waveguide with small sinusoidal perturbations in the boundaries. Both of these investigations were intended as the first step toward treating the case of a waveguide with statistically rough boundaries. The technique employed is a straightforward perturbation expansion in which the boundary condition at the sinusoidal surface is expanded about the mean planar surface. The result of the analysis in both cases is that a forward propagating wave is, with corrections to first order in the perturbation parameter, coupled to two other modes: a forward propagating wave mode and a backward propagating wave mode. Nayfeh (1974) showed that the perturbation expansion employed by Samuels (1959) and Salant (1972) is not uniform near stopband frequencies, where the mode coupling is strong, and that a multiple scales perturbation technique yields a uniformly valid expansion. Nayfeh (1975) essentially repeated the treatment of Nayfeh (1974), but allowed for the possibility of a net fluid flow through the waveguide. Nusayr (1980) employed a multiple scales perturbation technique in the analysis of a rectangular waveguide with sinusoidal boundaries. In all of the above cases the finding is that the periodically perturbed boundary couples a forward propagating mode with both a second forward propagating mode and a backward propagating mode. As is made evident in the section on the travelling wave spectral representation of Bloch wave functions (Sec. 3.4), the secondary modes found in the perturbation analyses are the first higher order components of the travelling wave spectrum.

Bai and Keller (1987) treated the case of a rectangular waveguide loaded with a periodic array of rigid spheres. They based their approach on the Webster horn equation and compared the results of a strained parameter perturbation analysis and a numerical analysis. The perturbation analysis yields values for the low frequency limit of the phase velocity and the bounding frequencies of the first three stopbands. The results of the two analyses compare very well, but the validity of the Webster horn equation at frequencies above the second stopband, for the waveguide geometry treated, is doubtful. Because of the symmetry of their axial location, the spheres will very effectively scatter sound into the even higher order modes of the waveguide. Additionally, because the first even higher order mode is above cutoff for frequencies above the second stopband frequency, sound will be propagating in two modes simultaneously. The Webster horn equation is a one dimensional wave equation and is therefore valid for the case of a single mode of propagation only.

While all of the works discussed above treat the general problem of interest, acoustic wave propagation in a fluid-filled periodic waveguide, they are inapplicable for the waveguide of this study. The large and infinitely rapid changes in waveguide cross sectional area which occur at the side branches simply cannot be regarded as "small". A perturbation expansion, as used in the above analyses, would therefore be a poor choice of analysis technique. While the side branches do not generally represent *small* perturbations in the cross sectional area of a waveguide, they do represent *spatially localized* perturbations. An approach which is readily applicable when the nonuniformity in the waveguide is spatially localized (and more generally applicable) is that of Achenbach and Kitahara (1987). They treat the problem of wave propagation in an elastic solid that has a three dimensional rectangular lattice of spherical cavities. Because they concentrate on excitation along a symmetry axis of the medium, their problem is identical to that of a waveguide which is filled with an elastic solid which contains a periodic array of spherical cavities along the axis. The paper also concentrates on the low frequency or plane wave mode case which, under purely longitudinal excitation, has a purely longitudinal wave solution (i.e., there is no shear mode excitation). The problem is therefore identical to a fluid acoustics problem. The result of the analysis is a dispersion relation that depends upon the scattering characteristics of the spherical cavities. The approach of Achenbach and Kitahara is that employed here in the derivation of the dispersion relation.

1.4 The Waveguide Under Study

The variables representing the various dimensions of the waveguide are shown in Fig. 1.2. The waveguide is aligned along the z axis with the side branches parallel to the y axis. The origin of the coordinate system is midway between side branches and centered on the bottom wall. The walls of the waveguide are located at $x = \pm a/2$,

$y = 0$, and $y = b$. The resultant waveguide cross sectional area is therefore $A_w = ab$. The side branches are placed at intervals of h along z, and are located in the bottom wall. The side branch walls are at $x = \pm a/2$, $y = -d$, $z = nh + (h - l)/2$, and $z = nh + (h + l)/2$, where n is an integer. In other words, the side branches are rectangular waveguides of cross sectional area $A_s = al$ and depth d.

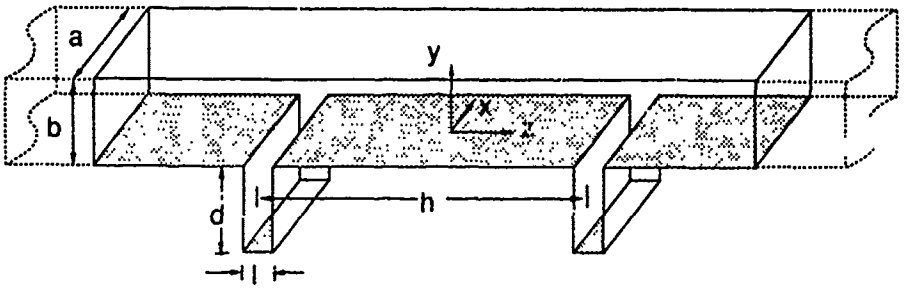

FIGURE 1.2
The periodic waveguide is a rectangular duct loaded with rigidly terminated rectangular side branches. Two cycles of the waveguide are shown.

AS-91-332

We now introduce some terminology:

- The "waveguide sections" are the sections of rectangular duct of length $h - l$ located between side branches. An example of a waveguide section is the segment between $z = \pm(h - l)/2$.
- The "port regions" are those regions above the side branch openings and in-between adjacent waveguide sections. An example of a port region is the volume $(h - l)/2 < z < (h + l)/2$, $0 < y < b$, $-a/2 < x < a/2$.
- A "cell" is a section of the periodic waveguide of length h along z centered on a waveguide section with side branches at each end. An example of a cell is the section defined by $-h/2 < z < h/2$.

In addition to those imposed later in the text, several approximations and assumptions are used from the onset of the analysis. They are as follows:

- The system is under time harmonic excitation. The arbitrary excitation case can be treated by Fourier synthesis.

- The system is under low frequency excitation. The frequency is below the cut-on frequency of the first higher order mode of both the waveguide sections and the side branches.

- The structure is, in the lossless case, effectively two dimensional. The waveguide boundaries normal to x are symmetric with respect to x and the structure within those boundaries is invariant with respect to x. We further assume that the excitation is independent of x, which, by symmetry arguments implies that the acoustic field is invariant with respect to x. The waveguide and the acoustic field can therefore be treated as being invariant and having infinite extent with respect to x; i.e., the waveguide and the field are two dimensional. In other words, the wave solution would be unchanged if the width a of the waveguide were allowed to become infinite.

- The waveguide is of infinite length. The problem of a semi-infinite or a finite periodic waveguide is considered in the section on truncation of the structure (Sec. 3.5).

1.5 The Scope of the Investigation

The remaining chapters are divided as follows. In Chap. 2 we begin with a system of governing equations and boundary conditions for the waveguide of interest and show that the solution wave functions are Bloch wave functions. Several functional representations of Bloch wave functions are shown. Chapter 3 consists of derivations of the dispersion relation, the impedance function, and the Bloch wave function for the waveguide. The effects of the truncation of the periodic structure are considered. In Chap. 4 the measurement of the Bloch wave dispersion is described. The various measurements are compared with theoretical results. Chapter 5 consists of brief concluding remarks and suggestions for future work.

2. THE FLOQUET THEOREM AND BLOCH WAVE FUNCTIONS

In this chapter it is shown that the mathematical system of governing equations and boundary conditions describing lossy, linear acoustic waves in a periodic waveguide is, under the appropriate frequency restrictions, of a class which has Bloch wave solutions. In order to show that Bloch wave functions are the solutions of the system, we apply the Floquet theorem to the mathematical system. While the Floquet theorem is penned so as to apply to a class of ordinary differential equations, an inspection of its proof shows that it is more generally applicable to a class of *systems* of partial differential equations and boundary conditions. In order to be eligible for the application of the Floquet theorem, the system must (1) exhibit a translational invariance, and (2) have two linearly independent solutions. It will be shown that the Floquet theorem is indeed applicable to the system of interest and that the application results in a restriction on the solution wave functions: they must be Bloch wave functions.

The chapter is organized as follows. We begin with a discussion of the system of governing equations and boundary conditions and show that the system exhibits an invariance under translation. It is then shown that, under a frequency restriction, the system can be considered to be one dimensional and has two linearly independent solutions. The Floquet theorem is then applied to the system to show that the solution of the system must obey the Bloch wave condition; i.e., the solution wave functions are Bloch wave functions. Finally, several functional representations of Bloch wave functions are presented.

2.1 The System Under Study and its Translational Invariance

The aim of this section is to present the mathematical system to be solved and show that it exhibits invariance under a certain class of translation operations. While the derivations of the equations themselves are not shown, the assumptions implicit therein are presented. The reader interested in the details of the derivations are referred to the book by Pierce (1981).

2.1.1 The Governing Equations and Boundary Conditions

The set of equations that governs the dynamics of a viscous, heat conducting fluid is composed of statements of fundamental conservation laws and thermodynamic relations. These equations relate the field variables representing mass density, pressure, temperature, entropy, and fluid velocity:

$$\begin{aligned} \hat{\rho} &= \rho_0 + \rho, \\ \hat{P} &= P_0 + p, \\ \hat{T} &= T_0 + T, \\ \hat{s} &= s_0 + s, \\ \hat{\mathbf{u}} &= \mathbf{u}, \end{aligned} \tag{2.1}$$

respectively, where the total value of a field variable (denoted by a hat) is expressed as the sum of the ambient value (subscripted with a zero) and the acoustic or fluctuating value.[1] The equations are derived under the following assumptions:

- The fluid is Newtonian; i.e., the viscous shear stress is proportional to the rate of shear.[2]
- The fluid transfers heat by conduction only and according to the Fourier law of heat conduction; i.e., the local heat flux is proportional to the local temperature gradient. In assuming that the heat transfer is by conduction *only* we neglect convective and radiative heat transfer.
- The fluid is in thermodynamic equilibrium; i.e., the thermodynamic state of the fluid is dependent upon *two* independent thermodynamic variables.
- The fluid is homogeneous; i.e., the ambient values of the field variables are constant and uniform.
- The dynamics of the fluid are well described by linearized governing equations; i.e., the magnitude of the acoustic disturbance is very small. The small parameter that the equations are linearized with respect to is the acoustic Mach number $\epsilon = |\mathbf{u}|_{\max}/c_0 \ll 1$.

Under these assumptions, linearized statements of the conservation of mass, momentum, and entropy are

[1] Note that we have assumed that $\mathbf{u}_0 = 0$; the fluid has no dc or net velocity.

[2] We have also assumed that the bulk viscosity is zero (or, equivalently, that the dilational viscosity is equal to -2/3 the shear viscosity), which is Stokes' assumption.

$$\frac{\partial \rho}{\partial t} + \rho_0 \nabla \cdot \mathbf{u} = 0, \tag{2.2}$$

$$\rho_0 \frac{\partial \mathbf{u}}{\partial t} = -\nabla p + \mu \left[\nabla^2 \mathbf{u} + (1/3) \nabla (\nabla \cdot \mathbf{u}) \right], \tag{2.3}$$

and

$$\rho_0 T_0 \frac{\partial s}{\partial t} = \kappa \nabla^2 T, \tag{2.4}$$

where μ is the coefficient of shear viscosity and κ is the coefficient of thermal conductivity. Linearized expansions of the thermodynamic relations $\hat{\rho} = \hat{\rho}(\hat{P}, \hat{s})$ and $\hat{T} = \hat{T}(\hat{P}, \hat{s})$ yield

$$\rho = \left(\frac{1}{c_0^2} \right) p - \left(\frac{\rho_0 \beta_0 T_0}{C_p} \right) s, \tag{2.5}$$

and

$$T = \left(\frac{1}{\rho_0 C_p} \right) p + \left(\frac{T_0}{C_p} \right) s, \tag{2.6}$$

where c_0 is the small-signal lossless sound speed, β_0 is the coefficient of thermal expansion, and C_p is the specific heat at constant pressure, all evaluated at the ambient condition. Equations 2.2-2.6, the dissipative governing equations, consist of seven scalar equations (four scalar equations and one vector equation) in seven scalar unknowns (four scalars and one vector).

In order to arrive at a set of boundary conditions, we assume that the boundary (the waveguide wall) is rigid, impenetrable, and has infinite heat capacity (i.e., is isothermal). We will also assume that the boundary is at rest with respect to the quiescent medium. Because the boundary is rigid and impenetrable, the velocity normal to the boundary must be zero:

$$\mathbf{u} \cdot \hat{\mathbf{n}}|_S = 0, \tag{2.7}$$

where $\hat{\mathbf{n}}$ is the unit vector normal to the surface of evaluation S, the wall of the waveguide. Because the fluid is viscous, it cannot slide with respect to itself or a boundary, and the tangential velocity at the surface must also be zero:

$$\mathbf{u} \times \hat{\mathbf{n}}|_S = 0. \tag{2.8}$$

Because the fluid has a nonzero heat conductivity, the fluid at the boundary must have the same temperature as the boundary. Because the boundary, by assumption, is always at the ambient temperature T_0, the fluid at the boundary must have zero acoustic temperature:

$$T|_S = 0. \tag{2.9}$$

Equations 2.7-2.9 are the boundary conditions on the dissipative system.

The Nondissipative System

In order to find the nondissipative governing equations, we simply use the dissipative equations in the limit as the heat conductivity and viscosity approach zero. In such a limit the mass continuity equation (Eq. 2.2) is unchanged, the momentum equation (Eq. 2.3) becomes a first degree equation, and the entropy equation (Eq. 2.4) becomes trivial:

$$\frac{\partial \rho}{\partial t} + \rho_0 \nabla \cdot \mathbf{u} = 0, \tag{2.10}$$

$$\rho_0 \frac{\partial \mathbf{u}}{\partial t} = -\nabla p, \tag{2.11}$$

and

$$s = 0. \tag{2.12}$$

As is expected, the lossless system is isentropic.[3]

The thermodynamic relations likewise simplify. Because $s = 0$ the density and temperature simply become directly proportional to the pressure:

$$p = c_0^2 \rho \tag{2.13}$$

$$T = (1/\rho_0 C_p) p. \tag{2.14}$$

Equations 2.10, 2.11, and 2.13 consist of five scalar equations in five scalar field variables. The system is therefore determined without the inclusion of the pressure-temperature relation (Eq. 2.14). The system of governing equations is therefore limited to Eqs. 2.10, 2.11, and 2.13 and the pressure-temperature relation simply yields temperature information once the pressure field is determined.

The boundary conditions on the nondissipative system are likewise a simplification of the boundary conditions on the dissipative system. When the viscosity and thermal conductivity of the fluid become zero the fluid is able to slip relative to the boundary and attain a non-zero acoustic temperature at the boundary. The only surviving boundary condition is the normal velocity restriction, which, by the use of the nondissipative momentum equation (Eq. 2.11) may be written in terms of the normal derivative of the acoustic pressure:

$$\nabla p \cdot \hat{\mathbf{n}}|_S = 0. \tag{2.15}$$

[3] In the lossless limit Eq. 2.4 becomes $\partial s/\partial t = 0 \rightarrow s =$constant, but any constant component of s is by definition incorporated into s_0, the ambient value of $\hat{s}$, and s becomes zero.

2.1.2 The Translational Invariance of the System

In order to establish the translational invariance of the system we must show that a translation operation exists under which the system remains unchanged. It is shown here that the dissipative system exhibits such an invariance. The nondissipative system is simply a special case of the dissipative system and therefore exhibits the same invariance.

We define $\mathcal{L}_i$ to be the i^{th} operator in the set of operators $\mathcal{L}$ which includes those found in the dissipative system of equations (Eqs. 2.2-2.6):

$$\mathcal{L} = \left\{1, \frac{\partial}{\partial t}, \frac{\partial}{\partial x_l}, \frac{\partial^2}{\partial x_m \partial x_n}\right\}, \tag{2.16}$$

where l, m, and n can each assume the values 1, 2, or 3 and $x_1 = x$, $x_2 = y$, and $x_3 = z$. We likewise define Ψ_i to be the i^{th} field variable in the set Ψ which consists of those found in the dissipative system of equations (Eqs. 2.2-2.6):

$$\Psi = \{\rho, p, s, T, u_1, u_2, u_3\}. \tag{2.17}$$

Each of the governing equations (Eqs. 2.2-2.6) can be represented as a linear combination of the operators in $\mathcal{L}$ acting on the field variables in Ψ:

$$(\Lambda_{ij}\mathcal{L}_i)\Psi_j = 0, \tag{2.18}$$

where the Λ_{ij}'s are constant coefficients and the summing convention is in effect. Likewise, each of the boundary conditions can be represented in the form

$$(\Omega_{ij}\mathcal{L}_i)\Psi_j|_S = 0, \tag{2.19}$$

where the Ω_{ij}'s are constant coefficients. In either case, the field variable Ψ_j is being operated on by the operator $\Lambda_{ij}\mathcal{L}_i$ or $\Omega_{ij}\mathcal{L}_i$.

The operators in the set $\mathcal{L}$ all belong to a class of operators that exhibit the property of *translational invariance*. That is, the operators all remain unchanged under the arbitrary spatial translation

$$(x_1, x_2, x_3) \rightarrow (x_1 + \Delta x_1, x_2 + \Delta x_2, x_3 + \Delta x_3).$$

An example is

$$\frac{\partial^2}{\partial x_m \partial x_n} \rightarrow \frac{\partial^2}{\partial(x_m + \Delta x_m)\partial(x_n + \Delta x_n)} = \frac{\partial^2}{\partial x_m \partial x_n}.$$

Because the operators that act on the field variables ($\Lambda_{ij}\mathcal{L}_i$ and $\Omega_{ij}\mathcal{L}_i$) are just the operators in $\mathcal{L}$ multiplied by constants, they are likewise invariant under arbitrary

translations. The set of governing equations is therefore translationally invariant. The set of boundary condition operators is also invariant under arbitrary translations, but the surface of evaluation S is not. It is, however, invariant under the more restricted set of translations $z \rightarrow z+nh$, where n is an integer, as the surface repeats at intervals of h along z. Because the set of governing equations is invariant under arbitrary translations and the set of boundary conditions is invariant under translations of h along z, the *system* is invariant under translations of h along z. The nondissipative system is just a simplification of the dissipative system and therefore has the same invariance.

It should be noted that the translational invariance depends on the homogeneity of the medium. An inhomogeneous medium has nonuniform ambient conditions such as $\rho_0 = \rho_0(x,y,z)$ or $T_0 = T_0(x,y,z)$. In such a medium the Λ_{ij}'s and Ω_{ij}'s (and therefore the operators $\Lambda_{ij}\mathcal{L}_i$ and $\Omega_{ij}\mathcal{L}_i$) are dependent upon the spatial coordinates and the translational invariance of the system is generally spoiled. If the medium is *periodically inhomogeneous* with a spatial period which is commensurate with the period of the surface of evaluation, an invariance is restored.

2.2 Wave Equations and the Zeroth Order Guided Wave Solutions

In this section solutions of the dissipative and nondissipative systems of equations and boundary conditions are shown. We begin with the nondissipative case and show the exact modal field solution in the vicinity of a side branch. We next introduce a frequency restriction that ensures that the evanescent higher order modes generated at a side branch are confined to the near vicinity of the port region. Under this restriction the system behaves as though the zeroth order or plane wave mode were the only mode present: the waveguide sections and side branches are effectively transmission lines. The approximation that the solution is well represented by the zeroth order field alone is referred to as the zeroth order approximation. It is then argued that under the same frequency restriction the solution of the *dissipative* system is well approximated by the zeroth order solution alone, and a method of finding such a solution is outlined.

2.2.1 The Nondissipative Case

In the nondissipative case the continuity equation (Eq. 2.10), the momentum equation (Eq. 2.11), and the pressure-density relation (Eq. 2.13) can readily be combined to form a single equation in the acoustic pressure,

$$\nabla^2 p - \frac{1}{c_0^2}\frac{\partial^2 p}{\partial t^2} = 0, \tag{2.20}$$

the classical wave equation. The solutions of Eq. 2.20 with Neumann, waveguide type boundary conditions are very well known (Morse and Ingard, 1986; Skudrzyk, 1971). The solutions are usually expressed as a sum over a discrete set of modes, some of which are evanescent and some of which are not. The analysis presented here is limited to frequencies for which every mode *except* the zeroth order mode is evanescent. In this context it is apparent what further frequency restrictions are necessary to treat the system as a one-dimensional wave system.

The Modal Solution

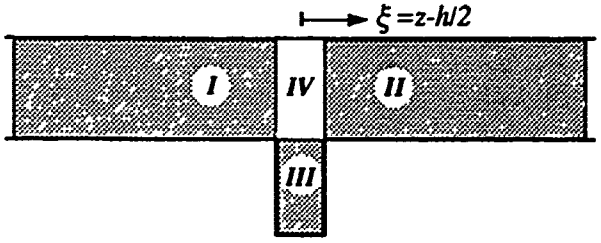

FIGURE 2.1
The four regions in the vicinity of a side branch.

In order to show the frequency constraints under which the solution can be well represented by the zeroth order field alone, we consider the solution of the nondissipative system in the vicinity of a side branch. The acoustic pressure wave function in the waveguide sections on either side of a side branch (regions I and II in Fig. 2.1) and in the side branch itself (region III in Fig.2.1) can be expressed as a sum over the discrete set of allowed modal solutions. It is assumed that the frequency is below the cut-on frequency of the first higher order mode, in which case the solutions can be expressed as the sum of the propagating zeroth order field and an infinite series representing the evanescent higher order modes. It is also assumed that the fields incident upon the side branch are purely zeroth order. Let $\xi = z - h/2$ be the shifted axial coordinate that is centered on a side branch. The waves incident from $\xi < 0$ and $\xi > 0$ have amplitudes A_0 and B_0, respectively. The time dependence, which under the time harmonic assumption is chosen to be $e^{-j\omega t}$, is suppressed and the acoustic pressure is treated as a function of the spatial coordinates only.

The wave solution in the presence of a scatterer is simply the sum of the incident wavefields and the resultant scattered fields. The zeroth order wave of amplitude A_0 incident on the side branch from $\xi < 0$ generates reflected and transmitted zeroth order waves of amplitudes $S_{11}A_0$ and $S_{21}A_0$, respectively, where the S_{ij}s are the zeroth order scattering matrix elements as defined by Rano, Whinnery, and Van Duzer (1965).[4] In addition to the zeroth order scattered fields there are generally also

[4] S_{11} and S_{22} are reflection coefficients and S_{12} and S_{21} are transmission coefficients. In simple

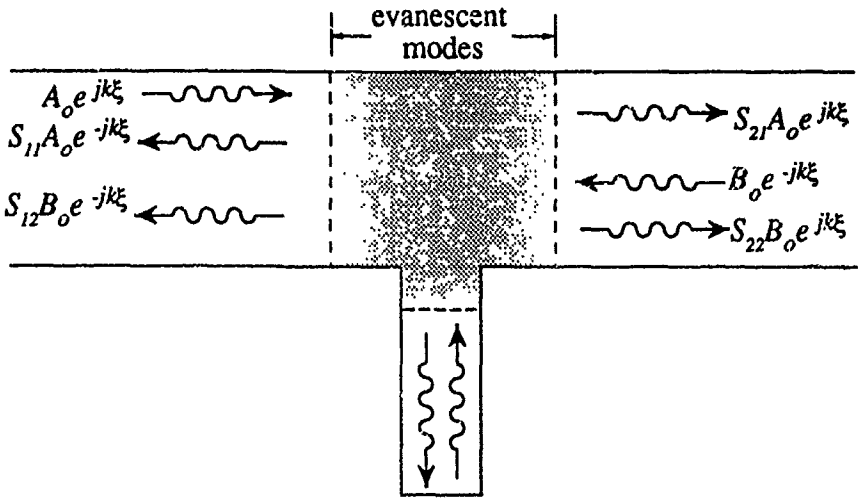

FIGURE 2.2
Zeroth order waves incident upon a side branch and the resultant scattered field. The scattered field consists of forward and back scattered zeroth order waves, zeroth order waves in the side branch, and evanescent modes. The evanescent modes are all confined to the near vicinity of the port region, as shown.

AS-91-333

forward and back scattered higher order modal fields. In a similar manner, the zeroth order wave of amplitude B_0 incident from $\xi > 0$ generates reflected and transmitted zeroth order waves of amplitudes $S_{22}B_0$ and $S_{21}B_0$, respectively, and higher order modal fields as well. The acoustic pressure field in region I (the waveguide section $\xi < -l/2$) can therefore be expressed as

$$p(y,\xi) = A_0 e^{jk\xi} + S_{11}A_0 e^{-jk\xi} + S_{12}B_0 e^{-jk\xi} + \sum_{n=1}^{\infty} A_n \cos(k_{n,y}y) e^{jk_{n,\xi}\xi},$$

where the various wave numbers are defined as

$$k_{n,y} = n\pi/b,$$

$$k_{n,\xi} = \left[(\omega/c_0)^2 - k_{n,y}^2\right]^{1/2},$$

and

$$k = \omega/c_0.$$

Because the analysis is restricted to frequencies below the cut-on frequency of the $n = 1$ mode, the axial wave number is imaginary for all but the zeroth order mode:

$$k_{n,\xi} = \pm j|k_{n,\xi}| \text{ for } n \geq 1.$$

terms, S_{ij} is the amplitude of the wave in region i due to a wave of unit amplitude incident upon the scatterer from region j.

The field in region I is therefore

$$p(y,\xi) = A_0 e^{jk\xi} + (S_{11}A_0 + S_{12}B_0)e^{-jk\xi} + \sum_{n=1}^{\infty} A_n \cos(k_{n,y}y)e^{|k_{n,\xi}\xi|}. \tag{2.21}$$

By similar reasoning, the field in region II (the waveguide section $\xi > l/2$) is

$$p(y,\xi) = B_0 e^{-jk\xi} + (S_{21}A_0 + S_{22}B_0)e^{jk\xi} + \sum_{n=1}^{\infty} B_n \cos(k_{n,y}y)e^{-|k_{n,\xi}\xi|}. \tag{2.22}$$

The field in region III (the side branch) can likewise be written as the sum

$$\begin{aligned} p(y,\xi) &= S_{sb}(A_0 + B_0)e^{jkd}2\cos(k(y+d)) \\ &\quad + \sum_{n=1}^{\infty} C_n 2\cos(k^{sb}_{n,\xi}(\xi - l/2))\frac{\cosh(k^{sb}_{n,y}(y+d))}{\cosh(k^{sb}_{n,y}d)}, \end{aligned} \tag{2.23}$$

where

$$k^{sb}_{n,\xi} = n\pi/l,$$

$$k^{sb}_{n,y} = \left[(\omega/c_0)^2 - (k^{sb}_{n,\xi})^2\right]^{1/2},$$

and S_{sb} is the coefficient of scattering into the side branch.

The Zeroth Order Approximation

The zeroth order approximation is that under which the system can be said to behave as though the zeroth order mode were the only mode present. For frequencies significantly below the cut-on frequencies of the higher order modes of the two guiding structures (the waveguide and the side branch), the evanescent field is confined to the port region. The evanescent modes will extend some distance into the waveguide on either side of the side branch and into the side branch itself (see Fig. 2.2), but the only *extended* field is the zeroth order field. The evanescent field is simply a *localized perturbation* to the zeroth order field and has no consequence with respect to the global behavior of the system.

One of the assumptions made in writing the solution in the form of Eqs. 2.21, 2.22, and 2.23 is that the fields incident upon the side branch are zeroth order. In order for this to be true, *the evanescent fields generated at each side branch must decay to a negligibly small amplitude over the distance h.* Since the first higher order mode has the most gradual attenuation of all the evanescent modes, the requirement is that the $n = 1$ mode be strongly attenuated over the distance h

$$e^{-[(\pi/b)^2 - (\omega/c_0)^2]^{1/2}h} \ll 1.$$

An equivalent statement is that the characteristic length associated with the decay of the evanescent field, i.e., $[(\pi/a)^2 - (\omega/c_0)^2]^{-1/2}$, must be small compared to h. Such a requirement leads to the frequency constraint

$$\omega \ll (c_0/h)[(\pi h/b)^2 - 1]^{1/2}. \tag{2.24}$$

Under this constraint, the system can be treated as a one dimensional system: a transmission line loaded with a periodic array of scatterers.

Although Eq. 2.24 is all that is required to treat the system as one dimensional, the derivation of the scattering matrix elements is much simplified if we make *another* zeroth order approximation, this time applied to the propagation of waves in the side branches. The field incident upon the port region from the side branch must be effectively zeroth order. For the side branch, the characteristic length associated with the decay of the lowest order evanescent field must be small as compared to $2d$, the "round trip" length of the side branch. The corresponding frequency constraint is

$$\omega \ll (c_0/2d)[(2\pi d/l)^2 - 1]^{1/2}. \tag{2.25}$$

It should be noted here that another low frequency constraint will need to be imposed when we consider the validity of the theory as it applies to a *real* periodic waveguide. The analysis thus far has all been under the assumption that the waveguide is effectively two dimensional. While this assumption is valid for the model waveguide (i.e., the ideal, mathematically defined waveguide), the *real* waveguide that the measurement is to be performed in will certainly have minor imperfections and not be perfectly invariant along x. These imperfections will lead to the excitation of higher order modes in x which have a structure $\sim \cos(m\pi x/a)$. To ensure that these modes decay to a negligible amplitude over the distance h, we require

$$\omega \ll (c_0/h)[(\pi h/a)^2 - 1]^{1/2}. \tag{2.26}$$

2.2.2 The Dissipative Case

In the dissipative case the system is much more complicated than the nondissipative system and does not reduce to a simple wave equation. A full three dimensional dissipative solution will not be shown. Instead we assume that the same argument used in the nondissipative case is valid to justify the use of the zeroth order field only. That is, we assume that when $\omega \ll (c_0/h)[(\pi h/a)^2 - 1]^{1/2}$ and $\omega \ll (c_0/2d)[(2\pi d/l)^2 - 1]^{1/2}$, the evanescent higher order modes are simply localized perturbations to the zeroth order field and need not be accounted for.[5] We are therefore left with the task of finding the zeroth order solution in each of the guiding structures (the waveguide sections and the side branches), each of which are simply rectangular waveguides.

[5]In the nondissipative, steady state case the evanescent modes, once established, exist entirely independently of the zeroth order field. There is no energy expenditure involved in maintaining the evanescent modes. In the dissipative case, however, the evanescent modes *do* dissipate energy, and represent an energy sink to the zeroth order field, which maintains their level. We assume that such a modification to the zeroth order field losses, particularly at low frequency where the evanescent modes have very little spatial extent, are negligible.

An elegant way of finding the zeroth order solution of the dissipative system is the modal field method (Pierce, 1981). The dissipative wavefield is decomposed into three component fields or modes: an acoustic mode, a vorticity mode, and an entropy mode. The field variables associated with a mode are subscripted with *ac*, *vor*, or *ent*, for acoustic, vorticity, or entropy mode, respectively. Each mode is governed by a partial differential equation that is derived from the the dissipative system of equations (Eqs. 2.2-2.6). The solutions of the three modal fields then sum to make up the total field. The method is only outlined here; the interested reader is referred to the detailed treatment in the book by Pierce (1981).

The equations governing the acoustic, vorticity, and entropy modes are

$$\nabla^2 p_{ac} - \frac{1}{c_0^2}\frac{\partial^2 p_{ac}}{\partial t^2} + \frac{1}{c_0^2}\left[\frac{4}{3}\frac{\mu}{\rho_0 c_0^2} + (\gamma - 1)\frac{\kappa/C_p}{\rho_0 c_0^2}\right]\frac{\partial^3 p_{ac}}{\partial t^3} = 0, \tag{2.27}$$

$$\nabla^2 \mathbf{u}_{vor} - \frac{\rho_0}{\mu}\frac{\partial \mathbf{u}_{vor}}{\partial t} = 0, \tag{2.28}$$

and

$$\nabla^2 s_{ent} - \frac{\rho_0 C_p}{\kappa}\frac{\partial s_{ent}}{\partial t} = 0, \tag{2.29}$$

respectively. The acoustic mode is governed by a wave equation that incorporates losses which, for small losses, are proportional to ω^2, which is typical of free field propagation in a thermoviscous fluid. The vorticity and entropy modes are governed by diffusion equations. The modes are independent except at the boundaries, where they are coupled; the acoustic mode acts as a source for the vorticity and entropy modes. Because the vorticity and entropy modes are governed by diffusion equations, they are confined to the vicinity of the source (the boundary), where they represent the modifications to the acoustic mode that make up the thermoviscous acoustic boundary layer. It should be noted that all the field variables of a particular mode can be found in terms of the field variable appearing in the equation for that mode. As an example, from p_{ac} alone we can find s_{ac}, $\mathbf{u}_{ac}$, T_{ac}, and ρ_{ac}. This is likewise true for the vorticity and entropy modes. The total field can then be found by summing the component modal fields:

$$p = p_{ac} + p_{vor} + p_{ent},$$

$$\mathbf{u} = \mathbf{u}_{ac} + \mathbf{u}_{vor} + \mathbf{u}_{ent},$$

and so on. One interpretation is that the acoustic mode drives the other two modes, which in turn have the appropriate structure to ensure that the *total* field satisfies the boundary conditions.

The modal formulation of the dissipative system of equations makes evident the two pathways by which acoustic energy is lost. One way is through the so called classical or ω^2 free field losses which occur independently of boundaries. This loss

pathway is described by the acoustic mode alone; the equation for p_{ac} is lossy and $s_{ac} \neq 0$ (entropy is generated by the acoustic mode alone). The other loss pathway is the "feeding" of the vorticity and entropy modes by the acoustic mode at the boundary. For a broad frequency range of interest, the latter loss pathway dominates the former, which can therefore be neglected.

The field is, except for the losses associated with the boundary layer, well described by the *acoustic mode alone.* The other modal fields represent modifications to the acoustic modal field only in the very near vicinity of the boundary, but are responsible for the dominant loss mechanism. It turns out that, for a wave propagating in the plane wave mode of a waveguide of given hydraulic radius, *the losses associated with coupling to the boundary layer can be incorporated into the acoustic mode.* The resultant field, which is found by a variational technique, is of the same form as that in the lossless case but the zeroth order wave number becomes

$$k = \omega/c_0 + (1+j)\frac{1}{\sqrt{2}R_H}\left[\left(\frac{\mu}{\rho_0 c_0^2}\right)^{1/2} + (\gamma-1)\left(\frac{\kappa/C_p}{\rho_0 c_0^2}\right)^{1/2}\right]\omega^{1/2}, \qquad (2.30)$$

where R_H is the hydraulic radius of the guiding structure and the free field (ω^2) losses have been considered to be negligible compared to the boundary layer ($\omega^{1/2}$) losses. This dispersion relation, up through the first term on the right hand side, is identical to that for the lossless case ($k = \omega/c_0$). The last term, which is complex and therefore introduces both losses *and* dispersion, is associated with the thermoviscous acoustic boundary layer. The range of validity of Eq. 2.30 is given by

$$\frac{c_0^2}{R_H^2}\frac{\mu}{\rho_0 c_0^2} \ll \omega \ll \left[\frac{c_0^2}{R_H^2}\left(\frac{\mu}{\rho_0 c_0^2}\right)^{-1}\right]^{1/3}, \qquad (2.31)$$

a result from Pierce (1981).

2.2.3 Linearly Independent, One Dimensional Solutions

At this point it can be shown that both the dissipative and nondissipative systems, under the frequency restrictions thus far compiled (Eqs. 2.24, 2.25, and 2.31) have two linearly independent solutions. Although we expect a one dimensional wave system to have two linearly independent solutions, the introduction of scatterers makes the system more complicated and worthy of discussion.

The most straightforward way to understand the types of solutions to expect is to consider the physical system as being a one dimensional wave system (i.e., a transmission line) that is loaded with a periodic array of scatterers. The solutions are composed of forward and backward travelling waves in each cell, as shown symbolically in Fig. 2.3. The amplitudes of the forward and backward travelling waves in

neighboring cells, however, *must be related as determined by the scattering matrix associated with the intervening scatterer.*

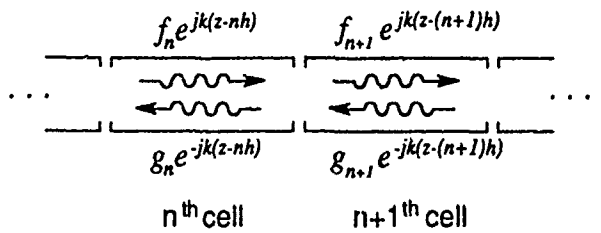

FIGURE 2.3
The zeroth order waves in the waveguide sections on either side of a scatterer.

AS-91-334

Consider the case wherein the complex amplitudes of the forward and backward travelling waves in a cell of the structure is known. The amplitudes of the forward and backward travelling waves at the center of the n^{th} cell are f_n and g_n, respectively. The corresponding amplitudes in the center of the neighboring cell, the $(n+1)^{\text{th}}$ cell, are f_{n+1} and g_{n+1}. The wave amplitudes in the n^{th} cell at the scatterer are then $f_n e^{jkh/2}$ and $g_n e^{-jkh/2}$, and those in the $(n+1)^{\text{th}}$ cell at the scatterer are $f_{n+1}e^{-jkh/2}$ and $g_{n+1}e^{jkh/2}$. The scattering relations, which relate the incoming and outgoing waves amplitudes at a scatterer, are

$$\begin{bmatrix} g_n e^{-jkh/2} \\ f_{n+1} e^{-jkh/2} \end{bmatrix} = \begin{bmatrix} S_{11} & S_{12} \\ S_{21} & S_{22} \end{bmatrix} \begin{bmatrix} f_n e^{jkh/2} \\ g_{n+1} e^{jkh/2} \end{bmatrix}. \tag{2.32}$$

Solving for f_{n+1} and g_{n+1}, we find

$$\begin{bmatrix} f_{n+1} \\ g_{n+1} \end{bmatrix} = \frac{1}{S_{12}} \begin{bmatrix} -|S|e^{jkh} & S_{22} \\ -S_{11} & e^{-jkh} \end{bmatrix} \begin{bmatrix} f_n \\ g_n \end{bmatrix}, \tag{2.33}$$

where $|S|$ is the determinant of the scattering matrix. The matrix in Eq. 2.33, which relates the travelling wave amplitudes at the cell centers on either side of a scatterer, is referred to as a tranmission matrix (Ramo, Whinnery, and Van Duzer, 1965). Given the amplitudes of the two travelling waves in a single cell, then, we can find the amplitudes of the two travelling waves in the cells neighboring that cell. In principle, we can continue this process until the wave amplitudes (and therefore the wave functions) in *all cells of the structure* are determined. The wave function of the entire system can therefore be expressed in terms of only the two constants f_n and g_n. These two constants are the two arbitrary constants associated with the general solution to a system that has two linearly independent solutions.

The Two Linearly Independent Solutions

The general solution function described above in terms of the two constants f_n and g_n can be considered to be composed of a linear combination of two component functions, $m^{(1)}(z)$ and $m^{(2)}(z)$. The conditions under which $m^{(1)}(z)$ and $m^{(2)}(z)$ are linearly independent is investigated by calculation of the Wronskian. It is shown that a very general class of pairs of functions are linearly independent.

The pair of functions $m^{(1)}(z)$ and $m^{(2)}(z)$ are defined in the n^{th} cell as

$$m^{(1)}(z) = M_n^{(1)} e^{jk(z-nh)} + N_n^{(1)} e^{-jk(z-nh)}$$

$$m^{(2)}(z) = M_n^{(2)} e^{jk(z-nh)} + N_n^{(2)} e^{-jk(z-nh)}.$$

Outside of the n^{th} cell, the functions are defined by successive applications of the transmission matrix as in Eq. 2.33. The Wronskian of $m^{(1)}(z)$ and $m^{(2)}(z)$ is

$$W = 2jk\left[N_n^{(1)} M_n^{(2)} - M_n^{(1)} N_n^{(2)}\right].$$

The functions are linearly independent if the Wronskian is nonzero (Arfken, 1985), which is true if

$$\frac{N_n^{(1)}}{M_n^{(1)}} \neq \frac{N_n^{(2)}}{M_n^{(2)}}.$$

In other words, $m^{(1)}(z)$ and $m^{(2)}(z)$ are linearly independent as long as they are not the same function.

2.3 The Floquet Theorem and the Bloch Wave Condition

In this section it is shown that because the mathematical system is translationally invariant and has two linearly independent solutions, it is a candidate for the application of the Floquet theorem.[6] The Floquet theorem is applied to the system to show the existence of two very unusual linearly independent solutions: the forward and backward travelling Bloch wave functions.

We begin with the consideration of $m^{(1)}(z)$ and $m^{(2)}(z)$, an arbitrary pair of linearly independent solution functions. Because $m^{(1)}(z)$ and $m^{(2)}(z)$ are linearly independent, we are able to express $\Gamma(z)$, an arbitrary solution, as the linear superposition

$$\Gamma(z) = \beta_1 m^{(1)}(z) + \beta_2 m^{(2)}(z), \tag{2.34}$$

[6]Proofs of the Floquet theorem, as it applies to second order ordinary differential equations with periodic coefficients, can be found in the books by Whittaker and Watson (1952) and Ince (1956).

where β_1 and β_2 are constant coefficients. It is evident that $|\beta\rangle$, a column vector composed of β_1 and β_2, is a *state vector*. The state vector is simply the projection of the solution $\Gamma(z)$ onto $|m(z)\rangle$, the linearly independent basis vector consisting of $m^{(1)}(z)$ and $m^{(2)}(z)$. As is seen in Eq. 2.34, the arbitrary solution $\Gamma(z)$ is simply the inner product of the state vector and the linearly independent basis vector:

$$\Gamma(z) = [\beta_1 \;\; \beta_2] \begin{bmatrix} m^{(1)}(z) \\ m^{(2)}(z) \end{bmatrix} = \langle \beta | m(z) \rangle. \tag{2.35}$$

Because the mathematical system is invariant under translations of h along z, $m^{(1)}(z+h)$ and $m^{(2)}(z+h)$ are also solutions to the system. These solutions can also be expressed in terms of the basis:

$$\begin{aligned} m^{(1)}(z+h) &= \alpha_{11} m^{(1)}(z) + \alpha_{12} m^{(2)}(z) \\ m^{(2)}(z+h) &= \alpha_{21} m^{(1)}(z) + \alpha_{22} m^{(1)}(z), \end{aligned} \tag{2.36}$$

or equivalently,

$$|m(z+h)\rangle = \tilde{\alpha} |m(z)\rangle \tag{2.37}$$

where the α_{ij}'s are constant coefficients.

We now look for the existence of a solution which has the property

$$\Gamma(z+h) = s\Gamma(z), \tag{2.38}$$

where s is a constant. With the introduction of $\mathcal{T}$, a translation operator, Eq. 2.38 becomes

$$\mathcal{T}\Gamma(z) = s\Gamma(z), \tag{2.39}$$

which is the eigenvalue problem associated with the operator $\mathcal{T}$. We next use Eq. 2.36 to expand $\Gamma(z+h)$ in terms of $m^{(1)}(z)$ and $m^{(2)}(z)$:

$$\begin{aligned} \Gamma(z+h) &= \beta_1 m^{(1)}(z+h) + \beta_2 m^{(2)}(z+h) \\ &= \beta_1 [\alpha_{11} m^{(1)}(z) + \alpha_{12} m^{(2)}(z)] + \beta_2 [\alpha_{21} m^{(1)}(z) + \alpha_{22} m^{(2)}(z)] \\ &= (\alpha_{11}\beta_1 + \alpha_{21}\beta_2) m^{(1)}(z) + (\alpha_{12}\beta_1 + \alpha_{22}\beta_2) m^{(2)}(z). \end{aligned} \tag{2.40}$$

In the state vector formulation, Eq. 2.40 is

$$\mathcal{T}\Gamma(z) = \Gamma(z+h) = \langle \beta | m(z+h) \rangle = \langle \beta | \tilde{\alpha} | m(z) \rangle. \tag{2.41}$$

Equations 2.37 and 2.41 both show that the operation of multiplication of a state vector by the matrix $\tilde{\alpha}$ is a *translation operation*. In other words, the equivalent of the translation operator $\mathcal{T}$ in the state vector formulation is the matrix $\tilde{\alpha}$. The substitution of Eqs. 2.35 and 2.41 into Eq. 2.39 results in a state vector formulation of the eigenvalue problem:

$$\mathcal{T}\langle \beta | m(z) \rangle = \langle \beta | \tilde{\alpha} | m(z) \rangle = s \langle \beta | m(z) \rangle$$

or

$$\tilde{\alpha}|\beta\rangle = s|\beta\rangle. \tag{2.42}$$

As is standard, we rewrite Eq. 2.42 in the form of a homogeneous equation,

$$(\tilde{\alpha} - s\tilde{1})|\beta\rangle = |0\rangle, \tag{2.43}$$

where $\tilde{1}$ is the identity matrix and $|0\rangle$ is the null vector. A nontrivial solution to Eq. 2.43 is guaranteed by the condition

$$|\tilde{\alpha} - s\tilde{1}| = 0,$$

which is satisfied by two values of s, the eigenvalues $s^{(1)}$ and $s^{(2)}$. Each of these eigenvalues is associated with an eigenvector, given by the equations

$$(\tilde{\alpha} - s^{(1)}\tilde{1})|\beta^{(1)}\rangle = |0\rangle$$
$$(\tilde{\alpha} - s^{(2)}\tilde{1})|\beta^{(2)}\rangle = |0\rangle.$$

In the spatial function representation, the eigenvectors correspond to eigen-*functions*, defined by

$$F(z) = \langle\beta^{(1)}|m(z)\rangle$$
$$G(z) = \langle\beta^{(2)}|m(z)\rangle.$$

The functions $F(z)$ and $G(z)$ are simply two linearly independent solution functions which we have found in terms of $m^{(1)}(z)$ and $m^{(2)}(z)$. The interesting property exhibited by the "new" basis composed of $F(z)$ and $G(z)$ becomes evident when the functions are operated on by the translation operator. The equivalent of Eq. 2.37 for this basis is

$$\begin{bmatrix} F(z+h) \\ G(z+h) \end{bmatrix} = \begin{bmatrix} s^{(1)} & 0 \\ 0 & s^{(2)} \end{bmatrix} \begin{bmatrix} F(z) \\ G(z) \end{bmatrix}. \tag{2.44}$$

We see that with this basis, the translation operation has a *canonical* form.

An alternative form of the eigenvalues, appropriate in the context of wave propagation, is

$$s^{(1)} = e^{jq_+h}$$
$$s^{(2)} = e^{jq_-h}, \tag{2.45}$$

where the constants $q_\pm$ are the (generally complex) Bloch wave numbers or Bloch spatial frequencies. The translation relations become

$$F(z+h) = e^{jq_+h}F(z)$$
$$G(z+h) = e^{jq_-h}G(z). \tag{2.46}$$

Equations 2.46 are referred to here as the Bloch wave conditions, and the linearly independent wave functions which meet these conditions are called Bloch wave functions.

2.4 Bloch Wave Functions

Bloch wave functions can be represented in a variety of functional forms. The various functional representations make evident the various unusual properties of Bloch waves. The two common forms of the Bloch wave function, here called the standard representation and the travelling wave spectral representation, are most often seen in work by solid state physicists and microwave engineers, respectively. A third functional form, here referred to as the convolution representation, is thought by the author to be a valuable alternative expression of the Bloch wave function, and is therefore included in this section.

2.4.1 The Standard Representation

A pair of wave functions which satisfy the Bloch wave conditions (Eq. 2.46) can be written

$$\begin{aligned} F(z) &= \Phi_{q_+}(z)e^{jq_+z} \\ G(z) &= \Phi_{q_-}(z)e^{jq_-z}, \end{aligned} \tag{2.47}$$

where $\Phi_{q_+}(z)$ and $\Phi_{q_-}(z)$ are periodic with the periodicity of the structure:

$$\begin{aligned} \Phi_{q_+}(z+h) &= \Phi_{q_+}(z) \\ \Phi_{q_-}(z+h) &= \Phi_{q_-}(z). \end{aligned} \tag{2.48}$$

In this representation, here called the standard representation, the Bloch waves are seen to be one dimensional travelling waves of spatial frequency $q_\pm$ that are modulated in amplitude and phase in a periodic manner by the functions $\Phi_{q_\pm}(z)$. The functions $\Phi_{q_\pm}(z)$, which are generally complex, are referred to here as the periodic modulation functions.

The two Bloch wave functions $F(z)$ and $G(z)$ can be seen to be very simply related to one another by considering a third solution function. Because the waveguide is invariant under reversal of the axial coordinate z, a third function

$$H(z) = \Phi_{q_+}(-z)e^{-jq_+z},$$

which is simply $F(z)$ under the symmetry transformation $z \rightarrow -z$, must also be a solution. Under a translation operation, $H(z)$ becomes

$$H(z+h) = e^{-jq_+h}H(z),$$

which is the Bloch wave condition for $G(z)$ *with* $q_- = -q_+$. The Bloch wave function $G(z)$ is therefore simply a backward travelling version of $F(z)$. Stated mathematically,

$\Phi_{q_-}(z) = \Phi_{q_+}(-z)$ and $G(-z) = F(z)$. We can therefore simplify the Bloch wave condition to

$$\begin{aligned} F(z+h) &= F(z)e^{+jqh} \\ G(z+h) &= G(z)e^{-jqh}, \end{aligned} \tag{2.49}$$

where $q = q_+ = -q_-$. The Bloch wave functions then become

$$\begin{aligned} F(z) &= \Phi_q(+z)e^{+jqz} \\ G(z) &= \Phi_q(-z)e^{-jqz}. \end{aligned} \tag{2.50}$$

In most of the analysis that follows, only the forward travelling Bloch wave $F(z)$ is considered. The backward travelling Bloch wave is identical to the forward travelling Bloch wave (they just propagate in opposite directions) so two analyses would be redundant. It is worth noting that up to this point, the axial inversion symmetry of the structure had not been exploited. A periodic structure with asymmetric cells would still have the two Bloch wave function solutions of Eq. 2.47, but these forward and backward travelling wave functions would not simply be reversed copies of one another.

The standard representation makes evident several features of Bloch waves in general which are noteworthy:

- Because the periodic modulation function $\Phi_q(z)$ has the periodicity of the structure, *the complex exponential (e^{jqz}) component of the Bloch wave function alone determines the net changes in phase and amplitude from a position in one cell to the corresponding position in a neighboring cell.* The phase change will be determined by $\mathrm{Re}\{q\}$ and the amplitude change by $\mathrm{Im}\{q\}$. If the wave function were sampled at intervals of h, the result would be identical to that of sampling the travelling wave e^{jqz}.

- Whereas the exponential component of $F(z)$ represents net wave function changes from cell to cell, $\Phi_q(z)$ *represents the wave function behavior within a single cell.* The exponential component represents a wave with phase that varies linearly with distance and amplitude that varies exponentially with distance. The $\Phi_q(z)$ component represents periodic deviations in phase and amplitude from the linear and exponential changes described by the exponential component.

- While $\Phi_q(z)$ is periodic, $F(z)$ is generally aperiodic. It is only for the discrete set of degenerate cases wherein the Bloch wavelength and the structure period are commensurate that the wave function is periodic.

2.4.2 The Travelling Wave Spectral Representation

In the standard form, the Bloch wave function, which is generally aperiodic, is expressed as the product of the two periodic functions $\Phi_q(z)$ and e^{jqz}. Because $\Phi_q(z)$ is periodic, it can be expressed in terms of a Fourier sum of discrete spatial frequency components:

$$\Phi_q(z) = \sum_{n=-\infty}^{+\infty} C_n e^{2\pi jnz/h}, \tag{2.51}$$

where

$$C_n = \frac{1}{h}\int_{-h/2}^{h/2} \Phi_q(z) e^{-2\pi jnz/h} dz. \tag{2.52}$$

The Bloch wave function can therefore be expressed

$$\begin{aligned} F(z) &= e^{jqz} \sum_{n=-\infty}^{+\infty} C_n e^{2\pi jnz/h} \\ &= \sum_{n=-\infty}^{+\infty} C_n e^{j(q+2\pi n/h)z}, \end{aligned} \tag{2.53}$$

which is called the travelling wave spectral representation of the Bloch wave function. It is readily seen that Eq. 2.53 is a sum over a discrete travelling wave spectrum, all components of which have the same temporal frequency (ω), but different spatial frequencies ($q + 2\pi n/h$). The phase velocity associated with the n^{th} travelling wave spectral component is seen to be

$$c_n = \frac{\omega}{q + 2\pi n/h}. \tag{2.54}$$

In the literature of periodic media, the travelling wave spectral components are often referred to as space harmonics (Ramo, Whinnery, and Van Duzer, 1965). It is interesting to note that because the range of the sum index n in Eq. 2.53 includes negative integers, half of the travelling wave spectral components have *negative* phase velocities. For this reason periodic structures are sometimes referred to as "backward wave structures" (Ramo, Whinnery, and Van Duzer, 1965).

2.4.3 The Convolution Representation

The apparent simplicity of the Bloch wave function in the concise, elegant, standard form (Eq. 2.50) is apt to be misleading. In fact, Bloch wave functions can be enormously complicated functions with a somewhat noise-like appearance owing to their general aperiodicity. A third expression of the Bloch wave function which bears a more intuitive relationship to the form of the Bloch wave can also be derived.

We first define the function that will be referred to as the cell wave function:

$$\psi(z) = \begin{cases} 0 & z < -h/2 \\ F(z) & -h/2 < z < h/2 \\ 0 & h/2 < z. \end{cases} \tag{2.55}$$

The cell wave function is simply the wave solution in a single cell of the periodic structure. We next use the Bloch wave condition (Eq. 2.49) to define the wave function anywhere in the structure in terms of its value in the cell defined by $-h/2 < z < h/2$:

$$F(z) = \begin{cases} \psi(z) & = \psi(z) * \delta(z) & -h/2 < z < h/2 \\ \psi(z-h)e^{jqh} & = \psi(z) * \delta(z-h)e^{jqh} & h-h/2 < z < h+h/2 \\ \quad \vdots & \quad \vdots & \quad \vdots \\ \psi(z-nh)e^{jnqh} & = \psi(z) * \delta(z-nh)e^{jnqh} & nh-h/2 < z < nh+h/2. \end{cases} \tag{2.56}$$

As is conventional, the asterisk ($*$) denotes the convolution operation as defined by

$$a(x) * b(x) = \int_{-\infty}^{+\infty} a(x-y)b(y)dy. \tag{2.57}$$

Because each shifted cell wave function is zero outside of its associated interval, the Bloch wave function can be expressed as the infinite sum of these functions. The Bloch wave function can therefore be expressed in the alternative form

$$F(z) = \psi(z) * \sum_{n=-\infty}^{+\infty} \delta(z-nh)e^{jnqh} \tag{2.58}$$

which is simply the cell wave function convolved with a phase weighted Shah or lattice function. The convolution of $\psi(z)$ with each phase weighted delta function in the lattice simply places a phase weighted copy of $\psi(z)$ at each lattice site. The Bloch wave function as expressed in Eq. 2.58, which will be referred to as the convolution representation, shows explicitly that the Bloch wave function is simply a string of repetitions of $\psi(z)$ at intervals of h with a cell to cell shift in phase of e^{jqh}. That is, aside from factors of the constant e^{jqh}, the Bloch wave function is simply a string of identical cell wave functions.

3. PROPERTIES OF THE BLOCH WAVES

In this chapter we derive expressions for some of the parameters which characterize Bloch waves. We begin with a derivation of the Bloch dispersion relation and an examination of the physical origins of some of the characteristics of the dispersion. The Bloch impedance function and explicit expressions of the Bloch wave function are derived. The multivalued nature of the dispersion relation is related to the travelling wave spectral form of the Bloch wave function. Finally, the consequences of truncation of the periodic structure are considered and Bloch wave reflection coefficients are derived.

3.1 Bloch Wave Dispersion

In order to derive a dispersion relation we exploit what is certainly one of the most significant attributes of the structure of Bloch waves: the analysis of wave propagation in an infinite periodic structure can be reduced to the analysis of wave propagation in a *single cell* of the structure. As is made evident by the convolution representation of the Bloch wave function, the infinite structure wave function can be expressed in terms of the wave function associated with a single cell of the structure.

A variety of methods have been employed in Bloch wave dispersion analyses (Collin, 1960; Slater, 1950; Kittell, 1986; Gasiorowicz, 1974). In each method, however, the dispersion relation is derived by imposing the same condition: the Bloch condition and the scattering relations must be consistent. That is, both the Bloch condition and the scattering relations place constraints on the relationship between the fields at the centers of neighboring cells. In order for these two constraints to be consistent with one another, a particular dispersion relation must exist. In the analysis presented here, which parallels that of Achenbach and Kitahara (1987), the Bloch condition is imposed in the form of boundary conditions. These boundary conditions, which are derived from the Bloch conditions, are applied at the centers of neighboring cells, as shown in Fig. 3.1. A general travelling wave solution in the vicinity of the intervening scatterer is expressed in terms of the S matrix elements as shown in Fig. 2.2. The application of the boundary conditions to this general travelling wave solution specifies the Bloch wave number in terms of the S matrix elements and k, the ordinary wave number. The S matrix elements associated with a rigidly terminated

side branch are found and substituted into the general dispersion relation. The result is the dispersion relation for our system. Features of the dispersion relation are then related to the various physical dimensions of the periodic structure.

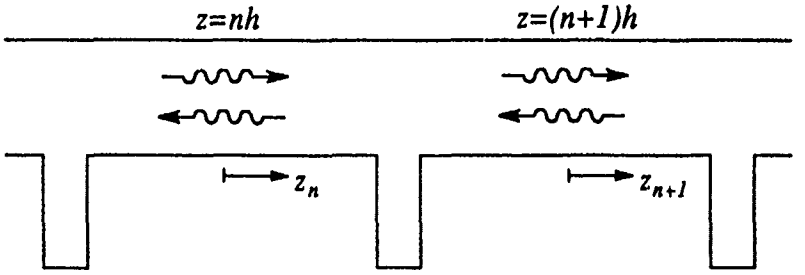

FIGURE 3.1
The dispersion analysis cell is centered on the side branch between the n^{th} and the $(n+1)^{th}$ cells. The Bloch boundary conditions are applied at the ends of the cell, at $z = nh$ and $z = (n+1)h$.

AS-91-335

3.1.1 The Bloch Boundary Conditions

The Bloch wave condition (Eq. 2.46) specifies the relationship that exists between the wave function at a point in the structure and that at a point one structure period distant. Such a condition is in effect a boundary condition (similar to a periodic boundary condition) which can be used in the analysis of the intervening section of the structure. A similar boundary condition can be derived for the *gradient* of the wave function. The standard representation of the Bloch wave function (Eq. 2.50) is a convenient functional form to use in such a derivation.

The evaluation of the Bloch wave function at $z = nh$ and $z = (n+1)h$ yields

$$p(z)|_{z=nh} = \Phi_q(nh)e^{jqnh}, \tag{3.1}$$

and

$$\begin{aligned} p(z)|_{z=(n+1)h} &= \Phi_q((n+1)h)e^{jq(n+1)h} \\ &= \Phi_q(nh)e^{jq(n+1)h}, \end{aligned} \tag{3.2}$$

respectively. Combining Eqs. 3.1 and 3.2, we find

$$p(z)|_{z=(n+1)h} = p(z)|_{z=nh}e^{jqh}, \tag{3.3}$$

which is the first Bloch boundary condition. Evaluation of the pressure gradient at $z = nh$ and $z = (n+1)h$ and introduction of Eq. 2.48 yields

$$\begin{aligned} \left.\frac{dp(z)}{dz}\right|_{z=nh} &= \left[\frac{d\Phi_q(z)}{dz}e^{jqz} + jq\Phi_q(z)e^{jqz}\right]_{z=nh} \\ &= \left[\left.\frac{d\Phi_q(z)}{dz}\right|_{z=nh} + jq\Phi_q(nh)\right]e^{jqnh}, \end{aligned} \tag{3.4}$$

and

$$\begin{aligned} \left.\frac{dp(z)}{dz}\right|_{z=(n+1)h} &= \left[\frac{d\Phi_q(z)}{dz}e^{jqz} + jq\Phi_q(z)e^{jqz}\right]_{z=(n+1)h} \\ &= \left[\left.\frac{d\Phi_q(z)}{dz}\right|_{z=nh} + jq\Phi_q(nh)\right]e^{jq(n+1)h}, \end{aligned} \tag{3.5}$$

respectively. Combining Eqs. 3.4 and 3.5 results in

$$\left.\frac{dp}{dz}\right|_{z=(n+1)h} = \left.\frac{dp}{dz}\right|_{z=nh} e^{jqh}, \tag{3.6}$$

which is the second Bloch boundary condition. It is interesting to note that the Bloch boundary conditions are simply phase shifted periodic boundary conditions on both the acoustic pressure and its gradient.

3.1.2 The Dispersion Relation for an Arbitrary Scatterer

The dispersion relation is found by imposing the condition that the field which, by definition, exists in the vicinity of the scatterer must meet the Bloch boundary conditions. The field in the n^{th} and the $(n+1)^{\text{th}}$ cells can generally be written as

$$p(z) = \begin{cases} f_n e^{jkz_n} + g_n e^{-jkz_n} & -h/2 < z_n < h/2 \\ f_{n+1}e^{jkz_{n+1}} + g_{n+1}e^{-jkz_{n+1}} & -h/2 < z_{n+1} < h/2, \end{cases}$$

where we define the shifted axial coordinate $z_m = z - mh$ which is centered on the m^{th} cell. This field is illustrated in Fig. 3.1. Equation 2.32 can be used to express g_n and f_{n+1} (the scattered waves) in terms of f_n and g_{n+1} (the incident waves), and the field can be written

$$p(z) = \begin{cases} f_n e^{jkz_n} + (S_{11}e^{jkh}f_n + S_{12}e^{jkh}g_{n+1})e^{-jkz_n} & -h/2 < z_n < h/2 \\ (S_{21}e^{jkh}f_n + S_{22}e^{jkh}g_{n+1})e^{jkz_{n+1}} + g_{n+1}e^{-jkz_{n+1}} & -h/2 < z_{n+1} < h/2. \end{cases} \tag{3.7}$$

The substitution of this solution into the Bloch boundary conditions leads to the system

$$\begin{bmatrix} S_{21} - e^{-jkh}e^{jqh} - S_{11}e^{jqh} & S_{22} + e^{-jkh} - S_{12}e^{jqh} \\ S_{21} - e^{-jkh}e^{jqh} + S_{11}e^{jqh} & S_{22} - e^{-jkh} + S_{12}e^{jqh} \end{bmatrix} \begin{bmatrix} f_n \\ g_{n+1} \end{bmatrix} = \begin{bmatrix} 0 \\ 0 \end{bmatrix}. \tag{3.8}$$

Because Eq. 3.8 is a homogeneous system, it has a nontrivial solution if and only if the coefficient matrix is singular:

$$\det \begin{vmatrix} S_{21} - e^{-jkh}e^{jqh} - S_{11}e^{jqh} & S_{22} + e^{-jkh} - S_{12}e^{jqh} \\ S_{21} - e^{-jkh}e^{jqh} + S_{11}e^{jqh} & S_{22} - e^{-jkh} + S_{12}e^{jqh} \end{vmatrix} = 0. \tag{3.9}$$

This requirement results in a dispersion relation for a general scatterer:

$$S_{12}e^{jqh} + S_{21}e^{-jqh} + (S_{11}S_{22} - S_{12}S_{21})e^{jkh} - e^{-jkh} = 0, \tag{3.10}$$

or

$$S_{12}e^{jqh} + S_{21}e^{-jqh} + |S|e^{jkh} - e^{-jkh} = 0, \tag{3.11}$$

where $|S|$ denotes the determinant of the scattering matrix.[1]

Symmetric Scatterer

If the scatterer is symmetric under reversal of the axial coordinate, then $S_{11} = S_{22}$ and $S_{12} = S_{21}$ (the reflection and transmission is the same for waves incident from either side), and Eq. 3.11 simplifies to

$$2S_{12}\cos(qh) + (S_{11}^2 - S_{12}^2)e^{jkh} - e^{-jkh} = 0.$$

Discrete Scatterer

If the axial extent of the scatterer is very small compared to a wavelength, the scatterer is effectively symmetric. In addition, the pressures on either side of the scatterer are approximately equal, resulting in the further simplification $S_{12} = 1 + S_{11}$. In such a case the dispersion relation becomes

$$\cos(qh) - e^{jkh} + \frac{j}{S_{12}}\sin(kh) = 0.$$

Impedance Load Scatterer

The characteristic acoustic impedance of a uniform waveguide of cross sectional area A_w is defined as $Z_{0a} = \rho_0 c_0 / A_w$, where the subscript a identifies the impedance

[1] If the medium is reciprocal (as well as isotropic), then, by the reciprocity principle, $S_{12} = S_{21}$ (Collin, 1960).

as being acoustic. If the scattering is caused by the loading of the waveguide by the shunt acoustic impedance Z_{La}, then $S_{12} = (1 + Z_{0a}/2Z_{La})^{-1}$ (Kinsler, Frey, Coppens, and Sanders, 1982). The dispersion relation then becomes

$$\cos(qh) - \cos(kh) + j\frac{Z_{0a}}{2Z_{La}}\sin(kh) = 0. \tag{3.12}$$

3.1.3 The Dispersion Relation and the Physical Origins of its Structure

The dispersion relation for the waveguide of this study can be found by substituting the expression for the acoustic impedance of a rigidly terminated side branch

$$Z_{La} = j\frac{\rho_0 c_0/A_s}{\tan(k_{sb}\hat{d})},$$

into Eq. 3.12. Note that in place of d, the *physical* depth of the side branch, we have substituted the *end corrected* length $\hat{d} = d + \Delta d$. The additional length Δd corrects for the inertial load on the side branch field due to the mass of the fluid in the port region. The end correction derived by Morse (1976) for a circular opening of radius a is $\Delta d = 8a/3\pi$. Using the side branch width l in place of the diameter of the circular opening we get

$$\hat{d} = d + 4l/3\pi,$$

which is the end correction used in this study. The resultant dispersion relation is

$$\cos(qh) = \cos(kh) - \frac{A_s}{2A_w}\tan(k_{sb}\hat{d})\sin(kh). \tag{3.13}$$

In order to investigate the relationships between the physical dimensions of the periodic structure and the resultant characteristics of the dispersion relation we begin by casting the dispersion relation in nondimensional form. Several dimensionless parameters are then identified and related to dispersion characteristics by direct analytical reasoning and graphical analysis. Dispersion curves for several combinations of values of the parameters are shown in this section with the hope that the effect of variation of these parameters is straightforward enough to allow the reader to generalize later results, which will be presented for a single set of parameters only.

It should be noted here that the Bloch dispersion relation is a *multivalued* dispersion relation. In order to evaluate the Bloch wave number, an inverse cosine function must be evaluated,

$$qh = \cos^{-1}[\cos(kh) - (A_s/2A_w)\tan(k_{sb}\hat{d})\sin(kh)], \tag{3.14}$$

which is a multivalued function. The branch of the dispersion relation shown in plots here is referred to as the *primary branch*. The primary branch is that which, in the

uniform waveguide limit ($d \rightarrow 0$ or $A_s \rightarrow 0$) degenerates to the nondispersive relation $qh = kh$. As was pointed out in Chap. 1, such a presentation scheme is referred to as the extended zone scheme. The choice of the primary branch also allows us the graphical interpretation of the dispersion curve: the slope of the line from the origin to a point on the dispersion curve is the phase velocity associated with that point on the curve, and the slope of the dispersion curve at that point is the group velocity associated with that point. It should also be noted that the branch shown is the primary branch associated with the *forward propagating* Bloch wave.

Nondissipative Dispersion

In order to make evident the parameters involved, we write the dispersion relation in a form which explicitly shows the frequency dependence. In the nondissipative case, $k = k_{sb} = \omega/c_0$, which can be introduced into Eq. 3.13 to result in

$$\cos[qh] = \cos[\omega h/c_0] - 1/2[A_s/A_w] \tan\left\{[\omega h/c_0][\hat{d}/h]\right\} \sin[\omega h/c_0], \tag{3.15}$$

where the dimensionless quantities appear in square brackets. In addition to the dimensionless Bloch wave number (qh) and frequency ($\omega h/c_0$), there appear the two geometrical parameters $\hat{d}/h$ and A_s/A_w, which are normalized side branch depth and area, respectively.

We begin the investigation of the significance of the nondimensional parameters with the definition of the functions v and w:

$$w = \frac{1}{2} \tan\left[(\omega h/c_0)\frac{\hat{d}}{h}\right] \sin(\omega h/c_0)$$

$$v = \cos(\omega h/c_0) + \frac{A_s}{A_w} w.$$

The dispersion relation can now be written

$$qh = \cos^{-1}[v].$$

Because $\omega h/c_0$ is real, v is also real. The inverse cosine of a real number is real if the argument is bounded by ± 1 and complex if the argument is larger than 1 or less than -1:

$$qh = \begin{cases} n\pi + j\cosh^{-1}(v) & (n \text{ even}) \quad 1 < v \\ \cos^{-1}(v) & \quad -1 \leq v \leq 1 \\ n\pi + j\cosh^{-1}(|v|) & (n \text{ odd}) \quad v < -1 \end{cases} . \tag{3.16}$$

Because stopbands occur when qh becomes complex, the condition $|v| > 1$ is the condition for the occurrence of a stopband.

The conditions under which $|v| > 1$, the stopband condition, can be found by investigating the behavior of w. Because the $\cos(\omega h/c_0)$ component of v is bounded

by ± 1, qh becomes complex only when w is able to "push" $\cos(\omega h/c_0)$ past ± 1. The function w, however, is generally quite small (easily bounded by ± 1) except in the region of the tangent singularity. The two situations in which $|v|$ is likely to become larger than 1 and cause the occurrence of a stopband are therefore:

- When the nondimensional frequency is in the vicinity of $kh = n\pi$ (n an integer). Since $\cos(n\pi) = \pm 1$, w can easily cause $|v|$ to become greater than 1. Because the magnitude of the function w is modulated by the parameter A_s/A_w, large values of this parameter increase the overall size and strength of the stopband, but not the *location* of the stopband. Such a dependence on A_s/A_w makes intuitive sense as increasing the side branch area relative to the waveguide area increases the reactive load on the waveguide without affecting the frequency dependence of the load.
- When the nondimensional frequency is in the vicinity of the tangent singularity: $\omega h/c_0 = (n + 1/2)\pi/(\hat{d}/h)$ with n an integer.

The first of the two stopband conditions, which results in stopbands near $\omega h/c_0 = n\pi$, is characteristic of wave propagation in periodic media (Slater, 1950; Gasiorowicz, 1974; Kittel, 1986; Brillouin, 1946). These stopbands correspond to the fitting of an integral number of half wavelengths into a single cell of the structure, which is simply the one dimensional Bragg condition. The stopbands near $\omega h/c_0 = n\pi$ are due to the periodicity of the structure, and will be referred to as the structure periodicity stopbands or the Bragg stopbands.

The second of the stopband conditions, which results in stopbands in the vicinity of $\omega h/c_0 = (n+1/2)\pi/(\hat{d}/h)$, is *not* typical of wave propagation in periodic media (see Fig. 1.1). The set of frequencies specified by the condition $\omega h/c_0 = (n + 1/2)\pi/(\hat{d}/h)$ is simply the set of resonance frequencies of the side branch.[2] These stopbands will be referred to as the side branch resonance stopbands.

We see from this analysis that A_s/A_w and $\hat{d}/h$ are parameters which gauge the overall strength of the stopbands and location of the side branch resonance stopbands, respectively. Figure 3.2 shows the real and imaginary parts of the nondimensional Bloch wave number (the dispersion and attenuation) for three values of A_s/A_w at a fixed value of $\hat{d}/h$. Recalling that stopbands occur when $|v| > 1$, we see that the effect of increasing A_s/A_w is as expected: the stopbands widen and increase in strength with no shift in location. Note the unusual structure of the side branch resonance stopband: $\mathrm{Im}\{q\}$ is cusped and $\mathrm{Re}\{q\}$ is discontinuous at the side branch

[2]Because a *single* side branch in an otherwise uniform waveguide causes total reflection of an incident wave if the frequency is a resonance frequency of the side branch, it is not surprising that a stopband occurs near such a frequency. In fact, because there is zero transmission across a single cell, we expect $\mathrm{Im}\{q\} \to \infty$ at the side branch resonance frequency.

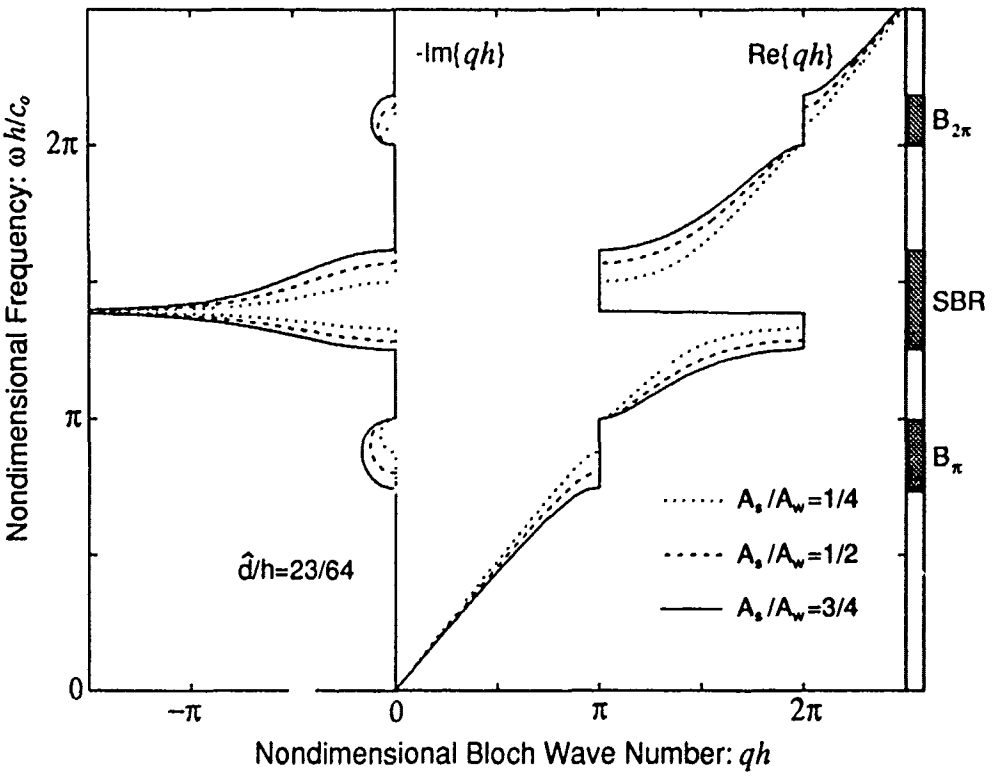

FIGURE 3.2

Nondissipative Bloch wave dispersion. Shown are Re$\{qh\}$ and -Im$\{qh\}$ for three values of the parameter A_s/A_w at a constant value of $\hat{d}/h$. The value of A_s/A_w determines the overall degree of loading of the waveguide by the side branches and therefore the overall magnitude of the periodic structure effect. The sizes and strengths of the stopbands are affected by changes in A_s/A_w, but the locations of the stopbands are not. The π and 2π Bragg stopbands and the side branch resonance stopband are marked B_π, $B_{2\pi}$, and SBR, respectively.

AS-91-336

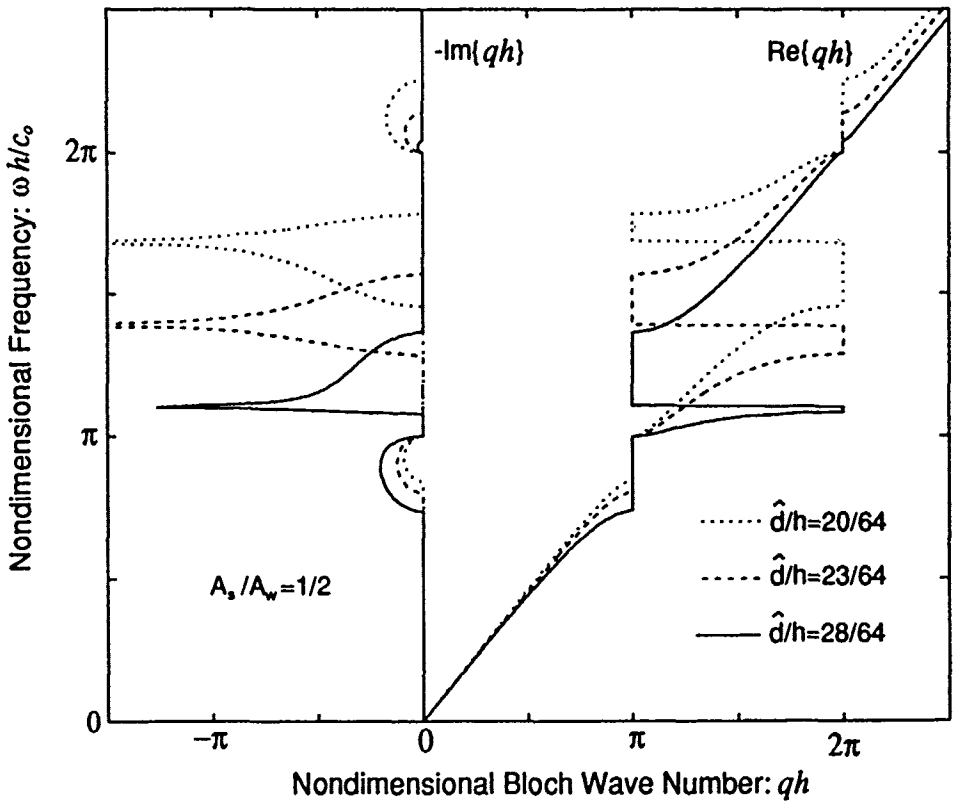

FIGURE 3.3

Nondissipative Bloch wave dispersion. Shown are Re$\{qh\}$ and -Im$\{qh\}$ for three values of the parameter $\hat{d}/h$ at a constant value of A_s/A_w. Varying $\hat{d}/h$ shifts the frequency of the side branch resonance stopband and alters the size and strength of the Bragg stopbands. The Bragg stopbands are wider (in frequency) and stronger when the side branch resonance stopband is near.

AS-91-337

resonance frequency. Figure 3.3 shows the dispersion and attenuation for three values of $\hat{d}/h$ with a fixed value of A_s/A_w. We see that changes in $\hat{d}/h$ affect both the Bragg and the side branch resonance stopbands. The location of the side branch resonance stopband shifts when $\hat{d}/h$ changes, and the Bragg stopbands are strongest when the side branch resonance stopband is nearby.

Dissipative Dispersion

When dissipation is present, the dispersion relation is, as might be expected, much more complicated. In the nondissipative case we were able to investigate the structure of the dispersion relation using mathematical reasoning. In the dissipative case we are left with little more than the rather crude technique of graphing the dispersion relation for a variety of parameter values.

We begin, as in the nondissipative case, by expressing the dispersion relation in the frequency-explicit form. The dissipative wave number, as defined in Eq. 2.30, is substituted into Eq. 3.13 to result in

$$\begin{aligned}\cos[qh] = \cos\left\{[\omega h/c_0] + (1+j)[\omega/\omega_{\mu\kappa}]^{1/2}[h/R_{Hw}]\right\} \\ -1/2[A_s/A_w]\tan\left\{[\omega h/c_0][\hat{d}/h] + (1+j)[\omega/\omega_{\mu\kappa}]^{1/2}[\hat{d}/R_{Hs}]\right\} \\ \cdot \sin\left\{[\omega h/c_0] + (1+j)[\omega/\omega_{\mu\kappa}]^{1/2}[h/R_{Hw}]\right\}. \qquad (3.17)\end{aligned}$$

The frequency $\omega_{\mu\kappa}$, defined as

$$\omega_{\mu\kappa} = 2\left[\left(\frac{\mu}{\rho_0 c_0^2}\right)^{1/2} + (\gamma-1)\left(\frac{\kappa/C_p}{\rho_0 c_0^2}\right)^{1/2}\right]^{-2}, \qquad (3.18)$$

is a frequency associated with thermoviscous losses, and R_{Hw} and R_{Hs} are the hydraulic radii of the waveguide and the side branch, respectively. In addition to those found in the nondissipative case, we have three more nondimensional quantities: the frequency $\omega/\omega_{\mu\kappa}$ and the two lengths h/R_{Hw} and $\hat{d}/R_{Hs}$.

At this point several qualitative observations about the effects of dissipation on the dispersion relation can be made. First, the fact that the dissipation terms (terms that did not appear in the nondissipative dispersion relation) all vary as $(\omega/\omega_{\mu\kappa})^{1/2}$ implies that $\omega_{\mu\kappa}$ is the characteristic frequency which defines the scale on which dissipative effects are measured. The other two nondimensional parameters are h/R_{Hw}, which is associated with propagation losses in the waveguide sections and $\hat{d}/R_{Hs}$, which is associated with similar losses in the side branches. The nondimensional parameters

$$\frac{h}{R_{Hw}} = \frac{h}{b} + \frac{h}{w} \qquad (3.19)$$

and

$$\frac{\hat{d}}{R_{Hs}} = \frac{\hat{d}}{l} + \frac{\hat{d}}{w}, \tag{3.20}$$

each associated with losses in a particular guiding structure, are dependent upon the length of the guiding structure as compared to its transverse dimensions. As is evident in Eq. 2.30, acoustic boundary layer effects result in both dissipation *and* dispersion, as they must to satisfy the Kramers-Kronig relations. We expect that the dispersion effects associated with h/R_{Hw} and $\hat{d}/R_{Hs}$ will cause slight shifts in the locations of the stopbands, as we found that the stopband locations are associated with resonance conditions, which will be shifted in frequency with the introduction of dispersion. The dissipative effects associated with h/R_{Hw} and $\hat{d}/R_{Hs}$ are more difficult to analyze. We know that h/R_{Hw} represents $\omega^{1/2}$ attenuation of the waves in the waveguide sections, and therefore expect some associated attenuation of the Bloch waves to result, but the functional behavior of $Im\{qh(\omega)\}$ is difficult to foresee. Likewise, $\hat{d}/R_{Hs}$ represents $\omega^{1/2}$ losses in the side branches and is therefore associated with a resistive component in the periodic load. Again, we expect that these losses will result in attenuation of the Bloch waves, but the frequency dependence of the attenuation is not obvious.

The effects of the parameters h/R_{Hw} and $\hat{d}/R_{Hs}$ are investigated graphically using constant values of A_s/A_w and $\hat{d}/h$ and varying the values of h/R_{Hw} and $\hat{d}/R_{Hs}$. Figure 3.4 shows the imaginary component of the dimensionless Bloch wave number for $\hat{d}/R_{Hs} = 0$ and h/R_{Hw}=0, 5, and 10. The effect of h/R_{Hw} is to introduce a roughly $\omega^{1/2}$ loss component in the passband Bloch wave number, which agrees nicely with intuition. Figure 3.5 shows the imaginary component of the Bloch wave number for $h/R_{Hw} = 0$ and $\hat{d}/R_{Hs}$=0, 5, and 10. The fact that the effect of $\hat{d}/R_{Hs}$ is most pronounced in the vicinity of the side branch resonance stopband makes sense as the acoustic field in the side branch has its greatest amplitude in the vicinity of resonance, and can therefore dissipate more acoustic energy. It is interesting to note that a nonzero value of $\hat{d}/R_{Hs}$ has no effect (i.e., $\mathrm{Re}\{qh\} = kh$ and $\mathrm{Im}\{qh\} = 0$) at $\omega h/c_0 = \pi, 2\pi$. Evidently at these frequencies (longitudinal resonance), the acoustic field in the side branch vanishes and the Bloch waves propagate at the uniform waveguide phase speed.

Figure 3.6 shows both the dissipative and nondissipative dispersion curves for a single set of parameters: $\hat{d}/h = .421$, $A_s/A_w = 3/8$, $h/R_{Hw} = 6.562$, and $\hat{d}/R_{Hs} = 5.531$. This set of parameters is, for reasons to be discussed in Chap. 4, the set to which the experimental portion of this work is dedicated. Note that the only significant effect of losses on the real component of the Bloch wave number is to smooth out the cusped corners.

It should be noted at this point that there are two distinctly different varieties of attenuation which occur in the periodic waveguide. One is the attenuation that occurs

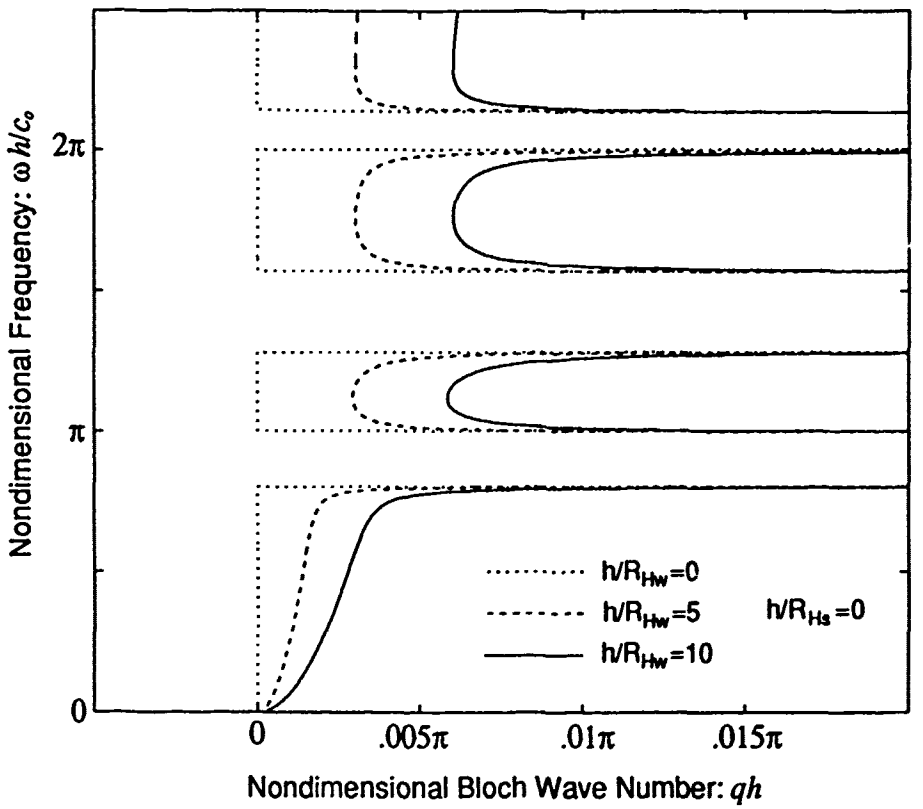

FIGURE 3.4

Bloch wave attenuation. Shown is $\mathrm{Im}\{qh\}$ for three values of the parameter h/R_{Hw} with $\hat{d}/R_{Hs} = 0$, which is the case of lossless (reactive) side branches but lossy waveguide sections. Varying h/R_{Hw} adjusts the amount of roughly $\omega^{1/2}$ loss, the standard waveguide loss. The losses are enhanced near both species of stopbands.

AS-91-338

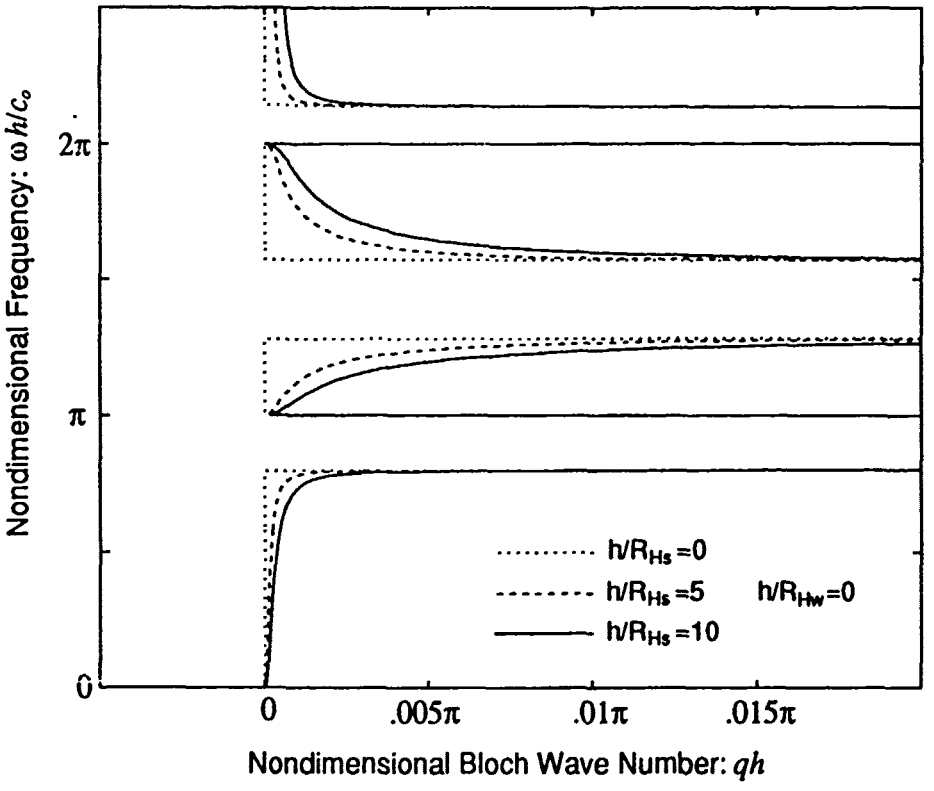

FIGURE 3.5

Bloch wave attenuation. Shown is $\mathrm{Im}\{qh\}$ for three values of the parameter $\hat{d}/R_{Hs}$ with $h/R_{Hw} = 0$, which is the case of lossless waveguide propagation but lossy (resistive) side branches. The effects of side branch losses are most pronounced in the region of the side branch resonance stopband, and are nonexistent at $\omega h/c_0 = n\pi$.

AS-91-339

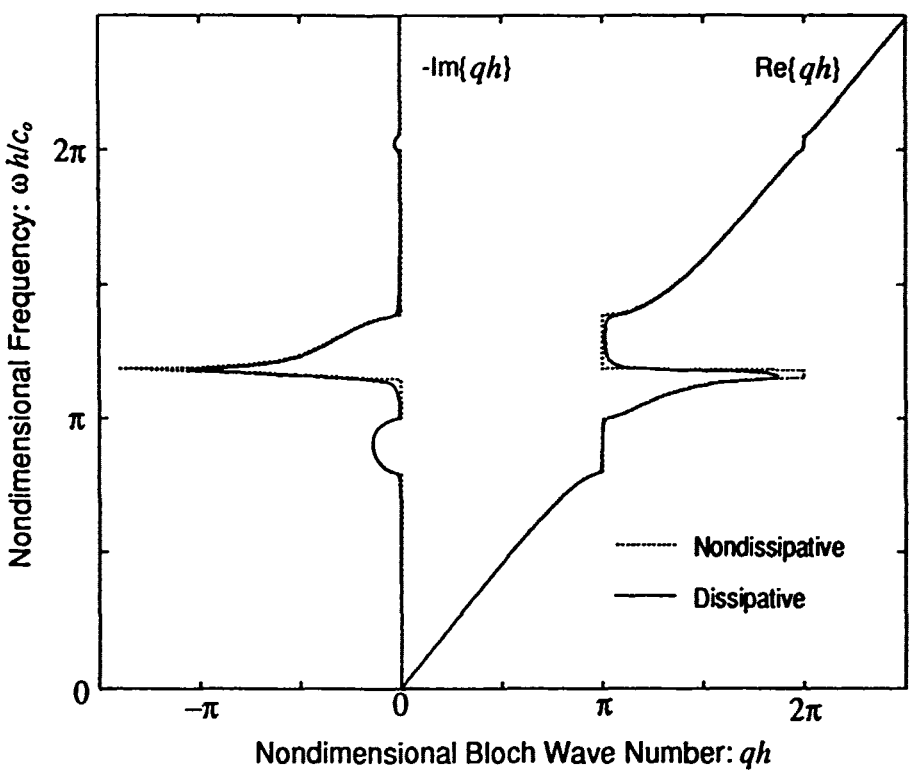

FIGURE 3.6
Dissipative and nondissipative Bloch wave dispersion for the values $\hat{d}/h = .421$, $A_s/A_w = 3/8$, $h/R_{Hw} = 6.652$, and $\hat{d}/R_{Hs} = 5.531$, which are those used in Chap. 4

AS-91-340

in the stopbands even in the nondissipative case. The other is the dissipative attenuation that is present at all frequencies but, owing to the magnitude of the dissipation in this study, most evident at passband frequencies. The dissipative attenuation, as was mentioned earlier, is due to thermal and viscous losses and is associated with the generation of entropy and the dissipation of acoustic energy. The nondissipative attenuation occurs in the absence of the entropy generating mechanisms and therefore cannot be associated with any energy dissipation. The nondissipative attenuation is very similar to the attenuation of evanescent modes in standard waveguides, which is also a type of nondissipative attenuation. As will be seen in Sec. 3.2, the impedance of the periodic waveguide at stopband frequencies, much like that of the evanescent modes in a standard waveguide, is reactive. For these reasons the two components of the attenuation will be referred to as the dissipative and the reactive components.

The main thrust of the theoretical component of this work, the derivation and discussion of the dispersion relation, is at this point complete. For this reason, further theoretical results will be presented graphically for only the single set of parameters listed above as the effects of adjustment of these parameters on the later theoretical results will be quite obvious.

3.2 The Iterative Bloch Acoustic Impedance

In this section we derive the Bloch acoustic impedance, which is simply the acoustic impedance at a point midway between side branches. The technique employed is similar to that used to derive the dispersion relation: we impose the condition that the Bloch wave function be consistent with the conditions at the scatterer. In the derivation of the dispersion relation, the Bloch wave condition was introduced in the form of the Bloch boundary conditions, which relate the field variable (and its gradient) in neighboring cells. Here, the Bloch wave condition is introduced through the iterative impedance condition, which relates the acoustic impedance in neighboring cells.

We begin by deriving the general Bloch impedance function for a waveguide loaded periodically with an arbitrary scatterer characterized by the scattering matrix S_{ij}. From that result, more specific results are found for the case of a symmetric scatterer, an arbitrary impedance load, and loading by a rigidly terminated side branch.

3.2.1 The Iterative Acoustic Impedance

The acoustic impedance associated with Bloch waves is what is referred to as an *iterative* impedance (Brillouin, 1946). Because the structure is invariant under translations of h, there is no discernible difference between the structure at one particular point and at a corresponding point an integer number of structure periods distant. In other words, because the structure has no preferred reference point, a quantity such as the acoustic impedance *must repeat with the periodicity of the structure.* The Bloch impedance is therefore referred to as an iterative impedance; one period of the structure transforms the impedance back into itself. Stated mathematically, the iterative impedance condition is

$$Z_a(z) = Z_a(z+h). \tag{3.21}$$

The iterative impedance condition can be derived rigorously by generalizing the results of Sec. 2 3. The Bloch wave condition can be written in terms of *any* of the acoustic variables, including the acoustic pressure and the particle velocity

$$p(z+h) = p(z)e^{jqh}$$

$$u(z+h) = u(z)e^{jqh}.$$

The impedance at a point z is, by definition

$$Z(z) = \frac{p(z)}{u(z)},$$

and that at $z+h$ is

$$Z(z+h) = \frac{p(z+h)}{u(z+h)} = \frac{p(z)e^{jqh}}{u(z)e^{jqh}} = Z(z).$$

It is evident that the iterative impedance condition is an inherent property of Bloch waves.

3.2.2 Impedance Analysis

The analysis begins with the definition of the travelling wave amplitudes at the centers of the n^{th} and $(n+1)^{\text{th}}$ cells. Recall from Fig. 3.1 that f_n and g_n are the amplitudes of the forward and backward travelling acoustic pressure waves at $z = nh$, while f_{n+1} and g_{n+1} are those at $z = (n+1)h$. The acoustic impedance at $z = nh$ is, by definition,

$$Z_a(nh) = Z_{0a}\frac{f_n + g_n}{f_n - g_n}, \tag{3.22}$$

and that at $z = (n+1)h$ is

$$Z_a(nh+h) = Z_{0a}\frac{f_{n+1}+g_{n+1}}{f_{n+1}-g_{n+1}}. \tag{3.23}$$

The acoustic pressure fields at $z = nh$ and $z = (n+1)h$ are related by the transmission matrix defined in Eq. 2.33:

$$\begin{bmatrix} f_{n+1} \\ g_{n+1} \end{bmatrix} = \frac{1}{S_{12}} \begin{bmatrix} -|S|e^{jkh} & S_{22} \\ -S_{11} & e^{-jkh} \end{bmatrix} \begin{bmatrix} f_n \\ g_n \end{bmatrix}.$$

Introducing these expressions for f_{n+1} and g_{n+1} into Eq. 3.23 results in

$$Z_a(nh+h) = Z_{0a}\frac{f_n[-|S|e^{jkh}-S_{11}]+g_n[S_{22}+e^{-jkh}]}{f_n[-|S|e^{jkh}+S_{11}]+g_n[S_{22}-e^{-jkh}]}. \tag{3.24}$$

We next use Eq. 3.22 to substitute $Z_a(nh)$ into Eq. 3.24 in place of f_n and g_n:

$$Z_a(nh+h) =$$

$$Z_{0a}\frac{(Z_a(nh)+Z_{0a})[-|S|e^{jkh}-S_{11}]+(Z_a(nh)-Z_{0a})[S_{22}+e^{-jkh}]}{(Z_a(nh)+Z_{0a})[-|S|e^{jkh}+S_{11}]+(Z_a(nh)-Z_{0a})[S_{22}-e^{-jkh}]}. \tag{3.25}$$

The iterative impedance condition states that the impedances at nh and $(n+1)h$ must be equal. Because the Bloch impedance is defined to be the impedance at the cell center, we have

$$Z_{Ba} = Z_a(nh) = Z_a(nh+h).$$

The introduction of the iterative condition makes Eq. 3.25 quadratic in Z_{Ba}/Z_{0a}:

$$(Z_{Ba}/Z_{0a})^2[|S|e^{jkh}-S_{11}-S_{22}+e^{-jkh}]$$

$$+(Z_{Ba}/Z_{0a})[2S_{22}-2S_{11}]+[-|S|e^{jkh}-S_{11}-S_{22}-e^{-jkh}]=0.$$

Solving for Z_{Ba} via the quadratic formula yields

$$Z_{Ba} = Z_{0a}\frac{S_{11}-S_{22}\pm e^{-jkh}[(|S|e^{2jkh}-1)^2-4S_{12}S_{21}e^{2jkh}]^{1/2}}{|S|e^{jkh}-S_{11}-S_{22}+e^{-jkh}}. \tag{3.26}$$

Symmetric Scatterer

If the scatterer is symmetric under reversal of the axial coordinate, then $S_{11} = S_{22}$ and $S_{12} = S_{21}$, and Eq. 3.26 simplifies to

$$Z_{Ba} = Z_{0a}\left[\frac{|S|e^{jkh}+2S_{11}+e^{-jkh}}{|S|e^{jkh}-2S_{11}+e^{-jkh}}\right]^{1/2}. \tag{3.27}$$

Discrete Scatterer

If the scatterer is discrete then $S_{12} = 1 + S_{11}$ as was described in Sec. 3.13. Equation 3.27 then simplifies to

$$Z_{Ba} = Z_{0a}\left[\frac{S_{11}(e^{jkh}-1)+j\sin(kh)}{S_{11}(e^{jkh}+1)+j\sin(kh)}\right]^{1/2}. \tag{3.28}$$

Impedance Load Scatterer

If the scattering is caused by the loading of the waveguide by the shunt acoustic impedance Z_{La}, then $S_{11} = -(1+2Z_{La}/Z_{0a})^{-1}$ (Kinsler, Frey, Coppens, and Sanders, 1982). The substitution of the expression for S_{11} into Eq. 3.28 results in the impedance function

$$Z_{Ba} = Z_{0a}\left[\frac{(Z_{0a}/Z_{La})[\cos(kh)-1]+\sin(kh)}{(Z_{0a}/Z_{La})[\cos(kh)+1]+\sin(kh)}\right]^{1/2}. \tag{3.29}$$

Side Branch Load

The substitution of the acoustic impedance of a rigidly terminated side branch,

$$Z_{La} = j\frac{\rho_0 c_0/A_s}{\tan(k_{sb}\hat{d})},$$

into Eq. 3.29 results in the Bloch impedance

$$Z_{Ba} = Z_{0a}\left[\frac{\frac{1}{2}(A_s/A_w)\tan(k_{sb}\hat{d})[\cos(kh)-1]+\sin(kh)}{\frac{1}{2}(A_s/A_w)\tan(k_{sb}\hat{d})[\cos(kh)+1]+\sin(kh)}\right]^{1/2}. \tag{3.30}$$

This is the Bloch acoustic impedance for the periodic waveguide of this study. It is of interest to note that in the lossless case the argument of the square root is positive or negative but real. This corresponds to an impedance that is either resistive or reactive, but never both. Figure 3.7 shows the Bloch acoustic impedance (normalized by the uniform waveguide impedance $Z_{0a} = \rho_0 c_0/A_w$) in both the dissipative and the nondissipative cases. In the nondissipative case, as might be expected, the impedance is real at passband frequencies and imaginary at stopband frequencies. When dissipation is present, the impedance is generally complex and the rapid transitions present in the nondissipative case are smoothed out.

The acoustic impedance at points away from the center of the waveguide section can be found in terms of the Bloch acoustic impedance. The definition of the acoustic impedance at the center of the zeroth cell (i.e., at $z = 0$)

$$Z_a = Z_{0a}\frac{f_0+g_0}{f_0-g_0},$$

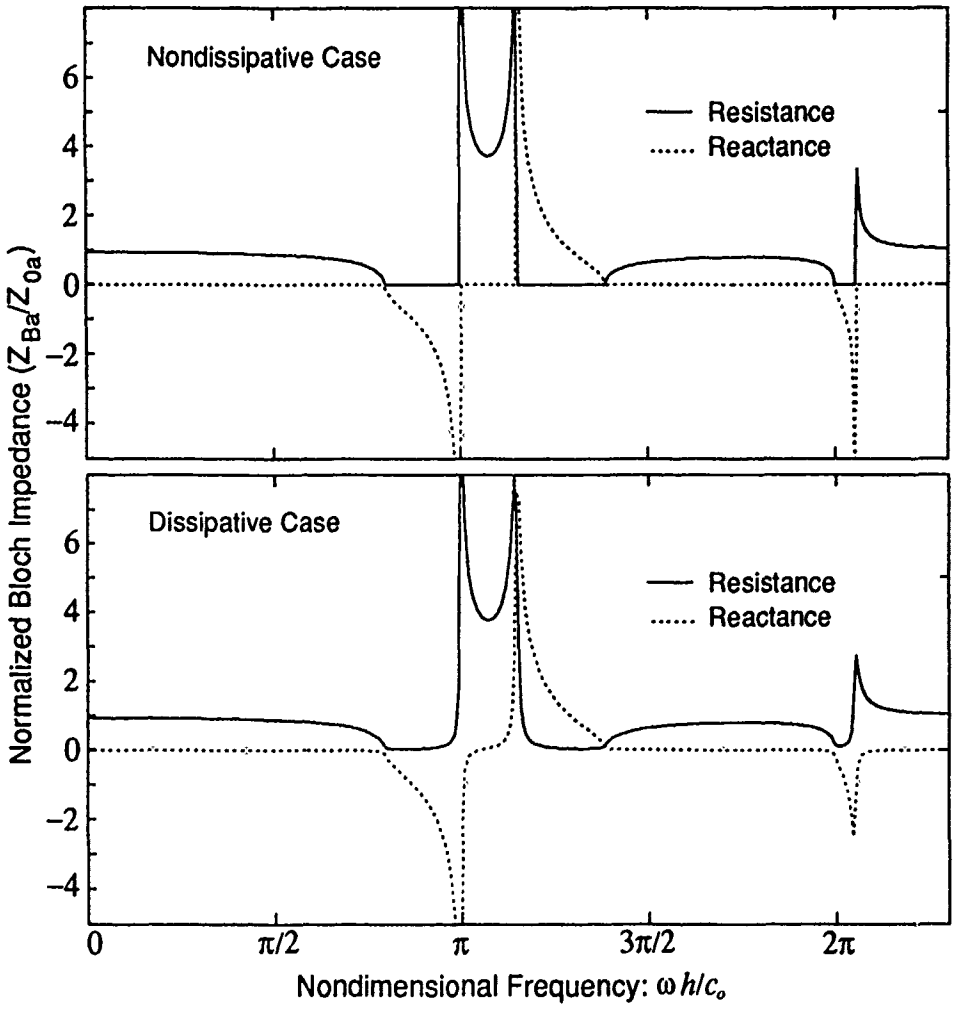

FIGURE 3.7

The Bloch acoustic impedance: the impedance of the periodic waveguide halfway between side branches. The impedance shown is normalized by the acoustic impedance of a uniform waveguide $Z_{0a} = \rho_0 c_0 / A_w$. In the nondissipative case the impedance is real for passband frequencies and imaginary for stopband frequencies.

AS-91-341

can be generalized to include the range $-h/2 < z < h/2$ by introducing phase corrections to the travelling wave components. The generalized impedance is

$$Z_a(z) = Z_{0a}\frac{f_0 e^{jkz} + g_0 e^{-jkz}}{f_0 e^{jkz} - g_0 e^{-jkz}}. \tag{3.31}$$

Solving for g_0/f_0 in terms of Z_{Ba} and Z_{0a} and substituting into Eq. 3.31 yields

$$Z_a(z) = Z_{0a}\frac{(Z_{Ba} + Z_{0a})e^{jkz} + (Z_{Ba} - Z_{0a})e^{-jkz}}{(Z_{Ba} + Z_{0a})e^{jkz} - (Z_{Ba} - Z_{0a})e^{-jkz}},$$

or

$$Z_a(z) = Z_{0a}\frac{Z_{Ba}\cos(kz) + jZ_{0a}\sin(kz)}{Z_{0a}\cos(kz) + jZ_{Ba}\sin(kz)}.$$

3.3 The Bloch Wave Parameter g/f and Bloch Wave Functions

In this section a Bloch wave parameter is identified that, in conjunction with the dispersion relation, completely specifies the Bloch wave function. As was stated in Sec. 2.4, the Bloch wave number q determines the global or cell-to-cell changes in the Bloch wave amplitude and phase. The Bloch wave parameter g/f, we will show, accounts for the wave function behavior *within* a single cell. It turns out that g/f bears a very simple relationship to the Bloch impedance and will therefore be expressed in terms of that quantity.

In Sec. 2.4.3 the Bloch wave function was expressed in the convolution form

$$p(z) = \psi(z) * \sum_{n=-\infty}^{+\infty} \delta(z - nh)e^{jnqh},$$

where $\psi(z)$ is the wave function in a single cell of the structure. Since a cell is any section of the structure with length equal to the periodicity of the structure, it is here defined to be centered on the waveguide section of the structure with side branches at each end. The wave function in this cell is simply a linear combination of the two linearly independent solutions of the wave equation: a forward propagating wave of amplitude f and a backward propagating wave of amplitude g:

$$\psi(z) = fe^{jkz} + ge^{-jkz} \qquad -h/2 < z < h/2.$$

As was pointed out in Sec. 2.4, the convolution of this cell wave function with the phase weighted lattice function simply places appropriately phased copies of $\psi(z)$ in each cell of the structure, as is illustrated in Fig. 3.8. An alternative expression of $\psi(z)$ is found by normalizing the f and g wave amplitudes by $f + g$, the total pressure at the cell center:

$$\psi(z) = \frac{fe^{jkz} + ge^{-jkz}}{f + g} = \frac{e^{jkz} + (g/f)e^{-jkz}}{1 + (g/f)} \qquad -h/2 < z < h/2. \tag{3.32}$$

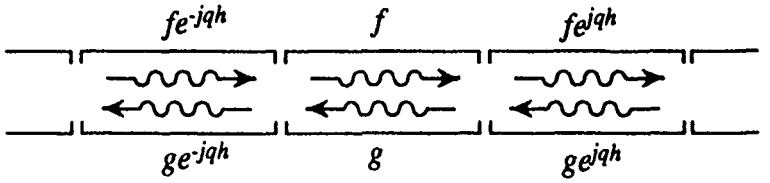

FIGURE 3.8
The forward travelling Bloch wave function is composed of a string of phase weighted copies of the cell wave function. The cell wave function is composed of a compound conventional wavefield: a wave of amplitude f (called an f wave) propagating in the direction of the Bloch wave and a wave of amplitude g (called a g wave) which propagates in the opposite direction.

AS-91-362

In this form it is evident that a coefficient multiplying the Bloch wave function for pressure (i.e., the Bloch wave pressure amplitude) is simply the pressure at the reference cell center, and that g/f is the only remaining unknown in the expression for the Bloch wave function. The acoustic impedance at the point midway between side branches, the Bloch acoustic impedance, is given by Eq. 3.30. In terms of the travelling wave components of the cell wave function (Eq. 3.32), the impedance is

$$Z_{Ba}A_w = \frac{p}{u} = \frac{f+g}{f/Z_0 - g/Z_0}, \tag{3.33}$$

which can be solved for g/f:

$$g/f = \frac{Z_{Ba} - Z_0/A_w}{Z_{Ba} + Z_0/A_w}. \tag{3.34}$$

The explicit form of g/f is found by introducing Eq. 3.30 into Eq. 3.34:

$$\begin{aligned} g/f = \Bigg\{ &\left[\frac{1}{2}(A_s/A_w)\tan(k_{sb}\hat{d})[\cos(kh) - 1] + \sin(kh)\right]^{1/2} \\ &- \left[\frac{1}{2}(A_s/A_w)\tan(k_{sb}\hat{d})[\cos(kh) + 1] + \sin(kh)\right]^{1/2}\Bigg\} \\ \div \Bigg\{ &\left[\frac{1}{2}(A_{sb}/A_w)\tan(k_s\hat{d})[\cos(kh) - 1] + \sin(kh)\right]^{1/2} \\ &+ \left[\frac{1}{2}(A_s/A_w)\tan(k_{sb}\hat{d})[\cos(kh) + 1] + \sin(kh)\right]^{1/2}\Bigg\}. \end{aligned} \tag{3.35}$$

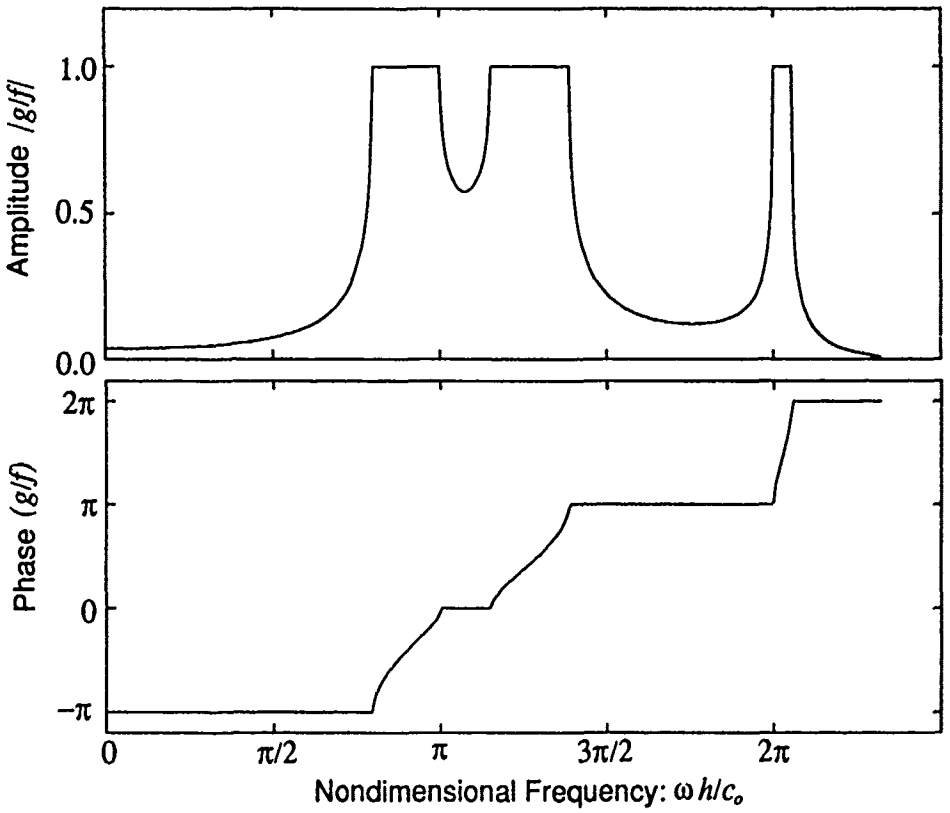

FIGURE 3.9

The amplitude and phase of the backward propagating component wave (the g wave) relative to the forward propagating component wave (the f wave). In the stopbands the backward propagating wave has an amplitude equal to the forward propagating component wave, indicating a longitudinal resonance condition.

AS-91-342

Figure 3.9 shows the amplitude and phase of g/f. The stopbands are clearly recognizable as the bands of frequencies in which the forward and backward travelling component waves of each cell have equal amplitudes, a longitudinal standing wave condition. It should be noted that this stopband condition ($|g| = |f|$) is consistent with the results of the impedance analysis: the impedance is reactive at stopband frequencies. The passbands are seen to be bands of frequencies in which the phase relationship between the component waves is fixed and equal to either 0 or π; the components are either perfectly in phase or perfectly out of phase. This type of phase relationship is consistent with the fact that the impedance is real at passband frequencies.

Stopband Bloch Wave Functions

As was noted above, the forward and backward travelling component waves of the stopband wave functions are equal in magnitude. The wave function is therefore simply a train of standing waves, the amplitudes of which vary exponentially with distance. For stopband frequencies, the periodic structure is essentially a sequence of coupled resonant tanks. Figure 3.10 shows stopband wave functions of the π stopband, the low frequency side of the side branch resonance stopband (in which $Re\{qh\} = 2\pi$), the high frequency side of the side branch resonance stopband (in which $Re\{qh\} = \pi$), and the 2π stopband. For each of the four frequencies, two plots of the wave function are shown. The upper of each pair of plots shows the wave function at $\omega t = 0$. The lower of each pair shows the wave function at $\omega t = 0, \pi/3, 2\pi/3, \pi, 4\pi/3$, and $5\pi/3$. Notice that the advance in phase from cell to cell is consistent with the associated values of $\mathrm{Re}\{qh\}$. Notice also the standing wave behavior characteristic of stopband Bloch wave functions.

Passband Bloch Wave Functions

Figure 3.11 shows some examples of passband Bloch wave functions. As might be expected, the wave functions are most unusual near the boundaries of the stopbands, where the dispersion is strongest. Note that particularly in the third and fourth waveform the pressure gradient is strongly discontinuous at the side branches, an occurrence which seems to disobey the law of conservation of mass. The side branch resonance, however, is zeroth order and is therefore a "breathing" mode which is alternately injecting and withdrawing mass from the port region, allowing the pressure wave function to become cusped. Note also that in spite of there being only a single temporal frequency present, there is obviously a rich spectrum of spatial frequencies. This phenomenon, which is characteristic of Bloch waves, is the basis of the travelling wave spectrum.

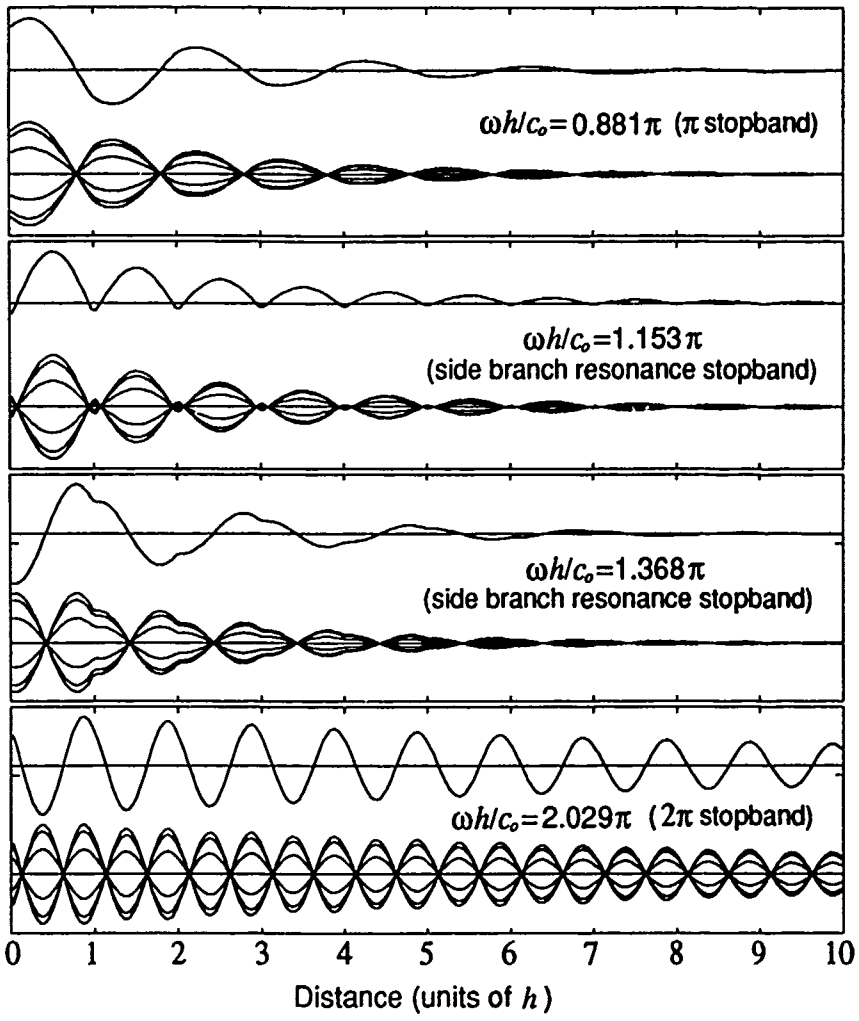

FIGURE 3.10

The Bloch wave function at four stopband frequencies. The second of each pair of plots shows the Bloch wave function at several instants of time, showing the longitudinal resonance condition typical of stopband Bloch wave functions.

AS-91-343

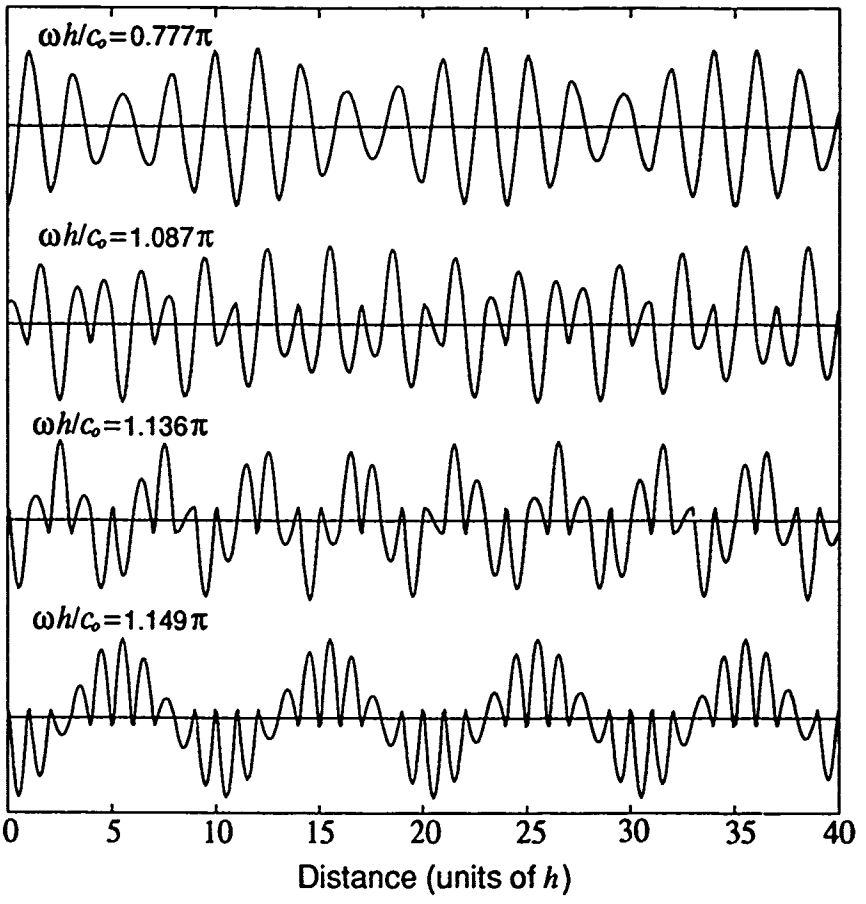

FIGURE 3.11
The Bloch wave function at four passband frequencies: $\omega h/c_0 = 0.777\pi$ (below the π stopband), 1.087π (above the π stopband), and 1.136π and 1.149π (both below the side branch resonance stopband).

AS-91-344

3.4 The Travelling Wave Spectrum and the Multivalued Dispersion Relation

In this section we concentrate on the travelling wave spectral representation of the Bloch wave function. We begin by finding an expression for the periodic modulation function $\Phi_q(z)$. We then evaluate the spectral amplitude integral (Eq. 2.52) for the spectral component amplitudes C_n. Finally, the physical significance of the multivalued nature of the dispersion relation is discussed.

3.4.1 The Travelling Wave Spectral Amplitudes

Equation 2.52, the spectral amplitude integral, can be evaluated if a closed form expression for $\Phi_q(z)$ can be found. Such an expression can be found by equating the standard expression and the convolution expression of the Bloch wave function. In the interval $-h/2 < z < h/2$ the standard expression is

$$p(z) = \Phi_q(z)e^{jqz},$$

and the convolution expression is

$$p(z) = \psi(z) = fe^{jkz} + ge^{-jkz}. \tag{3.36}$$

Equating these two forms of $p(z)$ yields an expression for the periodic modulation function:

$$\Phi_q(z) = fe^{j(k-q)z} + ge^{-j(k+q)z} \qquad -\frac{h}{2} < z < \frac{h}{2}. \tag{3.37}$$

The substitution of this expression for $\Phi_q(z)$ into the spectral amplitude integral (Eq. 2.52) results in the following expression for the spectral amplitudes

$$C_n = \int_{-1/2}^{1/2} \left[fe^{j(kh-qh-2\pi n)(z/h)} + ge^{-j(kh+qh+2\pi n)(z/h)} \right] d(z/h).$$

The integration is straightforward and we find

$$C_n = fj_0(n\pi + (q-k)h/2) + gj_0(n\pi + (q+k)h/2), \tag{3.38}$$

where $j_0(x)$ is the spherical Bessel function of order zero. The amplitudes of the travelling wave spectral components are shown in Fig. 3.12 for the six lowest spatial frequency components above and below the primary ($n = 0$) component.

An excellent example of the rich spectrum of spatial frequencies that can occur in a Bloch wave function is evident in the last function of Fig. 3.11. The primary

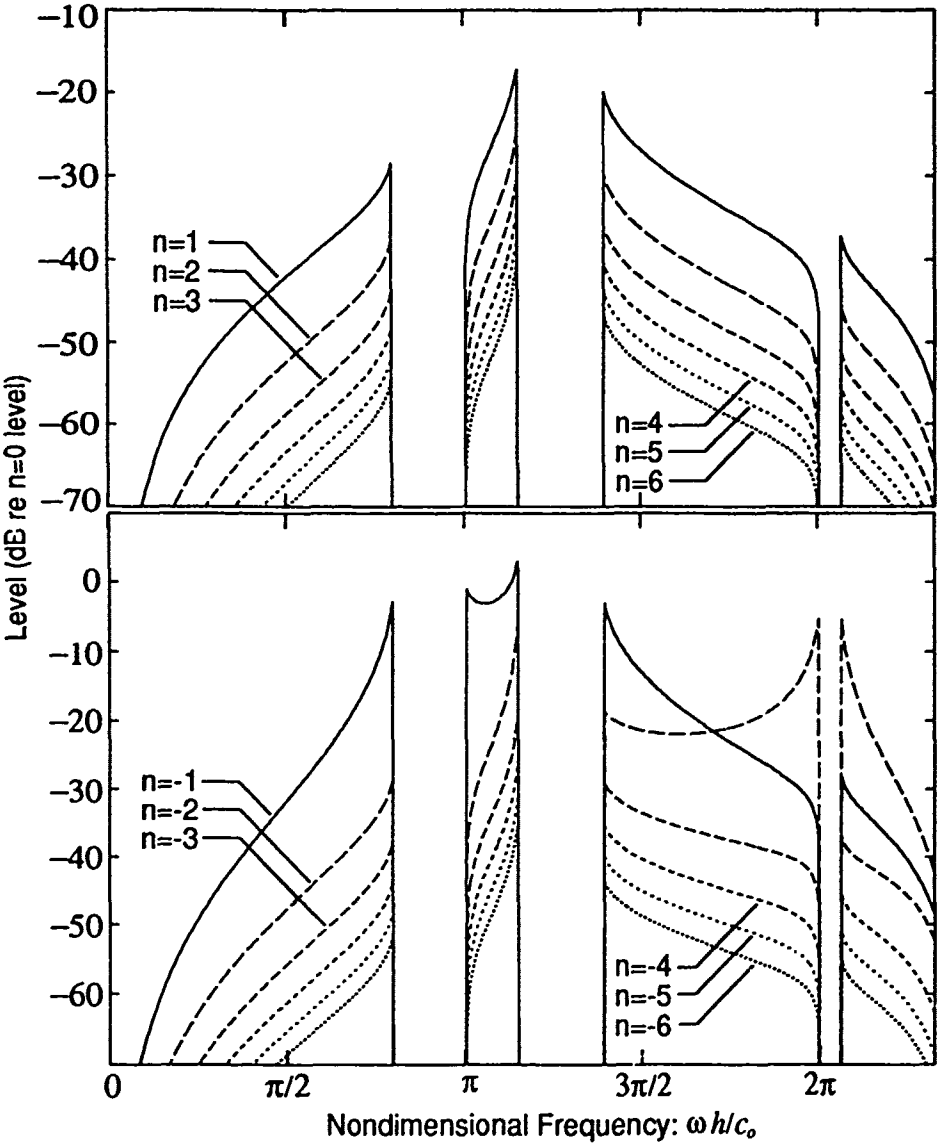

FIGURE 3.12

The amplitudes of the components of the travelling wave spectrum. The upper plot shows the spectral amplitudes for the $n > 0$ components and the lower shows those for the $n < 0$ components. The amplitudes are normalized to the value of the primary ($n = 0$) branch.

AS-91-345

spatial frequency (i.e., Bloch wave number) corresponds to a wavelength of about one structure period. It is obvious that in addition to higher spatial frequencies due to the sharply cusped waveform, there is a strong low spatial frequency component corresponding to a wavelength of about ten structure periods. Figure 3.12 shows that this low spatial frequency component, the $n = -1$ component, is expected to have an amplitude which is larger than the principal component amplitude near the side branch resonance stopband.

3.4.2 The Multivalued Dispersion Curve

The physical significance of the fact that the dispersion relation is multivalued becomes apparent when we note that the components of the travelling wave spectrum occur at the same interval along the spatial frequency axis as the repetitions of the dispersion relation. In Sec. 3.1 it was noted that the dispersion function is multivalued and repeats at intervals of $2\pi/h$ along q. An interval of $2\pi/h$ is the same interval as that between the spatial frequency components of the travelling wave spectrum. Figure 3.13 shows the complete dispersion function including all branches of the inverse cosine function. The primary branches associated with both forward and backward travelling Bloch waves are shown as unbroken lines, and all other branches are shown as dotted lines. This representation, the "periodic zone representation" which was referred to in Chap. 1, relates *each temporal frequency to an infinite set of spatial frequencies.* The infinite set of spatial frequencies are simply the spatial frequencies of the travelling wave spectra associated with both forward and backward propagating Bloch waves. A forward propagating Bloch wave of Bloch wave number q_0 is composed of travelling waves of spatial frequency $q_0 + 2\pi n/h$, where n is a positive or negative integer. The same Bloch wave propagating in the opposite direction is composed of travelling waves of spatial frequency $-q_0 + 2\pi n/h$. We see that the full dispersion curve is composed of two families of curves, one associated with forward propagating Bloch waves and the other with backward propagating Bloch waves. These families of curves are shown in Fig. 3.14 as unbroken and dotted lines, respectively. The family of curves associated with forward propagating Bloch waves is simply an infinite set of repeats of the primary branch curve associated with forward propagating Bloch waves, each occurring at intervals of $2\pi/h$ along the spatial frequency axis. Likewise, the family of curves associated with backward propagating Bloch waves is a set of copies of the primary branch curve associated with backward propagating Bloch waves, distributed at intervals of $2\pi/h$ along the spatial frequency axis. Each of these "copies" of the primary branch represents a spectral component; the n^{th} travelling wave component is represented by the copy shifted by $2\pi n/h$ along the spatial frequency axis. Figure 3.14 shows the travelling wave spectral components of one forward travelling and two backward travelling Bloch waves. Each horizontal row of circles connected by a dashed line represents the travelling wave spectral components of a Bloch wave. In the stopbands, the two families of curves are confluent;

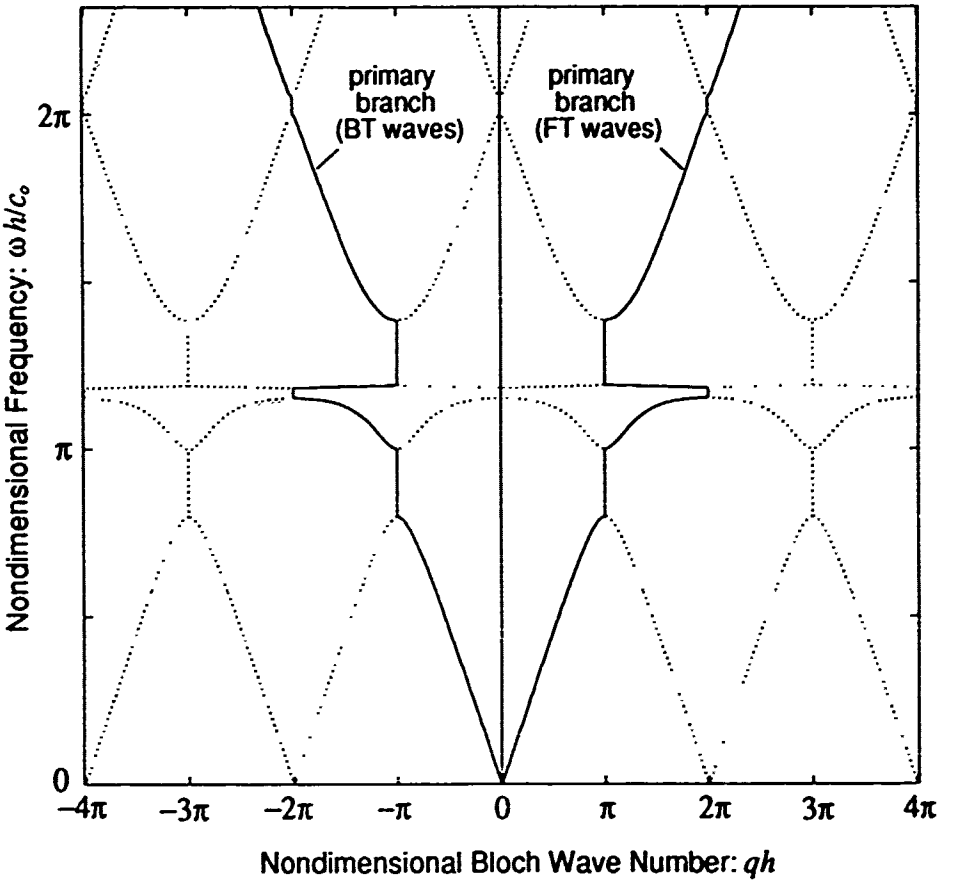

FIGURE 3.13

The complete dispersion curve including branches other than the primary branch. The primary branches associated with both forward and backward propagating Bloch waves are shown as unbroken lines, and the other branches are shown as dotted lines. This presentation of the Bloch wave dispersion is referred to as the "periodic zone" scheme.

AS-91-346

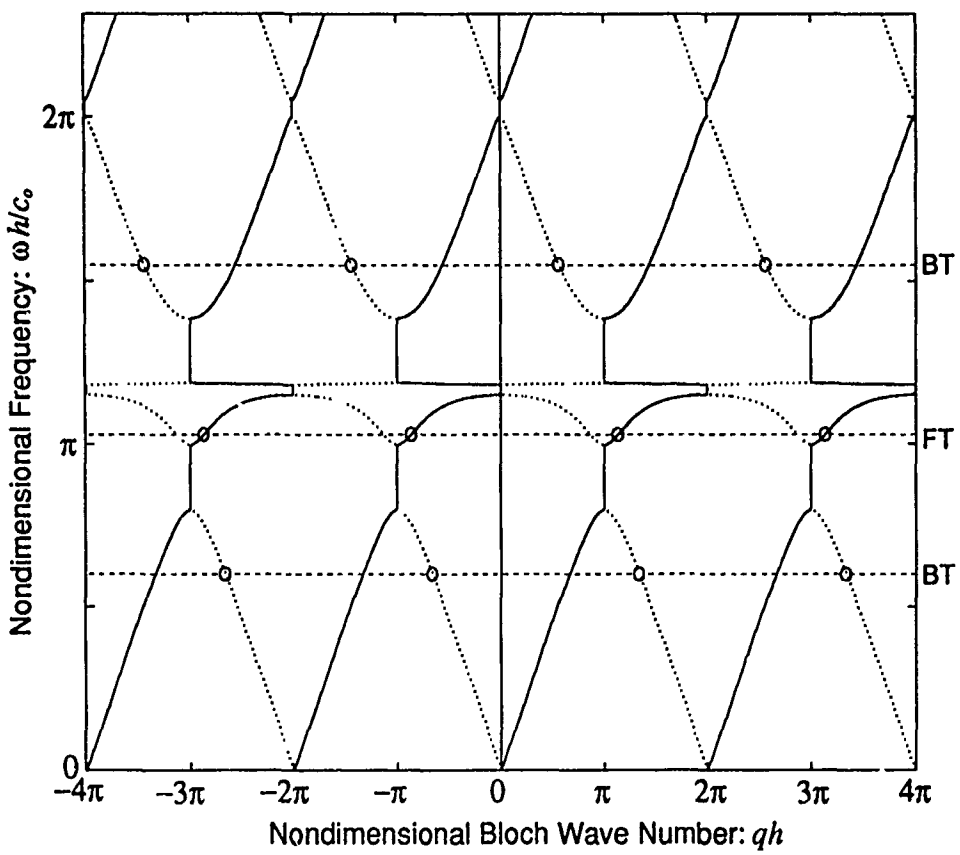

FIGURE 3.14

The complete dispersion curve showing the travelling wave spectra of several Bloch waves: a forward travelling (FT) Bloch wave of frequency $\omega h/c_0 = 1.043\pi$, and backward travelling (BT) Bloch waves of frequency $\omega h/c_0 = 0.574\pi$ and 1.530π. The branches of the dispersion relation associated with forward propagating Bloch waves are shown as unbroken lines and those associated with backward propagating Bloch waves are shown as dotted lines. Each horizontal row of circles connected by a dashed line represents the travelling wave spectral components of a Bloch wave.

AS-91-347

the forward and backward propagating waves are strongly coupled, as is implied by Fig. 3.9.

Notice that the complete dispersion relation contains no information about the amplitude or phase of the components of the travelling wave spectrum. Equation 3.38 is the source of that information. The interesting thing about the periodic zone representation of the travelling wave spectrum is that the graphical interpretation of the dispersion curve holds for all of the spatial frequency components. That is, the slope of the line from the origin to a point on the dispersion curve associated with a component of the travelling wave spectrum is the phase velocity associated with that component, and the slope of the dispersion curve at that point is the group velocity associated with that component. This graphical interpretation makes obvious two points of interest. First, each travelling wave component of a Bloch wave has the same group velocity, and this group velocity is directed in the direction of propagation of the Bloch wave. Second, each travelling wave component of a Bloch wave has a *different* phase velocity, and this phase velocity can be *directed opposite the group velocity*! This peculiarity is the reason periodic structures are sometimes referred to as "backward wave structures" (Ramo, Whinnery, and Van Duzer, 1965).

3.5 Effects of Truncation of the Structure: Bloch Wave Reflection and Transmission

Up to this point, all of the theoretical findings have been based upon the assumption that the periodic waveguide is of infinite length. The whole of Chap. 2 is devoted to showing the conditions under which we can expect to find Bloch wave solutions. The first of these conditions is that the system exhibits a translational invariance, which can occur only in the case of an infinite structure. This naturally raises the question as to the validity of the analysis as it applies to a physically realizable system.

We consider several situations involving non-infinite periodic waveguides. We begin with a semi-infinite periodic waveguide that is connected to a semi-infinite uniform waveguide. The uniform waveguide may be considered the termination for the periodic waveguide. The purpose of the analysis is to illustrate the way Bloch waves are able to satisfy interface conditions. We then consider the more general case of Bloch waves in a semi-infinite periodic waveguide incident upon an arbitrary terminating impedance. Next we treat the reverse case, that in which conventional waves in a uniform waveguide are incident upon a semi-infinite periodic waveguide. Various reflection and transmission coefficients are derived. Given the above findings, we conclude with a discussion of a guided wave system which includes a *finite* section of periodic waveguide.

3.5.1 A Periodic Waveguide Terminated by a Uniform Waveguide

We begin by considering a compound Bloch wavefield, a field composed of both forward and backward travelling Bloch waves. The convolution representation of the Bloch wave function shows the Bloch waves to be composed of a compound conventional wavefield which repeats (with shifted phase) at intervals of h. That is, the forward travelling Bloch wave consists of both forward and backward travelling component waves which are both advanced in phase by the factor e^{jqh} in propagating from one cell to the neighboring cell in the positive z direction. The amplitudes of the forward and backward travelling component waves are f^+ and g^+, with the ratio g^+/f^+ determined by Eq. 3.35. The backward travelling Bloch wave likewise consists

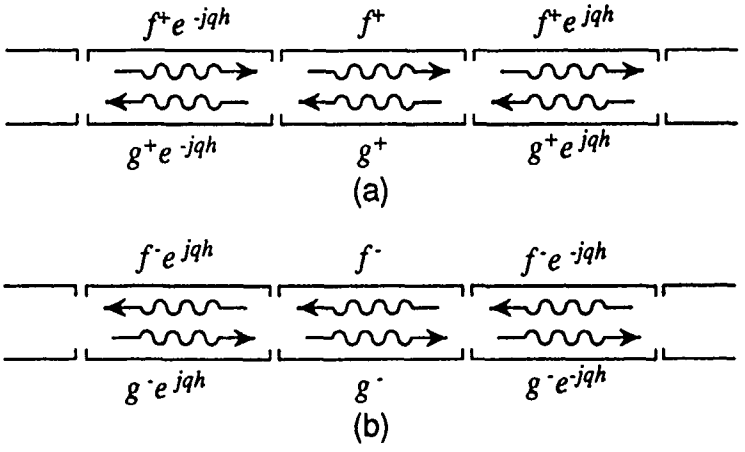

FIGURE 3.15
The component waves of (a) forward and (b) backward propagating Bloch waves. The values of the component wave pressure at the center of each cell are shown. The center cell is the reference cell.

AS-91-363

of a compound wavefield, but the phase advances in the negative z direction. The amplitudes of the component waves associated with the backward travelling Bloch wave are f^- and g^-, where f^- is the component propagating in the direction of the Bloch wave. Again, the ratio g^-/f^- is determined by Eq. 3.35. The forward and backward travelling Bloch waves are illustrated in Fig. 3.15.

We now consider the situation shown in Fig. 3.16(a), wherein both forward and backward travelling Bloch waves occur simultaneously in the same guiding structure. A reference cell is chosen to define the component wavefields such that in the center of the reference cell $p = f^+ + g^+ + f^- + g^-$ (i.e., the z origin is at the center of the reference cell). If the amplitude and phase of the backward travelling Bloch wave are

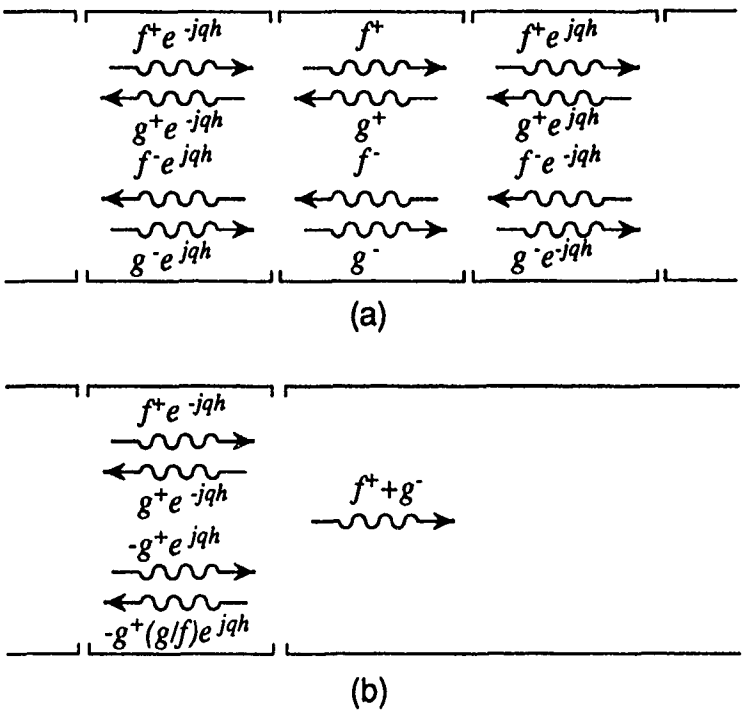

FIGURE 3.16
(a) Forward and backward propagating Bloch waves occurring simultaneously in the same structure with the amplitude/phase relationship $f^- = -g^+$. (b) The same situation as in (a), but with the periodic structure to the right of the center of the reference cell replaced by an infinite uniform waveguide.

AS-91-348

chosen so that $f^- = -g^+$, then *the g wave component of the forward travelling Bloch wave and the f wave component of the backward travelling Bloch wave cancel in the reference cell.* The wavefield in the reference cell is therefore purely progressive, as shown in Fig. 3.16(b). We can therefore replace the periodic structure to the right of the center of the reference cell with a semi-infinite, uniform waveguide with no disruption of the wavefield to the left of (and inside of) the reference cell. Conversely, it can be stated that the effect of replacing the periodic structure at some point with a semi-infinite, uniform waveguide is the generation of a backward travelling Bloch wave with amplitude and phase defined by $f^- = -g^+$.

3.5.2 The General Impedance Termination

While the arguments of the last section demonstrate qualitatively the way compound Bloch waves can satisfy the conditions at an interface, a quantitative analysis leads to much more general results. We consider the case of a periodic waveguide terminated by the acoustic impedance Z_{ta} at the center of the reference cell (at $z = 0$). As in the last section, f^+ and f^- are, respectively, the amplitudes of the f waves of the forward and backward propagating Bloch waves in the periodic waveguide which occupies the half space $z < 0$. We will call the pressure on the $z > 0$ side of the interface f_t. If no waves are incident on the interface from $z > 0$ (the field in the terminating medium is progressive), f_t is simply the transmitted pressure wave amplitude.

As usual, the continuity conditions must be met at the interface. Continuity of pressure requires

$$(f^+ + g^-) + (f^- + g^+) = f_t. \tag{3.39}$$

Since the relationship between the f and g waves is given by Eq. 3.35 for *any* Bloch wave

$$\frac{g}{f} = \frac{g^+}{f^+} = \frac{g^-}{f^-}, \tag{3.40}$$

we can write Eq. 3.39 as

$$(f^+ + f^-)(1 + g/f) = f_t. \tag{3.41}$$

Likewise, continuity of particle velocity at the interface requires

$$\frac{(f^+ + g^-)}{Z_{0a}} - \frac{(f^- + g^+)}{Z_{0a}} = \frac{f_t}{Z_{ta}}, \tag{3.42}$$

or

$$(f^+ - f^-)(1 - g/f) = f_t \frac{Z_{0a}}{Z_{ta}}. \tag{3.43}$$

The combination of Eqs. 3.41 and 3.43 results in a Bloch reflection coefficient,

$$R_B = \frac{f^- + g^-}{f^+ + g^+} = \frac{Z_{ta}(1 - g/f) - Z_{0a}(1 + g/f)}{Z_{ta}(1 - g/f) + Z_{0a}(1 + g/f)}$$

$$= \frac{Z_{ta} - Z_{Ba}}{Z_{ta} + Z_{Ba}}, \tag{3.44}$$

where we have chosen $f + g$, the pressure amplitude at the cell center, to represent the amplitude of the Bloch wave. Equation 3.44 is simply the standard definition of the reflection coefficient for a conventional wave in a medium of acoustic impedance Z_{Ba} incident on an interface between that medium and one of acoustic impedance Z_{ta}.

If the field in the terminating medium ($z > 0$) is progressive, then we can define a transmission coefficient by $T = f_t/(f^+ + g^+)$. Equations 3.41 and 3.43 can be combined to result in

$$T = \frac{f_t}{f^+ + g^+} = \frac{2Z_{ta}}{Z_{ta} + Z_{Ba}}. \tag{3.45}$$

This expression is identical to the corresponding expression for conventional waves.

Three Interesting Cases

The range of possible values of Z_{ta} includes three values of particular interest. In the case $Z_{ta} = Z_{0a}$, which is the case of the periodic structure terminated by a semi-infinite uniform waveguide, the transmission coefficient (Eq. 3.45) reduces to

$$T = 1 - g/f,$$

and the Bloch reflection coefficient (Eq. 3.44) becomes

$$R_B = -g/f, \tag{3.46}$$

or

$$f^- = -f^+\frac{g}{f} = -g^+, \tag{3.47}$$

which confirms the earlier result. In such a case the plot of $|R_B|$ is identical to the plot of $|g/f|$, shown in Fig. 3.9. In the case $Z_{ta} \to \infty$, the Bloch reflection coefficient (Eq. 3.44) reduces to

$$R_B = 1,$$

or

$$f^- = f^+, \tag{3.48}$$

which is what is expected for pressure wave reflection from a rigid termination. The form of R_B in Eq. 3.44 makes evident another case of interest, that in which $Z_{ta} = Z_{Ba}$, for which

$$R_B = 0$$

and

$$T = 1.$$

The reflected Bloch wave amplitude is zero; the incident Bloch wave energy is 100% transmitted.

3.5.3 A Uniform Waveguide Terminated into a Periodic Waveguide

We now consider the problem of a uniform waveguide of acoustic impedance Z_{ia} terminated by a periodic waveguide. The amplitudes of the incident and reflected conventional waves are f^+ and f^-, respectively, and the amplitude of the transmitted Bloch wave is $f_t + g_t$. Continuity of acoustic pressure at the interface requires

$$f^+ + f^- = f_t(1 + g/f), \tag{3.49}$$

and continuity of velocity requires

$$\frac{f^+}{Z_{ia}} - \frac{f^-}{Z_{ia}} = \frac{f_t}{Z_{oa}}(1 - g/f). \tag{3.50}$$

Equations 3.49 and 3.50 can be combined to yield

$$R = \frac{f^-}{f^+} = \frac{Z_{Ba} - Z_{ia}}{Z_{Ba} + Z_{ia}}.$$

Again, the reflection coefficient is identical to that describing the reflection of conventional waves. Note that when $Z_{ia} = Z_{Ba}$ (the impedance matched case) the reflected wave amplitude is zero.

Equations 3.49 and 3.50 can also be combined to yield the transmission coefficient (actually a *conversion* coefficient) for the transmitted Bloch wave

$$T_B = \frac{f_t + g_t}{f^+} = 2\frac{Z_{Ba}}{Z_{ia} + Z_{Ba}}. \tag{3.51}$$

Again, the result is identical to the conventional wave result. Note that when $Z_{ia} = Z_{0a}$ we get $T_B = 1 + g/f$ and $R = g/f$. In other words, $f_t = f^+$ and $f^- = (g/f)f^+$; the field in the conventional waveguide has the same f wave/ g wave makeup as a Bloch wave.

3.5.4 The Finite Periodic Waveguide

We are now in a position to deduce what sort of wavefields occur in a *finite* periodic waveguide. It has been shown that a conventional wave in a uniform waveguide incident upon a periodic waveguide generates a reflected conventional wave and a transmitted Bloch wave. It has also been shown that a Bloch wave incident upon a uniform waveguide generates a reflected Bloch wave and a transmitted conventional wave. From these findings we can arrive at the combination of Bloch and conventional wavefields that occur in a guided wave system that includes a finite section of periodic waveguide.

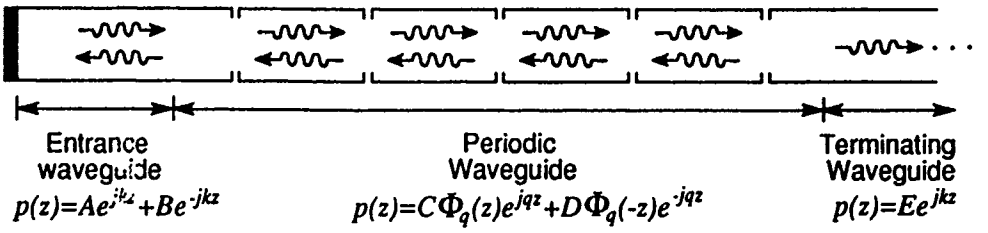

FIGURE 3.17
The Bloch and conventional wavefields in a guided wave system which includes a section of periodic waveguide.

AS-91-349

An example of a guided wave system that incorporates a section of periodic waveguide is shown in Fig. 3.17. The system is composed of a finite section of uniform waveguide (the entrance waveguide), a finite section of periodic waveguide, and a semi-infinite section of uniform waveguide (the terminating waveguide). A piston source in the entrance waveguide generates a forward travelling conventional wave which is incident upon the section of periodic waveguide. This incident wave is both reflected, resulting in a backward travelling conventional wave in the entrance waveguide, and transmitted, resulting in a forward travelling Bloch wave in the periodic waveguide. When the Bloch wave arrives at the terminating waveguide, it is likewise partially reflected, resulting in a backward travelling Bloch wave, and partially transmitted, resulting in a forward travelling conventional wave in the terminating waveguide.

Conclusion

The value of the analysis in this section is that it demonstrates that Bloch waves are *not* restricted to infinite periodic media. In fact, Bloch waves are *the* waves which occur in periodic media. A Bloch wave incident upon a termination *does not* generate a clutter of waves which then scatter in some complicated, disorganized manner from the side branches. Instead, a very specific, orderly backscattered field is generated: a backward propagating Bloch wave. Apparently the Bloch wave is not as "fragile" as one might be inclined to believe. Truncation of the periodic medium does *not* disrupt some sort of precarious balance, but simply causes a reflected Bloch wave to be generated.

To conclude, it appears that a periodic medium is very much like a conventional wave medium with a characteristic acoustic impedance equal to the Bloch acoustic impedance. The finite periodic medium problem discussed above is very similar to the classic three-medium problem. The three-medium problem is that in which a section of a medium of one characteristic impedance is sandwiched between media of another characteristic impedance. The solution shown above is essentially that of the three-medium problem. The difference is that, in our case, the waves in the middle medium are Bloch waves.

4. BLOCH WAVE DISPERSION MEASUREMENT

In this chapter an experimental verification of the dispersion relation derived in Sec. 3.1 is described. The measurement is made by spatially sampling the acoustic pressure in a compound Bloch wavefield. The reasoning behind this choice of measurement scheme and some of the inherent limitations are discussed. The set of design criteria that was developed to aid in the design of the waveguide is presented and the construction of the waveguide is described. The experimental setup is shown and the method of acquisition and processing of the data is described. Finally, the experimental results are compared to the theoretical predictions of Chap. 3.

4.1 The Experimental Paradigm

Here we describe the fundamental framework of the dispersion measurement. We begin by presenting the reasoning behind choosing to work with a compound as opposed to a progressive Bloch wavefield. The effect of spatially sampling a compound Bloch wavefield and the use of a linear regression to filter out some compound wavefield effects are discussed. Finally, we present the method of extracting the values of the Bloch wave number from field measurement data and some of the limitations associated with the measurement scheme.

4.1.1 Progressive versus Compound Bloch Waves

In Sec. 3.5 it was found that, depending upon the impedance of the termination, a truncated periodic waveguide can have either progressive or compound Bloch wave solutions. If the waveguide is terminated with the Bloch impedance, the resultant field is that of a progressive Bloch wave. Any other termination causes the incident Bloch wave to be reflected to some degree, resulting in a compound Bloch wavefield. In terms of a dispersion measurement, there are advantages and disadvantages to an experiment based on either a progressive or a compound Bloch wavefield.

In the case of a periodic waveguide terminated with the Bloch impedance, the resulting progressive Bloch wavefield makes the measurement of the dispersion trivial. If the pressure field is measured at two points an integral number of structure periods

apart (at $z = z_1$ and $z = z_2 = z_1 + nh$), then Eq. 2.46 relates the fields at the two points:

$$p(z_2) = p(z_1 + nh) = \left[e^{jqh}\right]^n p(z_1). \tag{4.1}$$

The dispersion is then found simply by solving for q in terms of the two field measurements:

$$q = \frac{1}{jnh} \ln \left[\frac{p(z_2)}{p(z_1)}\right]. \tag{4.2}$$

The major problem with an experiment based upon this scheme is the realization of the termination condition. Figure 3.7 shows that the Bloch impedance is a strongly frequency dependent function that would be enormously difficult to synthesize for anything more than a very limited range of frequencies. Another problem is that the precision of the measurement is strongly dependent on the degree to which the reflection from the termination is indeed zero. Even a very small reflection can cause sizeable perturbations in the otherwise progressive Bloch wavefield and ruin the precision of the measurement.

The termination of the periodic waveguide with a frequency independent termination essentially reverses the problems discussed above. A constant terminating impedance is very easily realizable, but the resultant compound Bloch wavefield complicates the measurement of the dispersion. The dispersion can still be derived from the measurement of the field at just two points, but such a scheme would involve an assumed knowledge of the relative amplitude and phase of the reflected Bloch wave. That is, the precision of the measurement depends upon exactly how well the termination is characterized and how well the theory describes Bloch wave reflection. A less "fragile" method is to sample the compound Bloch wavefield at a *number* of points. As will be shown in the following section, spatial sampling allows the dispersion information to be extracted from a compound Bloch wavefield without assuming anything about the reflected Bloch wave amplitude. This method also yields additional information about the field, such as the amplitude of the Bloch wave reflected from the termination.

A simple, frequency independent termination can be constructed by loading a section of uniform waveguide with a gently tapered fiberglass wedge. If the wedge is carefully tapered, it will be very nearly anechoic. The resultant input impedance of the section of waveguide is therefore that of a semi-infinite uniform waveguide, which is frequency independent.

4.1.2 Spatial Sampling of a Compound Bloch Wavefield

As was noted in Sec. 2.3, the result of spatially sampling a Bloch wave at intervals of the periodicity of the structure is indistinguishable from the result of sampling the

conventional travelling wave Ce^{jqz} at the same intervals. The n^{th} sample in a spatial series generated by sampling a forward travelling Bloch wave at the points $z = nh$ (where n is an integer) is

$$\begin{aligned} p_n &= \int_{-\infty}^{+\infty} \Phi_q(z) e^{jqz} \delta(z - nh) dz \\ &= \Phi_q(nh) e^{jnqh} \\ &= \Phi_q(0) e^{jnqh}. \end{aligned} \tag{4.3}$$

The same sampling performed on the conventional wave yields

$$\begin{aligned} p_n &= \int_{-\infty}^{+\infty} Ce^{jqz} \delta(z - nh) dz \\ &= Ce^{jnqh}. \end{aligned} \tag{4.4}$$

Comparison of Eqs. 4.3 and 4.4 shows that the travelling wave $p(z) = \Phi_q(0)e^{jqz}$ is, when sampled, indistinguishable from the sampled Bloch wave. The compound conventional wavefield equivalent of the compound Bloch wavefield for a terminated periodic waveguide is

$$p(z) = \Phi_q(0) \left[e^{jqz} + R_B e^{-jqz} \right], \tag{4.5}$$

where R_B is the Bloch wave reflection coefficient associated with the termination.

4.1.3 The Linear Regression as a Backward Travelling Wave Filter

One effect seen in compound conventional wavefields, and therefore in sampled compound Bloch wavefields as well, is spatial beating. The presence of the backward propagating wave causes the amplitude and phase of the field to deviate from that of a progressive wave. Whereas the phase of a progressive field increases linearly with distance in the direction of propagation, the backward travelling wave causes the phase of the field to oscillate periodically *about* a linear increase, as shown in Fig. 4.1. Likewise, the exponential decay associated with the amplitude of a progressive field takes on periodic oscillations *about* the exponential decay in the presence of a counter-propagating wave. The point of importance here is that although the amplitude and phase are different from those of a progressive field, the difference is *periodic*. The *net* amplitude decay is still exponential and the *net* phase advance is still linear. Therefore, *over a large enough number of cycles of the periodic perturbation the amplitude and phase average out to essentially exponential decay and linear increase, respectively.*

A very effective method of extracting the linear component of a series (such as the sampled phase series) is by using a linear regression.[1] A linear regression performed

[1]The linear regression is simply a first degree polynomial fit to a series. The fit is made in a least-square sense.

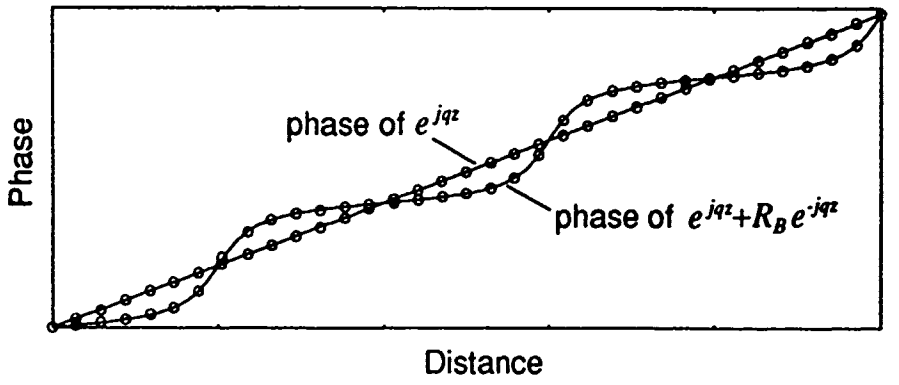

FIGURE 4.1
The phase of the travelling wave e^{jqz} alone and in the presence of a counter-propagating wave. The phase of the purely progressive field increases linearly with distance, and develops oscillations *about* the linear increase with the introduction of the reflected wave. The spatial frequency of the oscillations in both the amplitude and the phase series is $2q$.

AS-91-350

on the sampled phase series results in the *net slope* of the series; the oscillations due to the backward travelling wave are effectively filtered out. The net slope is the phase advance per unit distance of the forward travelling wave, which is the real part of the Bloch wave number. Likewise, a linear regression performed on the natural logarithm of the amplitude series effectively cancels the backward travelling wave's effect, and the resultant slope is the imaginary part of the Bloch wave number.

4.1.4 The Sampled Acoustic Pressure Series

Consider the case wherein we make $N+1$ measurements of the acoustic pressure field at spatial intervals of integral multiples of h. The measured pressures will be called p_0, p_1,...p_N, and the associated sample locations will be called z_0, z_1,...z_N. In polar form, these complex pressures are

$$p_i = |p_i|e^{j\vartheta_i} \qquad i = 0, 1, ...N. \tag{4.6}$$

We normalize the measurements by p_0, which will be referred to as the reference pressure, to get the relative pressure

$$\begin{aligned}\hat{p}_i &= \frac{p_i}{p_0} \\ &= \frac{|p_i|}{|p_0|} e^{j(\theta_i - \theta_0)} \\ &= |\hat{p}_i| e^{j\hat{\theta}_i} \qquad i = 0, 1, 2, ...N. \end{aligned} \tag{4.7}$$

Likewise the relative distance is defined as

$$\hat{z}_i = z_i - z_0 \qquad i = 0, 1, 2, ...N. \tag{4.8}$$

It is evident that $|\hat{p}_i|$ is the decay in amplitude and $\hat{\theta}_i$ the advance in phase of the wavefield over the distance $\hat{z}_i$. With the measured pressure so defined, the measured value of the real and imaginary parts of the Bloch wave number are

$$\begin{aligned} \mathrm{Re}\{q\} &\rightarrow \text{ linear regression of } \hat{\theta}_i \text{ against } \hat{z}_i \\ \mathrm{Im}\{q\} &\rightarrow \text{ linear regression of } \ln|\hat{p}_i| \text{ against } \hat{z}_i. \end{aligned} \tag{4.9}$$

It should be noted that this technique of extracting the real and imaginary components of the Bloch wave number from the spatially sampled field will work for *any* termination. Since the amplitude of the oscillations in the amplitude and phase of the field is dependent upon the amplitude of the counter-propagating Bloch wave, the results will simply be more precise for smaller reflected wave amplitudes. Another distinct advantage to this technique is that if we use one microphone for all the reference pressure measurements and another for all the downstream pressure measurements, then *no calibration of the microphones is necessary.* Any mismatch in the amplitude or phase response of the microphones will simply show up as a non-zero y-intercept in a plot of amplitude or phase against distance, and have no effect on the linear regression.

4.1.5 Limitations of the Measurement

The fact that we are counting on averaging out the effects of the backward travelling Bloch wave to make the measurement leads to the limitations associated with the measurement technique. The condition for the effective averaging out of the oscillations in the amplitude and phase is that we have a *sufficiently large number of oscillations over which to average.* Since the oscillations occur on the scale of a wavelength of the Bloch waves that compose the field, the limitation *appears* to be a low frequency limitation. It seems that we can ensure the effectiveness of the averaging technique simply by placing a restriction on the measurement frequencies: they must be high enough that several cycles of the Bloch waves occur over the spatial measurement interval. Such a restriction, however, would *not* be sufficient due to the fact that we are spatially *sampling* the field and the measurement is

therefore subject to the effects of spatial aliasing. Even in the case where we are operating at a frequency that is sufficiently high to ensure a large number of cycles of the oscillations, the number of oscillations in the *sampled* field may be arbitrarily small. Figure 4.2(b) shows an example of how the apparent frequency of a sampled field can be the low frequency alias of a higher frequency. In the sampled case, then, it is not simply low spatial frequencies that we must be cautious of, but *apparently* low spatial frequencies, those that have a low frequency alias. In the case of a spatial sampling interval of Δz_s, the Nyquist spatial frequency is $k_N = \pi/\Delta z_s$. The set of spatial frequencies that have k as an alias spatial frequency is $2nk_N \pm k$, where n is a positive integer. The spatial frequency of the oscillations in the amplitude and phase series is $2q$, so we expect measurement inaccuracy when

$$q \simeq nk_N. \tag{4.10}$$

Implicit in the measurement technique outlined above is yet another frequency restriction which should be acknowledged. The measurements are made a distance $h/2$ from the side branches, and are assumed to be a measurement of the zeroth order field alone. The evanescent modes generated at the side branches all have pressure maxima at $y = b$, where the measurements are made. The degree to which the measurements are representative of the zeroth order field is the degree to which the evanescent modes have decayed over the distance $h/2$. The requirement regarding the decay of the evanescent modes made in the development of the theory was that they decay significantly over a distance of h, so the validity of the measurement imposes a more severe frequency constraint than the validity of the theory, namely

$$\omega \ll (2c_0/h)\left[(\pi h/2b)^2 - 1\right]^{1/2}. \tag{4.11}$$

4.2 Design and Construction of the Periodic Waveguide

The design of the periodic waveguide was determined by two fundamental considerations: the dispersion must be measureable and the waveguide construction must be practical. In this section we present the set of design criteria that guided the choice of the waveguide dimensions. Details of the waveguide construction and the microphone positioning are shown.

4.2.1 Waveguide Design Criteria

In Sec. 3.1, several nondimensional parameters and their influence on the dispersion relation are identified. Using this information we derive a set of design criteria

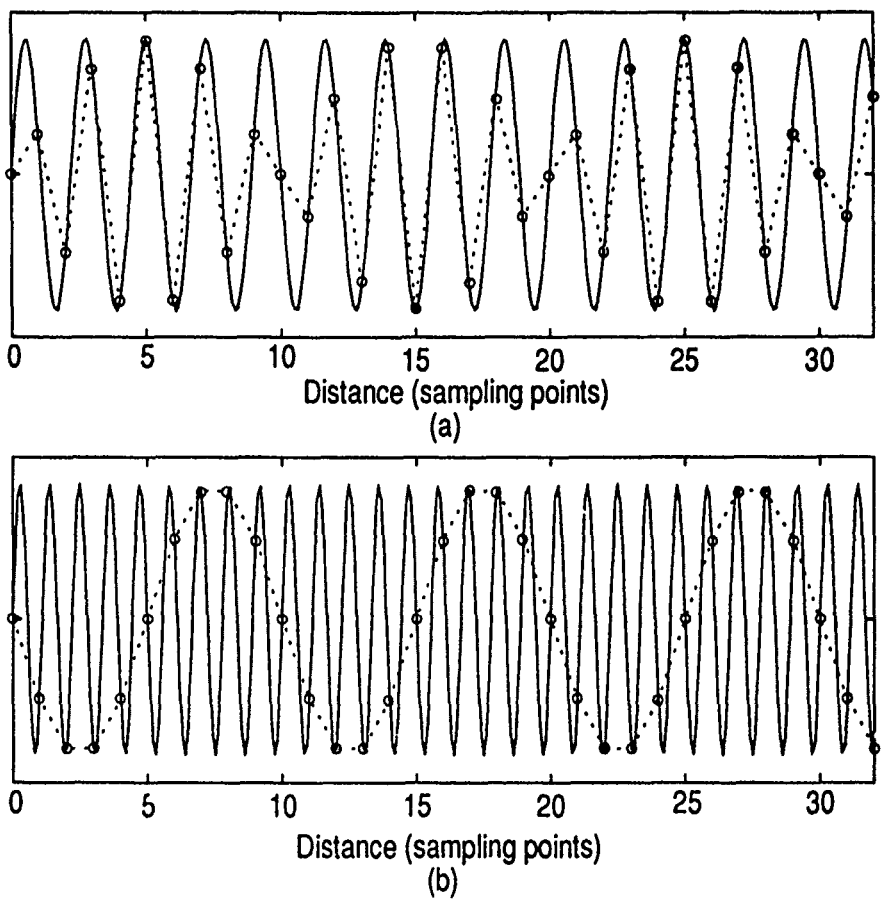

FIGURE 4.2
Sampling of an oscillatory waveform. In (a) the spatial frequency of the field is less than the Nyquist spatial frequency (k_N), so the sampled series is not aliased, but is greater than $k_N/2$, which is the condition for the beating effect seen. In (b) the spatial frequency is greater than k_N and the "folding down" in frequency characteristic of aliasing is seen.

AS-91-351

to aid in the specification of the dimensions of the waveguide. The criteria are as follows:

- The two species of stopbands should not overlap. The n^{th} Bragg stopband occurs in the vicinity of $kh = n\pi$, and the m^{th} side branch resonance stopband occurs in the vicinity of $k\hat{d} = (m+1/2)\pi$. The two coincide if $\hat{d}/h \simeq (m+1/2)/n$, a condition which we wish to avoid as we would like to independently verify the existence of and investigate the behavior of both stopband species.

- Both species of stopbands should occur at frequencies for which the analysis is valid. Again, this is to ensure a valid verification of both Bragg and side branch resonance stopbands.

- The dispersion should be strong enough to be easily measurable. There should be frequencies for which the characteristic length associated with dispersion

$$L_d = \frac{2\pi}{\mathrm{Re}\{q(2\omega)\} - 2\mathrm{Re}\{q(\omega)\}} \tag{4.12}$$

  is less than the overall length of the structure. This requirement assures us of easily measurable dispersion.

- The stopband attenuation should be relatively strong. There should be frequencies at which the characteristic length associated with attenuation

$$L_a = 1/\mathrm{Im}\{q\}$$

  is less than the overall structure length. The reasoning here is the same as for the strong dispersion criterion above.

- Thermoviscous losses should be minimized. This requirement keeps the band structure of the dispersion relation from being swamped by the attenuation and dispersion that results from acoustic boundary layer effects.

In Sec. 3.1 it was shown that the dimensionless parameters $\hat{d}/h$ and S/S_0 determine the location of the side branch resonance stopbands and the overall strength of the stopbands, respectively. It was likewise found that h/R_{Hw} and $\hat{d}/R_{Hs}$ are related to thermoviscous losses. The effects associated with these dimensionless parameters, the criteria listed above, and construction practicality considerations led to the following choices for the structure dimensions:

structure period: h=.1 m
side branch depth: d=.0381 m (1-1/2″)
side branch width: l=.0095 m (3/8″)
waveguide height: b=.0254 m (1″)
waveguide width: a=.0381 m (1-1/2″).

The length of the periodic waveguide is 50 cycles (5 meters), or 6 meters including the 1 meter anechoic termination. These dimensions result in the values of the nondimensional parameters reported in Sec. 3.1:

$$\begin{aligned} \hat{d}/h &= .421 \\ A_s/A_w &= 3/8 \\ h/R_{Hw} &= 6.562 \\ \hat{d}/R_{Hs} &= 5.531. \end{aligned}$$

According to Eq. 2.31, the frequency range over which Eq. 2.30 (the expression for the dissipative wave number) is valid is 40 mHz $\ll f \ll$ 400 kHz. The various frequency restrictions that were imposed to ensure the validity of the zeroth order approximation are as follows:

$$\begin{aligned} &\text{Eq. 2.24:} \quad f \ll 6,770 \text{ Hz} \\ &\text{Eq. 2.25:} \quad f \ll 18,100 \text{ Hz} \\ &\text{Eq. 2.26:} \quad f \ll 4,490 \text{ Hz} \\ &\text{Eq. 4.11:} \quad f \ll 6,700 \text{ Hz} . \end{aligned}$$

4.2.2 Waveguide Construction Details

The waveguide is a rectangular duct with one wall removed and replaced by a piece of nearly square stock with slots cut periodically across the width. The duct is a section of 38.10 mm x 69.85 mm (1-1/2"x 2-3/4", inner dimensions) rectangular extruded aluminum tubing with one of the narrow walls milled off, essentially making a piece of rectangular channel stock. The originally 6.4 meter (21′) length of duct was cut in half in order to make the machining of the duct practical. Five pieces of 44.45 mm x 50.80 mm (1-3/4"x2") aluminum stock 1.2 meters (47.24") in length were milled to a width of 38.10 mm (1-1/2") to fit into the width of the duct. Slots 38.10 mm (1-1/2") deep and 9.52 mm (3/8") wide were milled across the narrow width of the stock at 0.1 m intervals. The result is 12 such slots in each section of stock. Each of four aluminum binding plates 76.20 mm x 190.50 mm x 6.35 mm (3"x7-1/2"x1/4") was screwed to the side of the slotted sections opposite the slots with four 1/4-20 flathead screws to bind the sections end to end. The placement of the slots is such that the breaks between the sections of stock occur at one edge of a slot. The screw holes in the plates were countersunk off center so that the seating of the screws forces the ends of the slotted sections together, helping seal the intervening breaks.

Each of the two rectangular channel sections fits over the string of slotted sections in such a manner that an open 25.40 mm x 38.10 mm (1"x1-1/2") rectangular tube remains over the slotted sections. To ensure a good seal between the duct and the slotted sections, a piece of 31.75 mm (1-1/4") square extruded aluminum tubing is

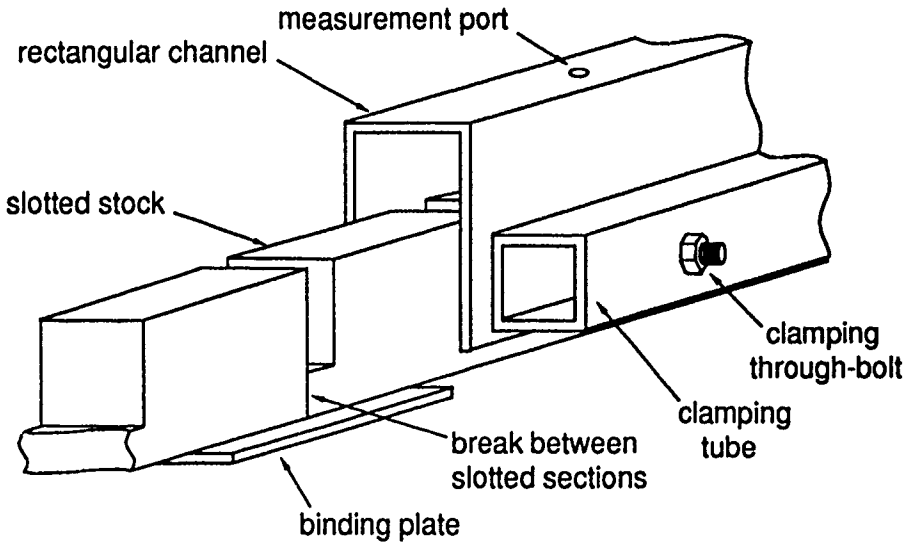

FIGURE 4.3
A cutaway perspective view of the waveguide.

AS-91-352

placed on either side of the duct below the open area that forms the waveguide and through-bolted to act as a clamp and force the duct walls into the sides of the slotted sections. Figure 4.3 illustrates the assembly. In order to further seal the joint between the duct and the slotted stock, vacuum grease was applied to the sides of the slotted stock prior to assembly. The through bolts are placed at two or three structure period intervals, as was convenient, and located midway between slots. Where the two duct sections are butted together, a rectangular U-shaped piece of aluminum stock was force fit over the joint to ensure the alignment of the duct sections and to tend to seal the joint. A similar U-shaped piece was fit over the source end of the waveguide and screwed into the slotted stock to act as a mounting flange for a compression driver.

The measurement ports are 9.53 mm (3/8") diameter holes drilled along the center of the side of the duct opposite the slotted sections (the top). The holes are located midway between side branches at *every other* period of the structure (every 0.2 meters), for a total of 23 ports: one reference port and 22 downstream ports. The holes are force fit with cylindrical aluminum plugs when not in use. The plugs are designed to form a flush surface on the inside of the waveguide when in place. During measurement the protective shrouds are removed from the microphones, which are slid into a teflon sleeve that fits into a mounting jig. The mounting jig is a rectangular U-shaped nylon block that straddles the waveguide and provides a stable mount for the microphone. The teflon sleeve buts into a shelf in the mounting block to ensure that the active face of the microphone is flush with the interior surface of the waveguide. This detail is illustrated in Fig. 4.4.

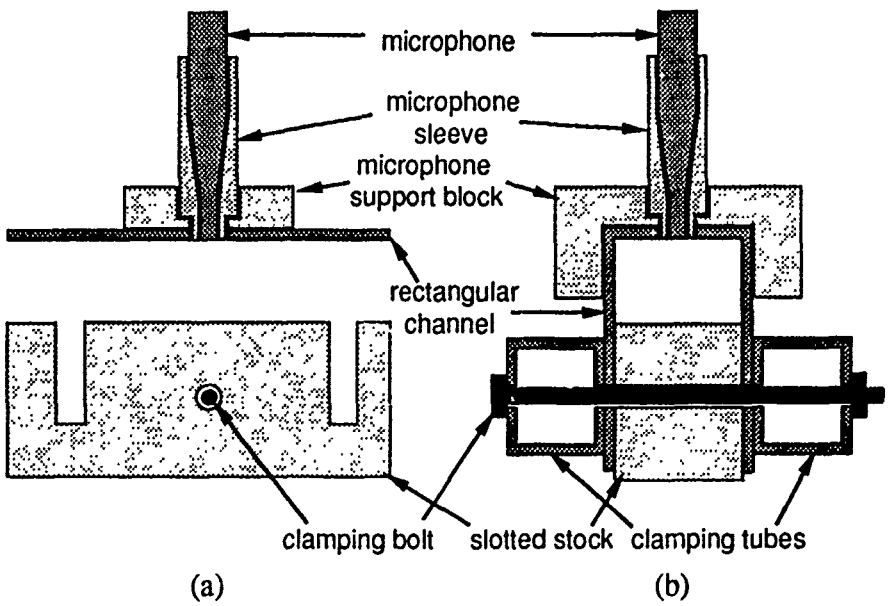

FIGURE 4.4
A sagittal cross-section (a) and a transverse cross-section (b) of the periodic waveguide showing the duct wall clamping system and the microphone placement.

AS-91-353

The anechoic waveguide termination is a roughly 1 m long fiberglass wedge which varies from a very fine trailing of a few fibers (at the upstream end) to densely packed (at the downstream end). As was discussed in Sec. 3.5, the termination of the periodic structure into a finite section of homogeneous waveguide which is loaded with an anechoic wedge (such as the fiberglass wedge) should simulate the termination of the structure into a semi-infinite section of waveguide. The periodic waveguide was terminated in such a manner, though the leading edge of the fiberglass termination was allowed to extend over the final two side branches. This was done because it was thought that such a transition between the Bloch impedance of the periodic structure and the purely resistive impedance of the anechoic termination section may reduce the magnitude of the reflected Bloch wave.

On the source end of the waveguide, the structure ends one period from the downstream side of the first side branch. The waveguide entrance is a 38.10 mm x 25.40 mm (1" x 1-1/2") rectangular opening, and the throat of the compression driver is a 50.80 mm (2") diameter circular opening. Because the driver is mounted directly onto the waveguide, a discontinuity in cross section results. The junction is sealed with a piece of neoprene gasket material with a circular hole that matches the driver throat.

4.3 The Experimental Setup and the Acquisition of Data

A computer controlled data acquisition system was used in the measurement portion of the experiment. Microphones were placed in the reference port and one of the downstream ports, and the computer was prompted to begin a data acquisition algorithm. The function of the algorithm is to measure $|\hat{p}_n|$ and $\hat{\theta}_n$, the amplitude and phase of the wavefield at the n^{th} measurement port relative to the amplitude and phase at the reference port, for a specified set of frequencies (the frequency set is discussed in Sec. 4.4). The downstream microphone was then moved to the next measurement point, and the process repeated for all 22 downstream ports. Following their acquisition, the data were postprocessed to correct for phase wrap-around effects and the limited dynamic range of the measurement system. Finally, linear regressions were performed on the spatial series associated with each frequency to result in values of $\mathrm{Re}\{q\}$ and $\mathrm{Im}\{q\}$ for each frequency.

4.3.1 The Experimental Setup

A block diagram of the experiment is shown in Fig. 4.5. At the heart of the setup is the Macintosh Mac II minicomputer, which runs National Instruments' LabVIEW, a data acquisition/analysis/display software package. The computer is linked via a

National Instruments NB-DMA-8-G interface board to the GPIB (General Purpose Instrumentation Bus), which serves as a communication and control link between the computer and the instrumentation.

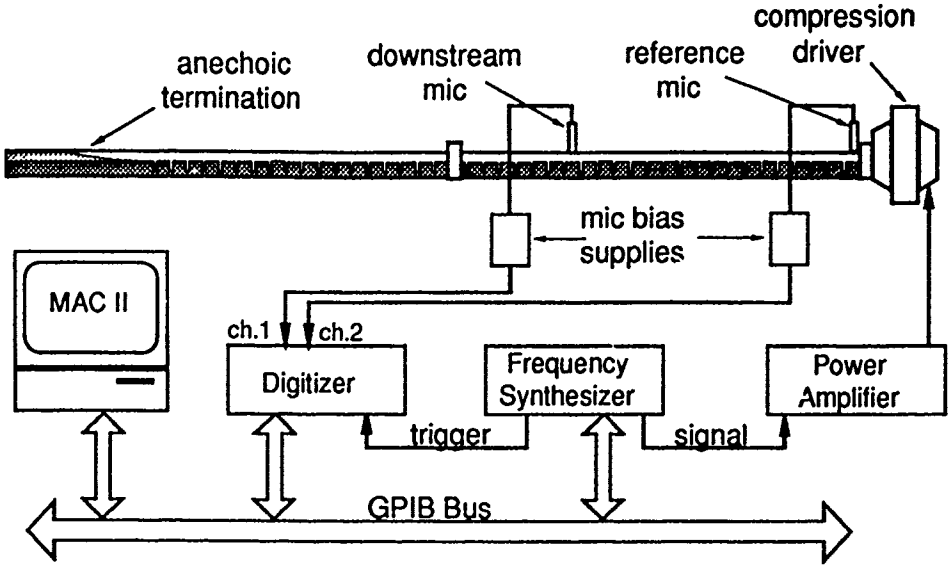

FIGURE 4.5
A block diagram of the experiment.

AS-91-354

The system operates as follows. The signal source is a Hewlett-Packard 3325A frequency synthesizer which, under computer control, sends a signal to a Crown D-150-A audio range power amplifier, which in turn drives a JBL 2485J compression driver. The resultant acoustic signal is picked up by two Brüel and Kjær 4136 1/4″ condenser microphones (with their associated preamplifiers and bias power supplies, the B&K 2619 and 2804, respectively) and routed to the inputs of a Tektronix RTD 710A digitizer. The digitizer is armed for waveform capture by the computer, and, upon receipt of a trigger, begins sampling as specified by the computer. Because the two-channel sampling is simultaneous and synchronous, the trigger (here conveniently supplied by the frequency synthesizer) is arbitrary. Upon completion of the waveform capture, the sampled waveform data are transferred to the computer for processing, display, and storage.

4.3.2 The Data Acquisition Algorithm

As mentioned above, the function of the data acquisition algorithm is to measure and store values of $|\hat{p}_n|$ and $\hat{\theta}_n$ for a specified set of frequencies. The user is

responsible for the specification of the frequency set and signal level, the positioning of the microphones, and the initiation of the acquisition algorithm. The computer then makes the measurements and stores the data for postprocessing.

The data acquisition algorithm, shown in flowchart form in Fig. 4.6, is outlined as follows:

- Initialize instruments. In the case of the frequency synthesizer the output voltage and output waveform are set. In the case of the digitizer, the initialization involves the specification of data transfer channels and several triggering and sampling parameters.
- Set synthesizer frequency and digitizer sampling rate. The sampling rate is set so that roughly 3 signal cycles are covered in the 1 kilosample capture (about 300 samples/signal cycle).
- Optimize digitizer input range. Because the digitizer has a limited dynamic range (roughly 55 dB for any single range setting), the information content and therefore the measurement accuracy can be maximized by making optimal use of the available dynamic range. For a given signal level, the *smallest* digitizer range setting at which the signal is not clipped results in the best use of the dynamic range. This optimal range setting was found by arming the digitizer and, upon completion of the waveform capture, requesting the maximum and minimum sample values. There are three possible outcomes:
  - Either the maximum or the minimum (or both) is at the limit of the range. In this case the amplitude setting is assumed under-range (signal clipped) and is set to the next larger available range. The process is repeated until the peak values of the acquired waveform fall within range.
  - The peak values are in range, but would be out of range at the next smaller available range setting. In this case the amplifier setting is optimal and the optimization routine ends.
  - The peak values are in range but would *not* be out of range at a smaller range setting. In this, the over-range case, the digitizer is set to the calculated optimal range.
- Capture and transfer waveforms. The digitizer is armed and, upon completion of the acquisition, the digitized waveform data are transferred to the computer.
- Resample the waveforms. The data vectors are resampled so that exactly one cycle of the waveform occupies a 256-bin timeseries vector. This resample algorithm is a linearly interpolating resampler, as diagrammed in Fig. 4.7 for the 8-bin case. The reason for resampling is two-fold:

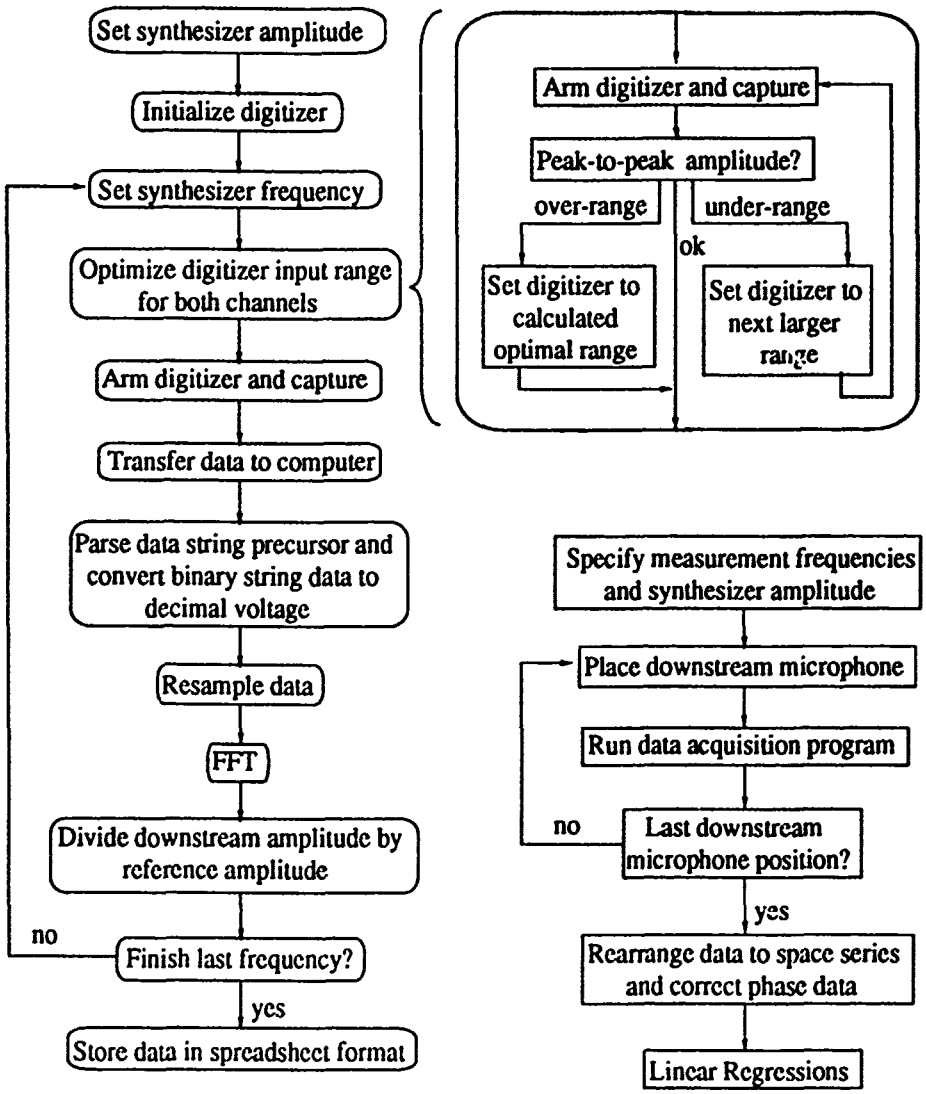

(a) Data Acquisition Algorithm

(b) User Algorithm

FIGURE 4.6
A flowchart of the data acquisition algorithm.

AS-91-355

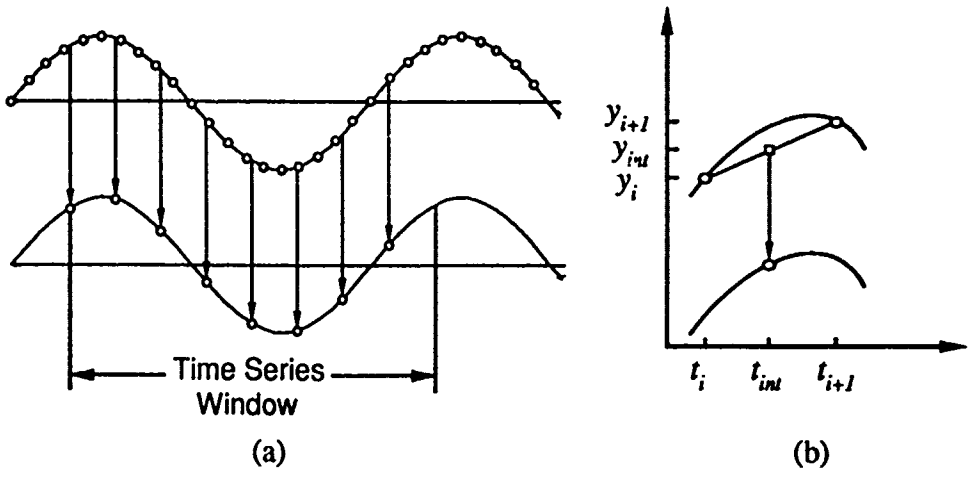

FIGURE 4.7

The linearly interpolating resample algorithm generates a timeseries which consists of exactly one cycle of the signal and has a number of bins equal to a power of two. Shown in (a) is an example for the case of eight time series bins. In (b) is shown the linear interpolation. The interpolated value is $y_{int} = y_i + (y_{i+1} - y_i)(t_{int} - t_i)/(t_{i+1} - t_i)$.

AS-91-356

- An FFT (fast Fourier transform algorithm) is used as a homodyning amplitude/phase detector. In such a scheme the sampling must be such that the frequency of interest has an *integral number of cycles in the time domain window.* This will ensure that the frequency of interest will *coincide exactly* with a single frequency domain bin. The number in the frequency bin is therefore the complex amplitude (i.e., magnitude *and* phase) of the signal at that frequency.
- In order to use a radix-2 FFT in place of the much more computationally intensive DFT (discrete Fourier transform algorithm), the number of bins in the timeseries must be a power of 2.

It should be noted that the amplitude and phase detection could be done much more efficiently by performing only the single fundamental homodyning integral. That is, because the timeseries is resampled so that exactly one cycle of the signal occupies the time domain window and the signal consists of a single frequency, the only integral of the Fourier transform which has a nonzero result is the fundamental integral.The remaining harmonic integrals are a computational waste. The reason for using the full FFT is that the data acquisition algorithm was developed both for use in this measurement and in later measurements in which the signal is expected to contain harmonic distortion components. In the latter case the algorithm will detect the amplitude and phase of all the

components of the signal.

- FFT the resampled timeseries and divide the complex amplitude of the downstream signal by that of the reference signal. Convert complex representation from cartesian to polar.
- Set the frequency synthesizer to the next frequency and repeat from the second step for each frequency in the set.
- Store data in spreadsheet format.

Once the data acquisition was complete, the data were reorganized into spatial series (one amplitude spatial series and one phase spatial series per frequency) to which some corrections were made. The first was the correction of the "wrap-around" effect in the phase series. Because the measured phase is restricted to the branch $-\pi < \hat{\theta}_n < \pi$, it is a sawtooth-like function of distance. The wrap-around problem was corrected by selectively adding 2π to the phase until a smooth, monotonically increasing function resulted. The other correction was to throw out data that fell below the floor of the dynamic range of the measurement system. At some stopband frequencies the waves are so strongly attenuated (over 260 dB/meter was measured) that the waves are rendered immeasurable beyond a certain distance from the driver. Beyond this point the measured amplitude is roughly constant (defining the floor of the dynamic range) and the phase is essentially random. These measurements of the noise floor were discarded.[2]

4.4 Experimental Results

Data were collected as described in the previous section for a set of 455 frequencies between 100 Hz and 4 kHz. The frequency interval was 10 Hz except in the vicinity of the side branch resonance stopband, where, because both the real and imaginary parts of the Bloch wave number vary rapidly with frequency, the interval was decreased to 4 Hz. The synthesizer level was set such that the acoustic signal was as strong as possible (for a good signal to noise ratio) without exceeding about 100 dB (re 20 μPa), which is safely within the realm of linear acoustics.

[2] Reduction in the length of the space series for stopband frequencies seems to imply that the resultant values of the Bloch wave number are less precise for these frequencies since the measurements at large distances from the driver contribute most strongly to the precision of the measurement. This implication is not necessarily true, however, as the strongly stopped waves are effectively reflectionless. The strong attenuation renders the reflected wave so weak there is essentially none of the oscillation in the space series associated with a compound wavefield and the resultant measurement is *more* precise. When the waves are *very* strongly stopped, however, we may have only two or three measurements of the amplitude and phase before the waves are immeasurable. In this case the experimental precision does suffer.

The low frequency end of the measurement frequency range was determined by the range of validity of the measurement technique. As was pointed out in Sec. 4.1, a linear regression can be used to filter out the effects of a counter-propagating Bloch wave provided the oscillations are numerous enough to make a good average possible. Since the oscillations occur at intervals of one half of a Bloch wavelength, the requirement is that the waveguide be several wavelengths long. Because we are measuring over about 4.5 meters, which is the wavelength associated with a frequency of about 70 Hz, we don't expect to get particularly good results below about 200 Hz.[3] The low frequency limit of 100 Hz was chosen with the expectation that the precision of the measurement technique would begin to break down at a somewhat higher frequency.

The high frequency end of the measurement frequency range was chosen to ensure the validity of the five frequency constraints associated with the zeroth order approximation (Eqs. 2.24, 2.25, 2.26, 2.31, and 4.11). Of the five constraints, that associated with higher order modes in x (Eq. 2.26) is the most limiting. That constraint, $f \ll 4494$ Hz, led to a choice of 4 kHz as the upper frequency limit for the measurements.

Although we are primarily interested in the measured values of the Bloch wave number q, it is nonetheless of interest to view some of the raw data. Figure 4.8 shows the amplitude spatial series for several frequencies in and below the π stopband. Notice that the 830 Hz series shows the characteristic exponential decay associated with lossy propagation, and no readily identifiable oscillations. The lack of oscillations indicates a nearly purely progressive Bloch wavefield. The 1200 Hz series shows both an increase in the exponential decay relative to the 830 Hz series and the appearance of oscillations. The increase in decay with frequency is expected of thermoviscous boundary layer losses, and the appearance of oscillations is consistent with the expected increase in reflected Bloch wave amplitude as a stopband frequency is approached. The 1350 Hz series shows the continuation of the trend of stronger decay and increasing oscillation amplitude with frequency. The remaining series (1380, 1400, 1420, and 1470 Hz) continue the decay trend as we move into the stopband, but the oscillations disappear. This phenomenon, discussed in Sec. 4.3, is due to the essentially nonexistent reflected Bloch wave due to the strong exponential decay. The other trend that is evident in the spatial series is the *decrease* in the spatial frequency of the oscillations with increasing frequency. This trend, evident in the 1200 Hz, 1350 Hz, and 1380 Hz series, seems to be exactly opposite the behavior expected of a compound wavefield. It is, however, exactly what is expected of a *sampled* compound wavefield as outlined in Sec. 4.1 (compare the 1200 Hz and 1350 Hz series to the examples of Fig. 4.2).

[3]Note that this is somewhat below the frequency at which we expect the termination to not be particularly anechoic. It is worth restating that the measurement technique will work regardless of the amplitude of the backward propagating Bloch wave component. The precision is simply better when the reflected wave amplitude is small. The behavior of the anechoic termination is therefore not critical to our measurement; it simply enhances the precision.

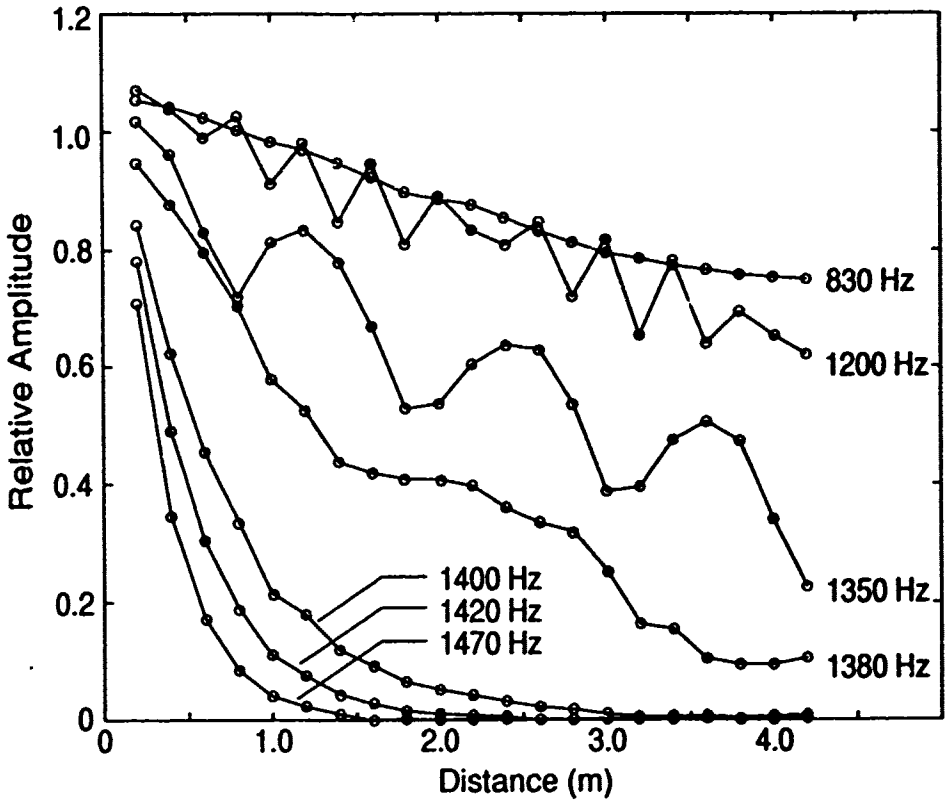

FIGURE 4.8
The amplitude spatial series for several frequencies in and below the π stopband.

AS-91-357

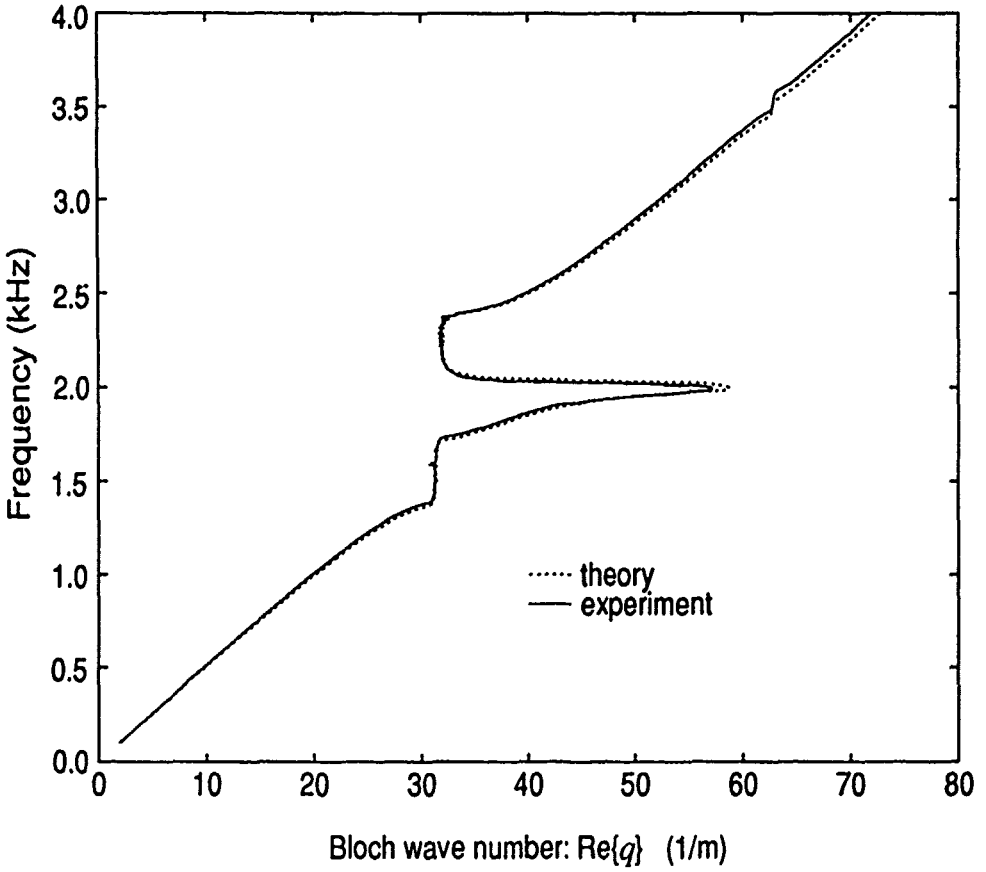

FIGURE 4.9
Theoretical and experimental values of $\mathrm{Re}\{q\}$.

AS-91-358

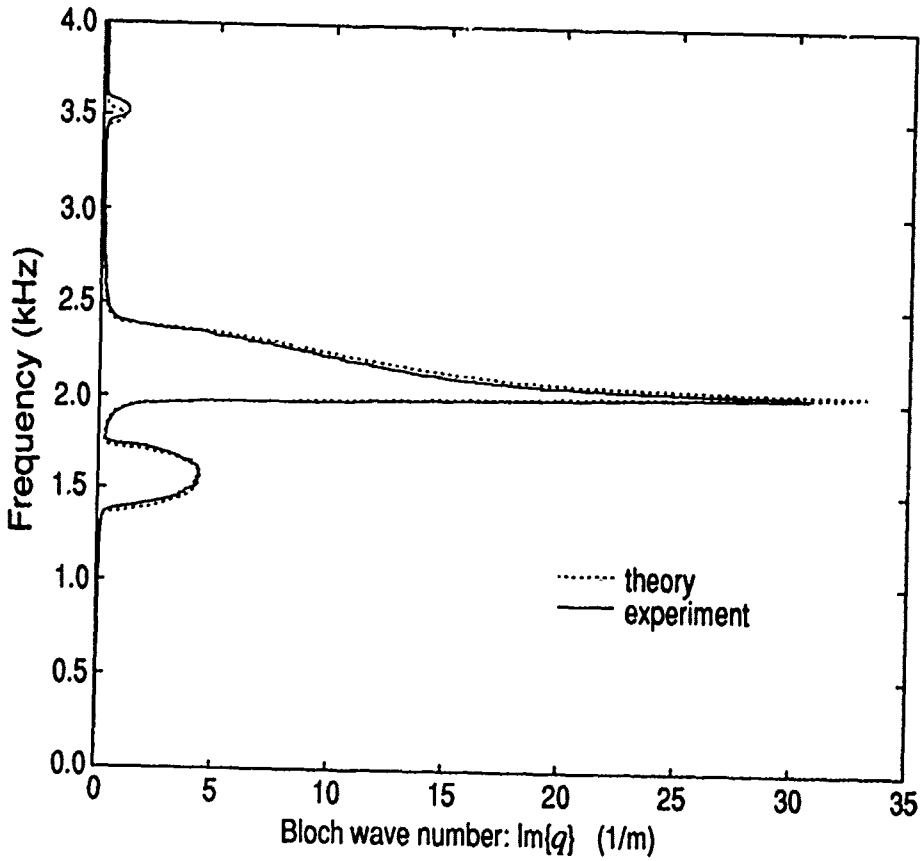

FIGURE 4.10
Theoretical and experimental values of $\mathrm{Im}\{q\}$.

AS-91-359

The theoretical and experimental values of the Bloch wave number show excellent agreement. Figures 4.9 and 4.10 show the real and imaginary components of q, respectively, for both theory and experiment. The π and 2π Bragg stopbands (centered at about 1.5 kHz and 3.5 kHz, respectively) and the side branch resonance stopband (at about 2.0 kHz) are clearly evident. In the vicinity of the 2π stopband the experimental curves begin to become shifted with respect to the theoretical curve, a trend that is evident for both $\mathrm{Re}\{q\}$ and $\mathrm{Im}\{q\}$. This may be due to the breakdown of one of the zeroth order assumptions. Figure 4.11 shows $\mathrm{Im}\{q\}$ on an expanded scale in q. The measured value of $\mathrm{Im}\{q\}$ is consistently about 0.02 m^{-1} larger than the theoretical prediction. This could be in part due to the fact that in the development of the theory

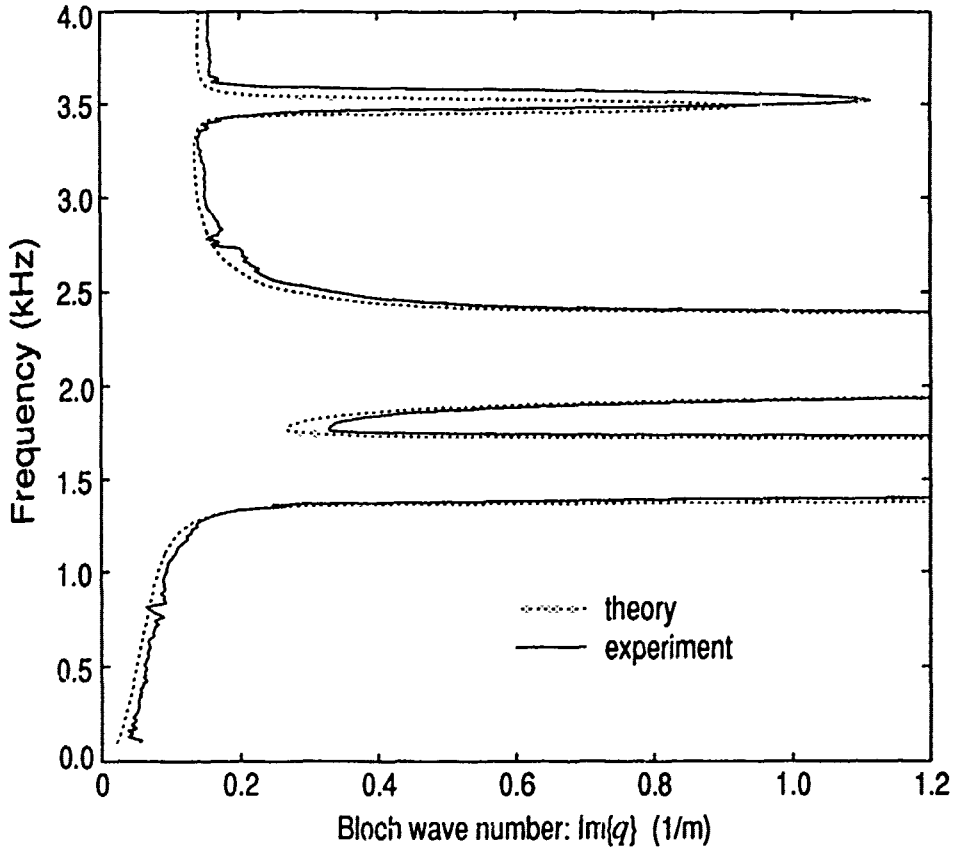

FIGURE 4.11
Theoretical and experimental values of $\mathrm{Im}\{q\}$ on an expanded scale.
AS-91-360

we accounted for losses in the zeroth order mode but none of the higher order modes. That is, we assumed that the evanescent higher order modes, once established, exist somewhat independently of the zeroth order mode, simply representing local lossless storage of acoustic energy. In fact, there are losses associated with the evanescent modes, losses which are "fed" by the zeroth order mode and which therefore represent additional dissipative attenuation of the zeroth order mode. It is also to be expected

that the various seals are imperfect and will leak or otherwise absorb acoustic energy. Note also that there are small patches of jitter in the plot near 800 Hz and 2700 Hz. These are frequencies at which the oscillations in the amplitude and phase series have zero frequency aliases and measurement inaccuracies are expected (see discussion of Eq. 4.10).

It was noted in Sec. 4.1 that the amplitude of the oscillations in the amplitude series is a measure of the reflected Bloch wave amplitude. Figure 4.12 shows the amplitude of the oscillations (which was found by taking half of the difference between the maximum and minimum values of the oscillations) and the theoretical value of the reflected Bloch wave amplitude. We see that albeit rough, there is a degree of agreement. The roughness is expected as we have simply looked for maxima and minima in the oscillations without accounting for lossy propagation (the oscillation amplitudes are larger near the termination end than near the source end) We may also be missing the absolute maxima and minima because of the intermittent nature of sampling. The technique breaks down at frequencies at which the attenuation is large (i.e., at and near stopband frequencies) as any noise-like jitter in the data is large compared to the very small amplitude of the wave incident upon the termination, making the reflected Bloch wave appear to be greater in amplitude than the incident wave amplitude. It can also be seen that the reflected Bloch wave amplitude is larger than expected below about 300 Hz, which is consistent with the predicted breakdown of the anechoic nature of the fiberglass wedge termination.

4.4.1 Conclusion

To conclude, it is first worth noting that the experimental findings are supportive of the validity of the theory (Figs 4.9, 4.10, and 4.11 provide the most conclusive testimony). Secondly, it is worth drawing attention to the *strength* of the dispersion and attenuation that we were able to achieve in a periodic waveguide. Phase speeds of 219 m/s and 465 m/s were measured at 1992 Hz and 2370 Hz, respectively. In other words, the phase speed changed by 246 m/s (a 112% increase) over a frequency interval of only 378 Hz (0.076 decades or 0.250 octaves). The attenuation was measured to be over 38 dB/m in the first Bragg stopband (the π stopband) and over 260 dB/m in the side branch resonance stopband. Another remarkable feature of the attenuation is the *sharpness* of the band structure. The measured attenuation was less than 9 dB/m at 1930 Hz, over 260 dB/m at 2028 Hz, and less than 4 dB/m at 2450 Hz. In other words, the attenuation increased by over 9200% (in dB/m) over an interval of only 98 Hz (0.022 decades or 0.072 octaves) and then decreased to 1.5% of the maximum value in the next 422 Hz (0.082 decades or 0.273 octaves)! The maximum attenuation slope was measured at over 20,230 dB/m/decade. For a propagation distance of 1.0 m (10 structure periods), the slope is over 20,230 dB/decade, which is larger than the slope associated with a 1000 *pole rolloff!*

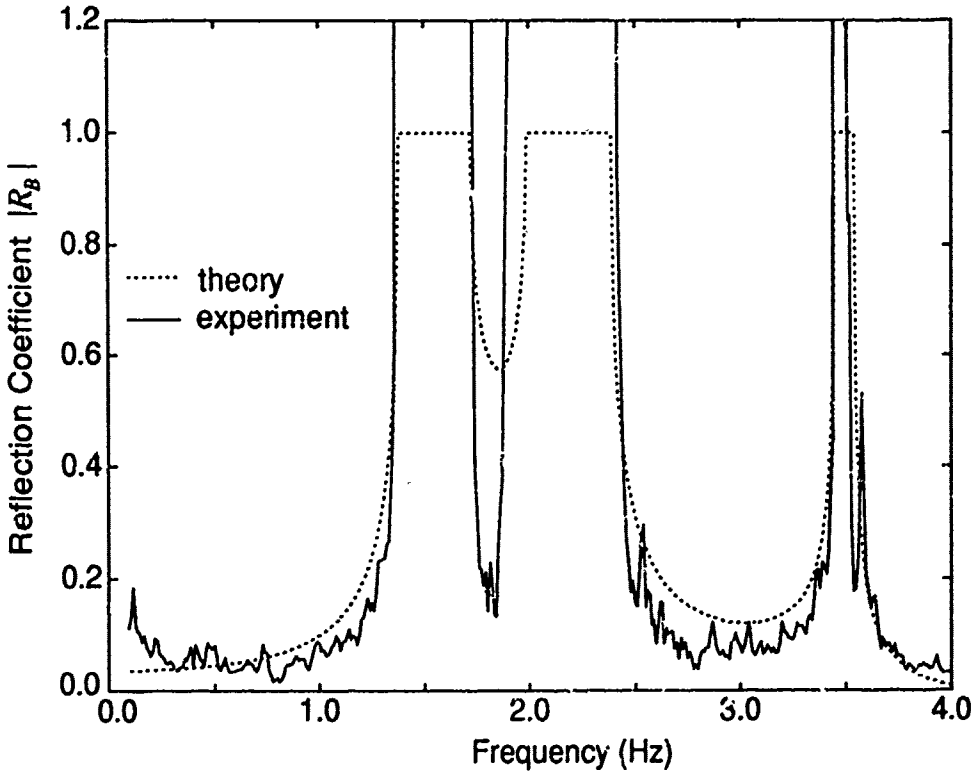

FIGURE 4.12
Theoretical and experimental estimates of the normalized amplitude of the Bloch wave reflected from the waveguide termination.

AS-91-361

5. CONCLUSION

A theoretical and experimental investigation of the properties of linear acoustic propagation in a periodic waveguide has been carried out. The waveguide under study is a rectangular duct loaded periodically with rigidly terminated side branches. In this chapter the results of the investigation are summarized, conclusions are drawn, and some suggestions for future work are presented.

Summary

This work is divided into three sections, each of which comprises a chapter. The first section (Chap. 2) is an investigation of the conditions under which one can expect to have Bloch wave solutions of a periodic waveguide problem. It is shown that there are two conditions under which the Floquet theorem may be applied to a mathematical system to show that the solution functions are Bloch wave functions. The system must (1) exhibit a translational invariance, and (2) have two linearly independent solutions. Condition (1) is shown to be satisfied *even in the dissipative case* for an arbitrary periodic waveguide. That is, the Bloch wave formalism retains its validity with the introduction of dissipative losses. Condition (2) is shown to be satisfied for our waveguide when the excitation frequency is low enough to ensure that the solution is well represented by the zeroth order mode of propagation alone. In other words, information must be transferred from cell to cell by the zeroth order mode of propagation only. In addition to the investigation of the above conditions, a new functional representation of the Bloch wave function, here called the convolution representation, is introduced. This representation bears a very straightforward relation to the functional form of the Bloch wave itself.

The second section (Chap. 3) is composed of derivations of the various quantities that characterize Bloch wave propagation. A dispersion relation for a waveguide loaded with a periodic array of arbitrary scatterers is derived. Various forms of the dispersion relation are shown for various types of scatterer. The dispersion relation for the waveguide of this study is derived and the features of the dispersion curve are related to the waveguide dimensions. The impedance function is derived for an arbitrary scatterer as well as for the scatterer used in this study. It is found that when expressed in the convolution representation, the Bloch wave function for a waveguide loaded with scatterers is completely specified by the two parameters q and g/f. An expression for g/f is derived. An analytic expression for the travelling wave spectral amplitudes is found in terms of q and g/f. The effect of truncating the

periodic waveguide is examined and a Bloch wave reflection coefficient is derived for a periodic waveguide terminated into an arbitrary terminating impedance.

The third section (Chap. 4) is the description of a measurement of the Bloch wave dispersion. A scheme for extracting precise dispersion information from a compound Bloch wavefield is developed and its implementation described. The resulting dispersion measurements show very good agreement with the theoretical results.

Conclusions

The goal of this study, to develop and experimentally verify a theory for acoustic Bloch wave propagation, appears to have been completed successfully. The theoretical results make some intuitive sense and agree well with the experimental results.

As was remarked upon in Sec. 4.4, the introduction of a periodic array of resonant scatterers into a guided wave system can cause both very strong dispersion and very sharply banded attenuation. The very rapid transitions in attenuation make the periodic waveguide a promising candidate for use as a band reject travelling wave filter (it was noted in Sec. 4.4 that the attenuation slope near the side branch resonance stopband is that of a 1,000 pole filter). Such a travelling wave filter would be tuneable simply by altering the resonance frequency of the scattering elements, as shown in Fig. 3.3. Such filtering techniques may be applicable in the design of exhaust noise mufflers or sound suppressing ventilation ducts. Low flow resistance, lightweight scatterers may be an attractive alternative to the duct lining in common use.

Suggestions for Future Work

As was pointed out in the introductory chapter, this work is preliminary to the study of *finite amplitude* acoustic propagation in a periodic waveguide. Suggestions for future work in the *linear* acoustic case are:

- Experimentally verify the f and g wave makeup of a Bloch wave. Such a measurement would also be an indirect measurement of the periodic structure impedance.
- Measure the (generally aharmonic) series of resonance frequencies of a rigidly terminated periodic waveguide. Such a measurement may be of interest in the nonlinear case as the nonlinearly generated harmonic distortion components would *not* coincide with resonances as they do in the uniform waveguide case.
- Investigate the propagation of transients in a periodic waveguide.
- Determine whether or not the introduction of periodic scatterers into ventilation ducting would be an effective means of suppressing noise transmission through

the duct.

- Apply the theory developed here to the case of a waveguide with *distributed* as opposed to spatially localized scatterers. The scattering matrix elements as defined in this work would then be non-causal functions of frequency (owing to the fact that the associated impulse responses would be non-zero for $t < 0$), but this will not be of concern as far as the dispersion relation is concerned. It would be interesting to treat the problem of a waveguide with sinusoidal walls by finding the S-matrix elements associated with a single sinusoidal bulge in a waveguide, introducing them into the general dispersion relation, and comparing the results to those of Nusayr (1980).

- Investigate the problem of wave propagation in a *temporally* periodic medium.

- Investigate propagation of a guided electromagnetic field through a guided acoustic field. To some degree, the acoustic field would represent an effectively static spatially periodic inhomogeneity.

REFERENCES

Achenbach, J. D., and M. Kitahara (1987). "Harmonic Waves in a Solid with a Periodic Distribution of Spherical Cavities," *J. Acoust. Soc. Am.* **81**, 595-598.

Arfken, G. (1985). *Mathematical Methods for Physicists* (Academic Press, Inc., New York).

Bai, D., and J. B. Keller (1987). "Sound Waves in a Periodic Medium Containing Rigid Spheres," *J. Acoust. Soc. Am.* **82**, 1436-1441.

Bell, D. T., and R. C. M. Li (1987). "Surface Acoustic Wave Resonators," *Proc. IEEE* **64**, 711-721.

Brillouin, L. (1946). *Wave Propagation in Periodic Structures* (McGraw-Hill Book Co., Inc., New York).

Collin, R. E. (1960). *Field Theory of Guided Waves* (McGraw-Hill Book Co., Inc., New York).

Drumheller, D. S. (1989). "Acoustical Properties of Drill Strings," *J. Acoust. Soc. Am.* **85**, 1048-1064.

Elachi, C. (1976). "Waves in Active and Passive Periodic Structures: A Review," *Proc. IEEE* **64**, 1666-1698.

Gasiorowicz, S. (1974). *Quantum Physics* (John Wiley and Sons, Inc., New York).

He, S., and J. D. Maynard (1986). "Detailed Measurements of Inelastic Scattering in Anderson Localization," *Phys. Rev. Letters* **57**, 3171-3174.

Hessel, A. (1969). "General Characteristics of Traveling-Wave Antennas," in *Antenna Theory*, Part 2, R. E. Collin and F. J. Zucker, Eds. (McGraw-Hill Book Co., Inc., New York).

Ince, E. L. (1926). *Ordinary Differential Equations* (Dover, New York).

Kinsler, L. E., A. R. Frey, A. B. Coppens, and J. V. Sanders (1982). *Fundamentals of Acoustics*, 3rd ed. (John Wiley and Sons, Inc., New York).

Kittel, C. (1986). *Introduction to Solid State Physics*, 6th ed. (John Wiley and Sons, Inc., New York).

Mead, D. J. (1970). "Free Wave Propagation in Periodically Supported, Infinite Beams," *J. Sound Vib.* **11**, 181-197.

Mead, D. J. (1973). "A General Theory of Harmonic Wave Propagation in Linear Periodic Systems with Multiple Coupling," *J. Sound Vib.* **27**, 235-260.

Morse, P. M. (1976). *Vibration and Sound*, 1st paperback ed. (American Institute of Physics for the Acoustical Society of America).

Morse, P. M., and K. U. Ingard (1986). *Theoretical Acoustics* (Princeton University Press, New Jersey).

Nayfeh, A. H. (1974). "Sound Waves in a Two Dimensional Duct with Sinusoidal Walls," *J. Acoust. Soc. Am.* **56**, 768-770.

Nayfeh, A. H. (1975). "Acoustic Waves in Ducts with Sinusoidally Perturbed Walls and Mean Flow," *J. Acoust. Soc. Am.* **57**, 1036-1039.

Nusayr, A. (1980). "Propagation in Rectangular Ducts with Sinusoidal Undulations," *J. Acoust. Soc. Am.* **67**, 1472-1476.

Pierce, A. D. (1981). *Acoustics: an Introduction to its Physical Principles and Applications* (McGraw-Hill Book Co., Inc., New York).

Ramo, S., J. R. Whinnery, and T. Van Duzer (1965). *Fields and Waves in Communication Electronics* (McGraw-Hill Book Co., Inc., New York).

Salant, R. F. (1973). "Acoustic Propagation in Waveguides with Sinusoidal Walls," *J. Acoust. Soc. Am.* **53**, 504-507.

Samuels, J. C. (1958). "On Propagation of Waves in Slightly Rough Ducts," *J. Acoust. Soc. Am.* **31**, 319-325.

SenGupta, G. (1970). "Natural Flexural Waves and the Normal Modes of Periodically-Supported Beams and Plates," *J. Sound Vib.* **13**, 89-101.

Skudrzyk, E. (1971). *The Foundations of Acoustics* (Springer-Verlag, Wein).

Slater, J. C. (1948). "The Design of Linear Accelerators," *Revs. Modern Phys.* **20**, 473-518.

Slater, J. C. (1950). *Microwave Electronics* (D. Van Nostrand Co., Inc., New York).

Ungar, E. E. (1966). "Steady State Responses of One-Dimensional Periodic Flexural Systems," *J. Acoust. Soc. Am.* **39**, 887-894.

Whittaker, E. T., and G. N. Watson (1952). *Modern Analysis* (Cambridge University Press, London).

DISTRIBUTION LIST FOR
ARL-TR-91-19
UNDER CONTRACT N00014-84-K-0574
AND GRANT N00014-89-J-1109

Copy No.	
	Office of Naval Research Department of the Navy 800 North Quincy Street Arlington, VA 22217-5000
1-2	Attn: L. E. Hargrove (Code 1112)
	Director Naval Research Laboratory Washington, D.C. 20375
3	Attn: Code 2627
	Commanding Office and Director Defense Technical Information Center Building 5, Cameron Station 5010 Duke Street
4-7	Alexandria, VA 22314
	Los Alamos National Laboratory Mail Stop K764 Los Alamos, NM 87545
8	Attn: G. W. Swift
	NOAA Ship Ferrel 439 W. York St. Norfolk, VA 23510
9	Attn: D. L. Gardner
	Naval Postgraduate School Monterey, CA 93940
10	Attn: Technical Library (Code 0212)
11	S. L. Garrett
12	A. A. Atchley
13	B. Denardo
14	T. J. Hofler
15	A. Larraza
	Naval Research Laboratory P.O. Box 8337 Orlando, FL 32856
16	Attn: B. E. McDonald
	Sandia National Laboratories Geothermal Research Division Albuquerque, NM 87185
17	Attn: D. S. Drumheller
	U.S. Naval Academy Physics Department Annapolis, MD 21403
18	Attn: M. S. Korman

Copy No.	
	Cornell University Department of Theoretical and Applied Mechanics Thurston Hall Ithaca, NY 14835
19	Attn: W. A. Sachse
	Drexel University Department of Electrical and Computer Engineering 32nd and Chestnut St. Philadelphia, PA 19104
20	Attn: M. M. Bilgutay
	George Mason University Department of Physics 4400 University Drive Fairfax, VA 22030
21	Attn: P. H. Ceperley
	Georgetown University Physics Department Washington, D.C. 20057
22	Attn: W. G. Mayer
	Georgia Institute of Technology School of Mechanical Engineering Atlanta, GA 30332
23	Attn: Y. H. Berthelot
24	J. H. Ginsberg
25	P. H. Rogers
	Johns Hopkins University Department of Mechanical Engineering Baltimore, MD 21218
26	Attn: A. Prosperetti
	Kalamazoo College Department of Physics Kalamazoo, MI 49007
27	Attn: W. M. Wright
	Northwestern University Center for Engineering and Failure Prevention 2137 N. Sheridan Rd. Evanston, IL 60208-3020
28	Attn: J. D. Achenbach
	The Pennsylvania State University Graduate Program in Acoustics University Park, PA 16802
29	Attn: A. D. Pierce
30	V. W. Sparrow

Distribution List for ARL-TR-91-19 under Contract N00014-84-K-0574 and Grant N00014-89-J-1109 (cont'd)

Copy No.	
	The Pennsylvania State University Physics Department University Park, PA 16802
31	Attn: J. D. Maynard
	Swarthmore College Department of Engineering Swarthmore, PA 19081-1397
32	Attn: E. C. Everbach
	University of Mississippi Physics Department University, MS 39677
33	Attn: M. A. Breazeale
34	L. A. Crum
35	H. E. Bass
36	W. P. Arnott
37	R. Raspet
	University of Rochester Electrical Engineering Dept. Hopeman Building Rochester, NY 14627
38	Attn: E. L. Carstensen
39	K. J. Parker
	U. of Wisconsin-Milwaukee Department of Physics Milwaukee, WI 53201
40	Attn: M. Levy
	University of Washington Applied Physics Laboratory 1013 NE 40th St. Seattle, WA 98105
41	Attn: K. L. Williams
	Washington State University Department of Mechanical and Materials Engineering Thurston Hall Pullman, WA 99164-2920
42	Attn: P. G. Vaidya
	Washington State University Department of Physics Pullman, WA 99164-2814
43	Attn: P. L. Marston
	Washington University Department of Physics Lindell and Skinner St. St. Louis, MO 63130
44	Attn: Y. Fu
45	G. Cwilich

Copy No.	
	Yale University Department of Engineering Mason Laboratory 9 Mill House Avenue New Haven, CT 06520
46	Attn: R. E. Apfel
	Stanford University W. W. Hanson Laboratory of Physics Stanford, CA 94305
47	Attn: C. F. Quate
	Chief Defence Research Establishment Atlantic P. O. Box 1012 Dartmouth, Nova Scotia B2Y 3Z7 CANADA
48	Attn: Technical Library
49	F. D. Cotaras
	Fukui Institute of Technology Department of Technology 3-6-1, G uen Fukui 910 JAPAN
50	Attn: A. Nakamura
	The Technical University of Denmark Industrial Acoustics Laboratory Building 352 DK-2800 Lyngby DENMARK
51	Attn: L. Bjorno
	The University of Electro-Communications 1-5-1, Chofugaoka Chofu-shi Tokyo JAPAN
52	Attn: T. Kamakura
	University of Bergen Department of Mathematics N-5014 Bergen-U NORWAY
53	Attn: S. Tjotta
54	J. Naze-Tjotta
55	Kjell-Eivind Froysa
	Cambridge University Department of Applied Mathematics and Theoretical Physics Silver Street Cambridge CB3 9EW UNITED KINGDOM
56	Attn: D. G. Crighton

Distribution List for ARL-TR-91-19 under Contract N00014-84-K-0574 and Grant N00014-89-J-1109 (cont'd)

Copy No.	
	Institute of Sound and Vibration Research The University Southampton S09 5NH UNITED KINGDOM
57	Attn: C. L. Morfey
	University of Bath School of Physics Claverton Down Bath BA2 7AY UNITED KINGDOM
58	Attn: H. O. Berktay
59	V. F. Humphrey
	Schlumberger Cambridge Research Seismic Dept. High Cross Madingley Road Cambridge CB3 OEL ENGLAND
60	Attn: M. A. Schoenberg
	Agency of Industrial Science and Technology Mechanical Engineering Laboratory 1-2 Namiki, Tsukuba Ibaraki 305 JAPAN
61	Attn: H. Mitome
	Institut fur Angewandte Physik Technische Hochschule Darmstadt Schlosgartenstr. 7, D-6100 Darmstadt Federal Republic of Germany
62	Attn: W. Lauterborn
	Tokyo Institute of Technology The Graduate School of Nagatsuta 4259 Nagatsuta, Midori-ku Yokahama JAPAN
63	Attn: T. Sato
	Osaka University Department of Mechanical Engineering Faculty of Engineering Science Toyonaka Osaka 560 JAPAN
64	Attn. N. Sugimoto
	Doshisha University Faculty of Engineering Imadegawa, Karasuma Kyoto 602 JAPAN
65	Attn: Y. Watanabe

Copy No.	
66	Anthony Bedford (EM:UT)
67	David T. Blackstock (ARL:UT)
68	Charles E. Bradley (ARL:UT)
69	Ilene J. Busch-Vishniac (ME:UT)
70	Thomas A. Griffy (PHY:UT)
71	Mark. F. Hamilton (ME:UT)
72	James A. Hawkins (ARL:UT)
73	Elmer L. Hixson (ECE:UT)
74	Bart Lipkens (ARL:UT)
75	F. M. Pestorius (ARL:UT)
76	James A. Tencate (ARL:UT)
77	ARL:UT Library
78-92	NAD Reserve